Par **Hossam AL GHOSSINI**

Contributions to the study of control for small-scale wind turbine connected to electrical microgrid with and without sensor

Thèse présentée
pour l'obtention du grade
de Docteur de l'UTC

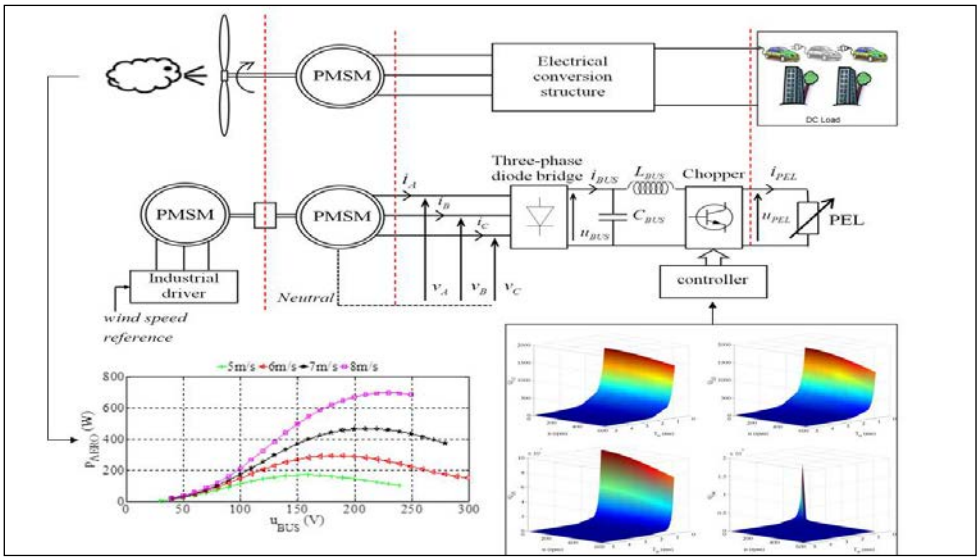

Soutenue le 23 novembre 2016
Spécialité : Réseaux Électriques : Laboratoire Avenues - GSU [EA 7284]

D2310

UNIVERSITE DE TECHNOLOGIE DE COMPIEGNE

THESE

Pour obtenir le grade de

DOCTEUR

Spécialité : Réseaux Electriques

Par

Hossam AL GHOSSINI

Contributions to the study of control for small-scale wind turbine connected to electrical microgrid with and without sensor

Laboratoire AVENUES - GSU - EA 7284

Soutenue le 23 Novembre 2016 devant le jury composé de :

Rapporteurs :	Xavier KESTELYN	L2EP, Lille
	Cristian NICHITA	GREAH, Le Havre
Examinateurs :	Franck BETIN	LTI, Amiens
	Christophe FORGEZ	LEC, Compiègne
Directeurs de thèse :	Fabrice LOCMENT	AVENUES, Compiègne
	Manuela SECHILARIU	AVENUES, Compiègne

Abstract

The aim of this thesis is to propose the most appropriate approach in order to minimize the cost of integration of a wind generator into a DC urban microgrid. A small-scale wind generator based on a permanent magnet synchronous machine (PMSM) is considered to be studied. A state of the art concerning the renewable energies, DC microgrid, and wind power generation is done. As the mechanical sensor for this structure is relatively of high cost, various types of wind conversion system control are presented in order to choose an energy conversion active structure and a sensorless PMSM. Therefore, a speed/position estimator is required to control the system. Thus, different methods proposed in literatures are considered and classified to be studied in details, and then the most effective and widely used ones are to be verified in simulation and experimentally for the studied system. The methods which are chosen are: rotor flux estimation with phase locked loop (PLL), sliding mode observer (SMO), Luenberger observer of reduced order, and extended Kalman filter (EKF). Facing to other methods, the EKF model-based estimator allows sensorless drive control in a wide speed range and estimates the rotation speed with a rapid response. The EKF parameters tuning is the main problem to its implementation. Hence, to solve this problem, the thesis introduces an adaptive method, i.e. adaptive-tuning EKF. As a result and grace to this approach, the total cost of conversion system is reduced and the performance is guaranteed and optimized.

Key words

Wind power generation, DC microgrid, small-scale wind turbine, permanent magnets synchronous machine (PMSM), sensorless control, phased locked loop (PLL), sliding mode observer (SMO), reduced order Luenberger observer, extended Kalman filter (EKF), adaptive tuning.

Résumé

L'objectif de cette thèse est de proposer l'approche la plus appropriée afin de minimiser le coût d'intégration de petite éolienne dans un micro-réseau DC urbain. Une petit éolienne basé sur un machine synchrone à aimant permanent (MSAP) est considéré à étudier. Un état de l'art concernant les énergies renouvelables, micro-réseau DC, et la production d'énergie éolienne, est fait. Comme le capteur mécanique de cette structure est relativement d'un coût élevé, les différents types de contrôle pour un système de conversion éolienne sont présentés afin de choisir une structure active de conversion d'énergie et un MSAP sans capteur. Par conséquent, un estimateur de vitesse/position est nécessaire pour contrôler le système. Ainsi, les méthodes différentes proposées dans la littérature sont considérées et classifiées à étudier dans les détails, puis les plus efficaces et largement utilisés sont à vérifier dans la simulation et expérimentalement pour le système étudié. Les méthodes choisies sont: estimation de la flux de rotor avec boucle à verrouillage de phase (PLL), observateur à mode glissement (SMO), observateur de Luenberger d'ordre réduit, et filtre de Kalman étendu (EKF). Face à d'autres méthodes, l'estimateur basé sur un modèle EKF permet une commande sans capteur dans une large plage de vitesse et estime la vitesse de rotation avec une réponse rapide. Le réglage des paramètres EKF est le problème principal à sa mise en œuvre. Par conséquent, pour résoudre ce problème, la thèse présente une méthode adaptative, à savoir réglage-adaptatif d'EKF. En conséquence, et grâce à cette approche, le coût total du système de conversion est réduite et la performance est garantie et optimisée.

Mots-clé

Production d'éolienne, micro-réseau DC, éolienne à petit puissance, machine synchrone à aimant permanent (MSAP), commande sans capteur, boucle à verrouillage de phase (PLL), observateur à mode glissement (SMO), observateur de Luenberger d'ordre réduit, filtre de Kalman étendu (EKF), réglage-adaptatif.

Acknowledgments

I thank all who in one way or another contributed in the completion of this thesis. First of all, I give my pure gratitude and thanks to God for His protection, His guidance and ability to do work. In this context, I offer all my scientific works humbly as lotus flower's petals before my beloved spiritual master Sathya Sai Baba whose precious and rich literatures have been accompanying me all along my working journey to finish this thesis.

I am so grateful to the Syrian scholarship team in the ministry of higher education and the AVENUES department at the University of Technology of Compiegne for making it possible for me to continue my studies in France. I give deep thanks to the professors and lecturers at the doctoral school, the librarians, and other workers. My special and heartily thanks to the supervisors of my thesis, Professor Fabrice LOCMENT and Professor Manuela SECHILARIU who encouraged me and directed all research works in this thesis. Their cooperation and discipline in work are highly appreciated. It is with their supervision that this work came into completion. I am also thankful to the team of AVENUES department. Their names cannot be disclosed, but I want to acknowledge and appreciate their amity and transparency during my research.

I am also so thankful to my fellow doctoral students namely Hongliang LIU, Hongwei WU, Changjie YIN, Leonardo TRIGUEIRO and all others not mentioned here whose challenges and productive thinking have provided new ideas to the work. I would like to thank especially my latter fellow doctoral students Issam Houssamo and BaoChao WANG who defended their thesis earlier than me and helped me a lot in the beginning years of my research works.

Last and not the least, from the depth of my heart I thank my family who encouraged me and prayed for me throughout the time of my research, especially my parents who encourage me in the path of science, my brothers who supported me emotionally and my wife who were by my side in the hard moments during the last two years. This thesis is heartily dedicated to my true friend the saint Abo Dawood Yousef Sobeh who took the lead to heaven before the completion of this work, and also to my first spiritual lecturer Nawwaf Alshibli; their spiritual and mental supports are beyond evaluation.

May the Almighty God abundantly bless all of you.

Table of contents

List of figures

List of tables

Abbreviations

AC	Alternative current
DC	Direct current
dSPACE	Digital signal processing and control engineering
EKF	Extended Kalman filter
EMF	Elector motive force
EEMF	Extended elector motive force
FPGA	Field-programmable gate array
HF	High frequency
HPF	High pass filter
HG-EKF	High gain extended Kalman filter
INFORM	Indirect flux detection by on-line reactance measurement
IPM	Interior permanent magnet
IP	Integral-proportional
LPF	Low pass filter
LTI	Linear time-invariant
MPP	Maximum power point
MPPT	Maximum power point tracking
MRAS	Model reference adaptive system
PEL	Programmable electronic load
PI	Proportional-integral
PLL	Phased-locked loop
PM	Permanent magnets
PMSM	Permanent magnets synchronous machine
P&O	Perturbation & observation
PV	Photovoltaic
SMO	Sliding mode observer

Nomenclature

φ_A, φ_B, φ_C	Stator flux in *A*-*B*-*C* reference (Wb)
v_A, v_B, v_C	Phase voltages in *A*-*B*-*C* reference (V)
i_A, i_B, i_C	Phase currents in *A*-*B*-*C* reference (A)
e_A, e_B, e_C	Electro motive forces (V)
v_α, v_β	Phase voltages in α-β reference (V)
i_α, i_β	Phase currents in α-β reference (A)
v_d, v_q	Stator voltages in d-q reference (V)
i_d, i_q	Stator currents in d-q reference (A)
φ_d, φ_q	Stator flux in d-q reference (Wb)
R_S	Phase resistance (Ω)
$[R]$	Matrix of resistance
L_s	Cyclic inductance of a stator winding (H)
L_0	Self inductance of a stator phase (H)
M_s	Mutual inductances between two stator phases (H)
$[L]$	Matrix of inductance
Ω	Rotational speed (rad/s)
ω	Electrical speed of the rotor (rad/s)
J	Moment of inertia (kg.m2)
T_{em}	Electromagnetic torque (N.m)

T_r	Resistant torque (N.m)
F	Viscose friction coefficient (N.m/rad)
p	Pole pairs number
θ	Angle between the rotational axis and the axis of stator (expresses the position of the rotor) (rad)
ψ	Induced flux by the permanent magnets (Wb)
K	flux magnets constant
L_d, L_q	Cyclic stator inductance respectively in direct axis ‘d’ and transverse axis ‘q’ (H)
u_{PEL}	Voltage at load terminals
i_{PEL}	Load current
u_{BUS}	DC bus voltage
i_{BUS}	DC bus current
L_{BUS}	Inductance of DC bus
C_{BUS}	Capacitor of DC bus
C_{PEL}	Capacitor at load terminals
p_{AERO}	Aerodynamic power (W)
p_{EM}	Electromagnetic power (W)
p_{BUS}	DC bus electric power (W)
ρ	Density (kg/m^3)
R	Radius of wind turbine blades (m)
c_P	Power coefficient of wind turbine

v	Wind speed (m/s)
λ	Tip-speed ratio of wind turbine
K_{SMO}	SMO gain
V	Lyapunov function
H	Sigmoid function
x	State vector
u	Control vector
y	Output vector
A	Matrix of transition
B	Matrix of control
C	Matrix of measurement
P	Covariance matrix
v	State noise
w	Measurement noise
Q	Covariance state noise
R	Covariance measurement noise
T_0	Observation horizons of auto tuning EKF

General introduction

1. Introduction

The global energy transition policy gives the main actions for the passage of the current electricity production, based mostly on fossil and fissile fuels that are finite and non-renewable resources at human scale, to an energy mix which includes a lot of renewable resources. Thus, knowing that the energy transition is a key concern in the various strata of society in many countries, in near future, almost all human activities, *i.e.* transport, industry, lighting, heating …, will be powered with renewable energy sources. The goal is to avoid an ecological crisis by means of reduction of environmental footprint, greenhouse gas emissions, and consumption of fossil/fissile fuels.

The World Energy Council, an international organization supporting renewable energy development across the planet, highlights that to provide sustainable energy policies it is important to take into account the three following dimensions:

- energy security: the effective management of primary energy supply from domestic and external sources, the reliability of energy infrastructure, and the ability of energy providers to meet current and future demand;
- energy equity: accessibility and affordability of energy supply across the population;
- environmental sustainability: the achievement of supply and demand side energy efficiencies and the development of energy supply from renewable and other low-carbon sources.

This is why the energy transition involves also a behavioral and socio-technical transition, avoiding overproduction and unnecessary consumption and leading to save more energy and benefit from better energy efficiency.

The utility power grid that operates today is confronting the demands to improve reliability, reduce costs, increase efficiency, comply with policies and regulations concerning the environment, integrate renewable energy sources and electric vehicles to power grid. Following the energy transition policy, the electricity production seeks to produce more and more energy from renewable sources, *i.e.* wind, solar, biomass, and geothermal sources, but integrating power from renewable resources into the utility power grid can be a huge challenge. The intermittent and random production of renewable sources is always a problem for their large-scale integration into the power grid. Often, the renewable energy sources are deployed as decentralized, or distributed, sources around the territory. Therefore, the decentralized electricity generation grows significantly and grid-connected system is proposed in most applications. However, the intermittent and unpredictable nature of renewable energy sources, such as wind turbine and photovoltaic, remains an issue for their integration into the utility grid resulting in: fluctuations of voltage and/or frequency, harmonic pollution, difficult load management, etc.

Regarding the environmental sustainability, one of the most energy intensive sectors is represented by urban area (buildings, transport, lighting, etc.), representing in the near future almost a half of total energy consumption and a quart of greenhouse gas emissions released into the atmosphere. Facing environmental challenges and knowing that urban areas have great potential for intensive development of these renewable energy sources, the urban areas are now positioned as a key player to achieve the energy transition. Therefore, the main goal is to reduce the environmental impact of existing and future urban areas and to find solutions to reduce energy consumption and increase the share of renewable energies. Actually the trend is to give more and more "local power" to urban areas to control the energy distribution as well as the production. Everything should be set up, throughout the territory of the city, to give the opportunity and the desire to produce its own energy. Thus, many calls for projects proposals are launched for the creation of positive energy buildings and territories, which undertake a path to achieve the balance between consumption and production of energy at the local level, aiming the renewable energy sources deployment.

2. *Decentralized electricity production*

Nowadays the energy distributed generation shows a very rapid growth and reveals an increasing complexity for grid managers. Indeed, there are many producer sites, but also some prosumer sites, which means producer and consumer sites based on distributed generation, as illustrated in Figure 1.

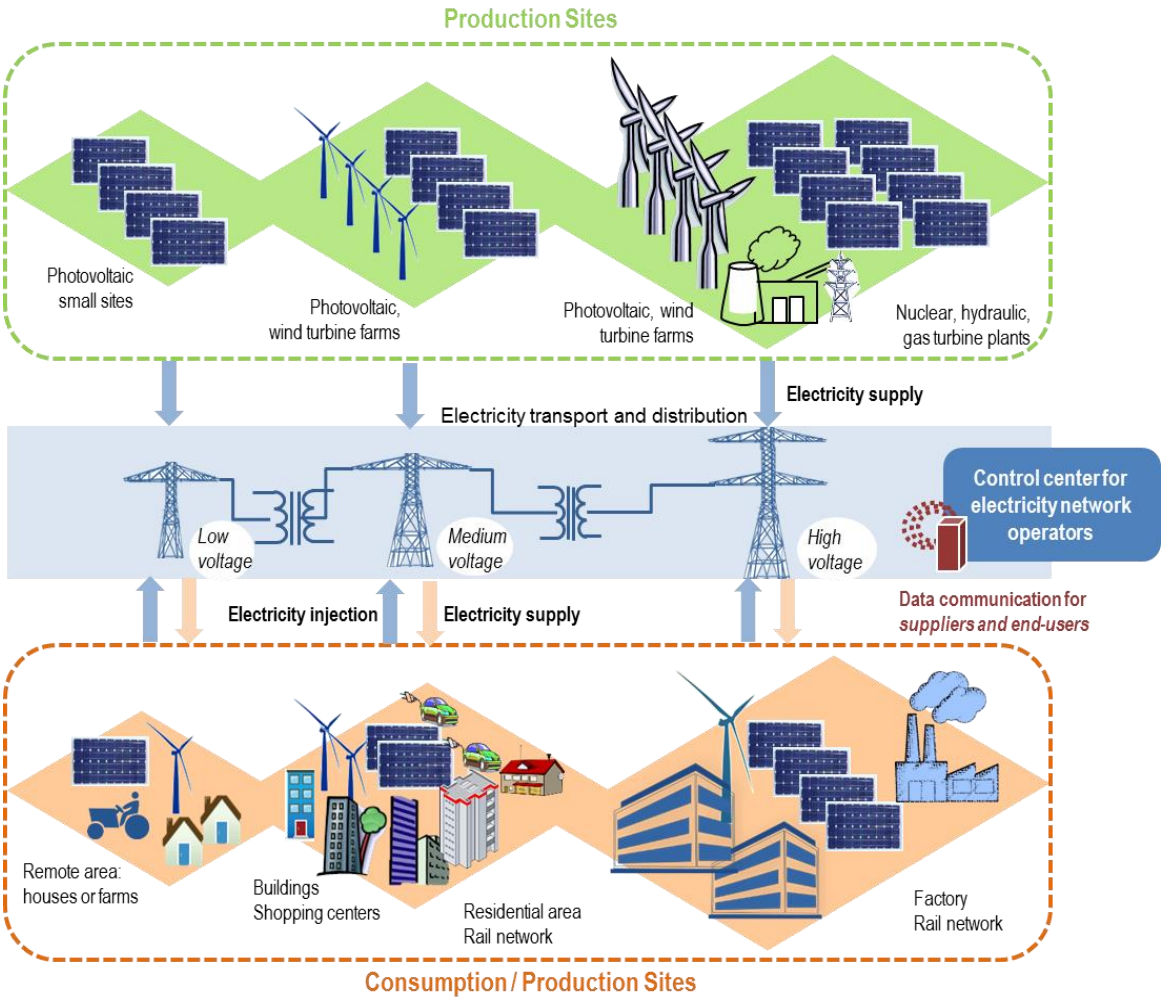

Figure 1. Distributed electricity generation around a territory [1]

This distributed generation requires grid management and their use must be optimized. Renewable energy production is mostly a distributed generation, and it is also intermittent and arbitrary; this is why, facing to the public grid, the renewable energy generation leads to new methods for balancing of production and consumption, especially for large scale implementation.

As shown in Figure 1, the production sites are connected to utility grid by unidirectional power flow while the prosumer sites are connected to utility grid by bidirectional power flow.

Therefore, the question is what is the best power grid technical regulation to integrate renewable energy sources to accommodate the utility grid in real time? Centralized regulation? Local regulation? Or both?

To make full use of distributed generation, requirements from both utility grid and end-user must be taken into account, and communication is required. Thus, the concept of smart grid appears, which can be seen as power grid equipped with communication and information technology. To increase renewable energy sources integration level and obtain a robust power grid, the smart grid could solve problems of peak consumption, optimal energy and demand response.

The smart grid is being designed primarily to exchange information on grid needs and availability, and to help balancing powers avoiding undesirable injection and performing peak shaving. Hence, the smart grid is defined as the power grid that employs an innovative monitoring, controls the transmission of information, and uses self-healing technologies to provide better services to electricity producers and distributors, flexible choice for end-users, good reliability and security of supply. This very complex smart grid, with bidirectional power flow and communication, requires a lot of work to implement it in reality.

In order to reduce losses and peak energy demand, and also to assume ancillary services (power grid technical regulations) through the data communication, the smart grid leads to microgrids concept, especially for prosumer sites. A microgrid is defined as a set of renewable and traditional sources, storage and utility grid connection, and controllable loads (urban infrastructures, buildings, electric vehicles, etc.). A controller is used to interact with the smart grid; it provides voltage control, power balancing, load sharing or load shedding, and takes into account the constraints of the public grid provided by smart grid communication. Therefore, with microgrids it is easier to manage and optimize the local energy with respect to the utility grid requirements. In addition, microgrids can better respond to both grid and user, and increase supply reliability.

Concerning the smart grid and microgrids, research areas include not only issues in power grid, but also data communication, dynamic pricing, as well as demand side management. Regarding microgrids, whether configured in AC, DC or hybrid, research studies relate to grid topology, power balancing control, energy management, and devices for protection.

Currently many countries are dealing with the formidable problem of financing of the smart grid and microgrids, from research project to implementation of experimental facilities that can become a demonstration and pilot site.

Specifically for microgrid projects, there are three leading countries: U.S.A., Japan, and South Korea. At European level, the more advanced countries are Denmark, Germany, Greece, and Spain. In France, several projects were started in last three years, both as research work and demonstrative site (*e.g.* Nicegrid, IssyGrid, PowerGrid Campus, etc.).

The main research issues on microgrid include following aspects: power converter (components, topology, and power quality), power balancing (droop control), and energy management. Concerning energy management, two kinds of approaches exist: the rule based approach, which is simple and robust but it does not guarantee the optimal performance in given conditions, and the optimization based approach that gives an optimal solution.

Nevertheless, the optimization approach is hard to implement in real-time operation, because optimization usually requires prediction. Prediction is often different from real conditions, and therefore, the prediction uncertainties can degrade operation or even result in failure. Regarding protection, the microgrid involves bi-directional power flow and flexible structure. It requires new protection device or algorithm that can handle the complex environment.

However, there is a research gap in the microgrid studies. Furthermore, these aspects are often studied separately; combining them together, especially implementing optimization in real-time power balancing has been reported in few publications. Because, optimization is usually treated as separate problem from the power balancing, and optimization is mostly studied by simulation, implementing optimization in real-time operation is difficult since lack of resistance to uncertainty. In addition, smart grid interaction is not always taken into consideration for microgrid control.

Thus, around the world, researchers and engineers are deploying increasingly efforts to design and implement intelligent microgrids to achieve the energy goals of the 21st century such as improved reliability based on diversification of sources of electricity production. Nevertheless, ensuring reliable distribution of electricity based on microgrid and realizing its integration into centralized larger production of the power grid are not easy to achieve.

3. *Microgrids research project of AVENUES EA 7284*

Our laboratory, AVENUES, works since more than eight years on the subject of *Urban microgrids for advanced local energy management with smart grid communication*. Our research project focuses to design a microgrid control strategy that optimizes the energy locally with respect to end-user demand, based on local information, and can participate in global smart grid interaction through communication.

The smart grid topology representation, given in Figure 2, displays our vision of the smart grid concept and the role of microgrids.

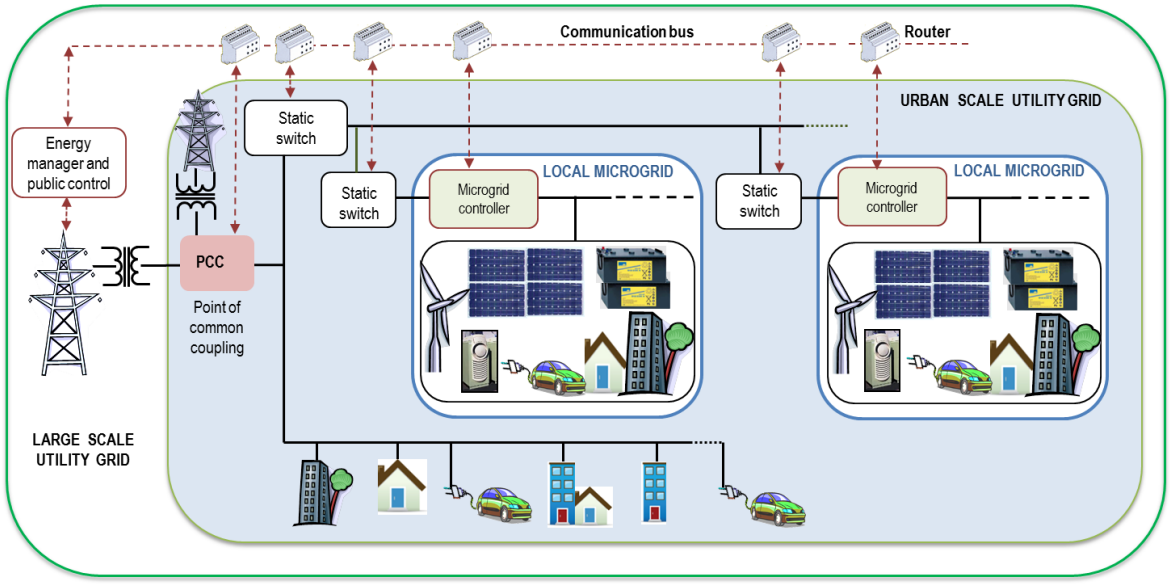

Figure 2. Smart grid topology [2]

At the local level, the microgrid can be integrated to the one of the urban prosumer infrastructure and connected to the main grid by an adapted controller. At urban scale there are several microgrids and parts of traditional utility grid, all are connected to the grid through the point of common coupling. It is assumed that intelligent switches allow connection and islanding of microgrids. A communication network is added, *e.g.* communication bus, whose routers are dedicated to direct messages following energy management priorities or special needs. In addition, all control interfaces generate and receive messages.

The urban microgrid developed by our laboratory is connected to the smart grid by mean of a controller that must provide the interface between the utility grid and the loads, *e.g.* urban infrastructures, buildings, electric vehicles, aiming an optimal power management. Figure 3 illustrates the power management interface principle based on the main data, which have to be exchanged between the microgrid and the public grid.

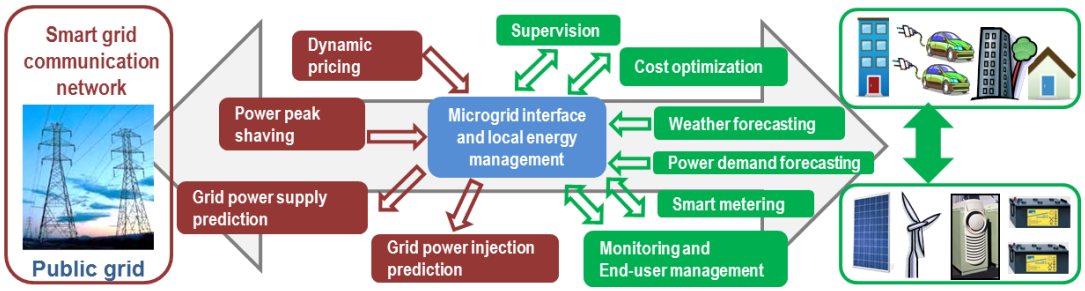

Figure 3. Power management interface principle [3]

Thus, the microgrid controller must take into account information about the public grid availability and dynamic pricing, inform the smart grid on injection intentions and power demand, meet the demand of the end-user with respect to all physical and technical constraints, and operate with the best energy cost for the public grid and for the end-user. To meet these objectives as well as other actions described in Figure 3 (forecasting, smart metering, monitoring…) a specific interface associated with the urban microgrid [4] was designed as proposed in Figure 4.

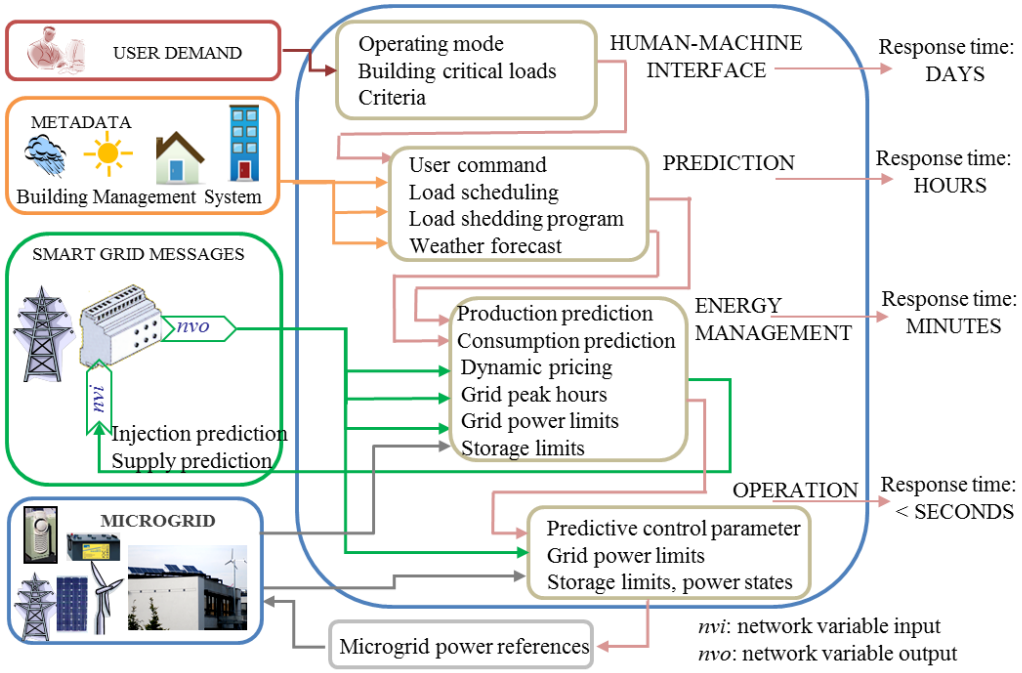

Figure 4. Microgrid controller

The developed microgrid controller presented in Figure 4 is a multilayer and multiscale design able to provide flexibility with respect to the necessary algorithms [5].

There are four functional layers whose response times range from days to less than a second. Human-machine interface allows taking into account the end-user options as predefined operating mode, or building critical loads, or load shedding limit, or other specific criteria. Prediction layer takes into account the end-user option, several forecast data (building operating mode, grid time-of-use, and weather), and aims to calculate two powers related to: renewable energy production prediction and

energy demand prediction. These two powers are given as inputs for the energy management layer which is the most important intelligent layer.

The energy costs optimization is calculated in this layer and is mainly based on the previously calculated predictions and the system constraints such as dynamic pricing, peak consumption, public grid vulnerabilities, and storage capacity. The optimization is solved by mixed integer linear programming and the solver could be CPLEX [6]. The obtained results are the optimal power evolution of each source for which the total cost is the minimum for the considered time duration. These powers cannot easily be implemented in real-time control. The solution is to translate the power flows into a single interface parameter for power balancing control, which is the predictive control parameter, one of the outputs of this layer. The second output concerns the predictions to be transmitted to smart grid (injection and supply). The predictive control parameter is applied in the operational layer, which algorithm controls the power balancing in the microgrid system. This last algorithm provides real-time references of the system powers and the coefficient of possible load shedding.

The main scientific issues are the difficulties of global optimization, due to the risk of mismatch between production/consumption predictions and the real time operating conditions, on the one hand, and the need to take into account the constraints imposed by the public grid, on the other hand.

For urban microgrids several operating strategies are developed based on sources that make up the microgrid (photovoltaic sources and wind turbine, storage, public grid connection, micro-turbine or bio-diesel generator) and loads. For buildings and electric vehicles charging stations, Figure 5 presents the main possible strategies.

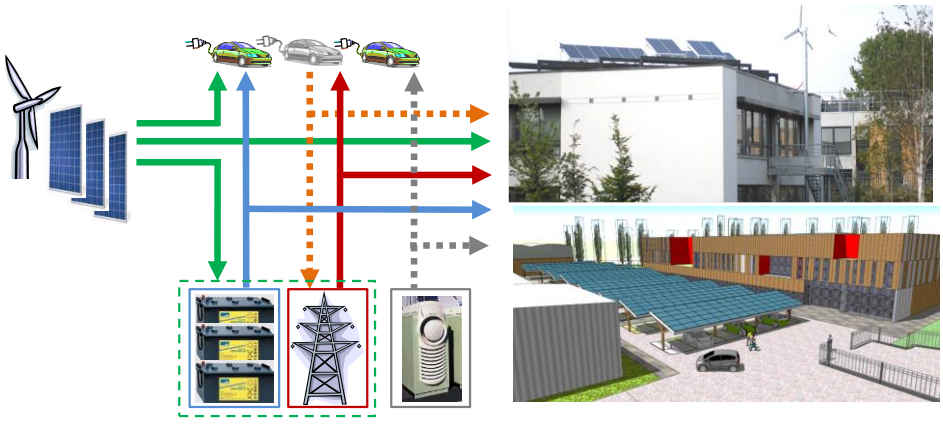

Figure 5. Energy management strategies for urban microgrid [3]

Renewable energies supply the building and charge the electric vehicles. The renewable excess energy could be stored and/or injected into the grid. The utility grid, if available, is used only as back-up for the building and the electric vehicles. The micro-turbine operates only if the grid is not available. The electric vehicles, if required for stringent situations, can supply the building and/or provide energy to

the grid. The messages received from the smart grid command the microgrid operating mode aiming compliance the actual availability of the grid.

4. *Small scale wind turbine integration in urban DC microgrid*

As defined earlier, microgrid aggregates distributed generation, loads, and storage together. These elements are coupled on the same bus, either in DC bus or AC bus [7], through converters and protection devices. It can work in both grid-connected mode and off-grid mode. As general information, the overview of the microgrid already designed and developed in our laboratory can be seen in Figure 6.

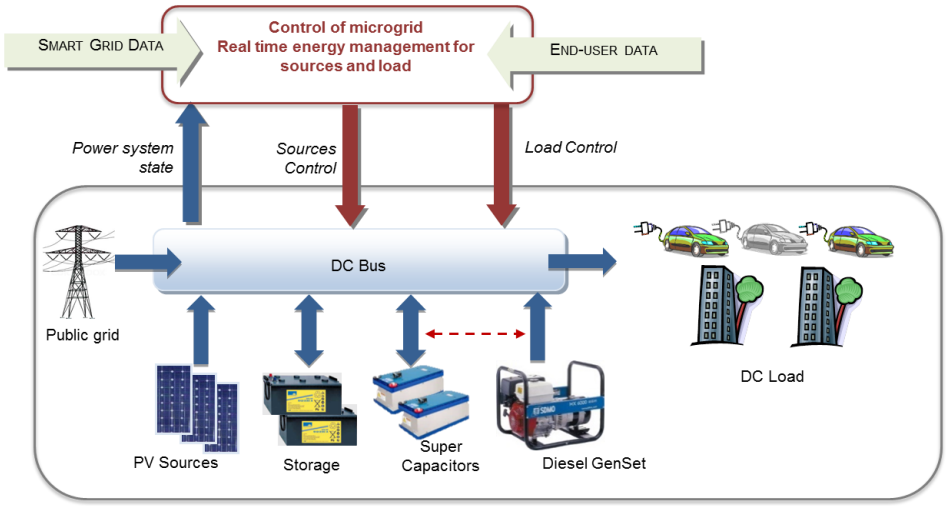

Figure 6. DC microgrid overview

The microgrid is proposed with DC bus link for an efficiently integration of other renewable sources and storage, for absence of phase synchronization, and because only the voltage must be stabilized. In addition, considering the DC bus and a DC load directly connected, the overall performance is improved by removing multiple energy conversions [8]. Indeed, a DC network building distribution may use the existing cables with the same power transfer as in AC distribution [9]. The DC bus can supply directly many building appliances (lighting, ventilation, electronic office equipment …) as well as an electric vehicle.

This DC microgrid consists of a power system and its real time control. The power system includes photovoltaic (PV) generator, connection to the public grid, electrochemical storage, electrostatic storage (as supercapacitors), diesel generator (Diesel GenSet) for traditional power source, and DC loads that could be the building as prosumer and electric vehicles. Diesel generator can play an important role for the off-grid operating mode. The control is assured through the controller shown in Figure 4. It is allowed communication with the end-user, databases, including weather forecast, building consumption prediction, and messages exchange with the smart grid.

To increase the efficiency of renewable generation for DC loads, the Microgrids research project of our laboratory considers a small-scale wind generator to be integrated to the described DC microgrid. Facing to PV sources, the small-scale wind generator is seen as a complementary renewable energy source. However, the energy potential and dynamic characteristics of the wind generator are very different from PV generators. The DC microgrid including the small scale wind generator principle overview is given in Figure 7.

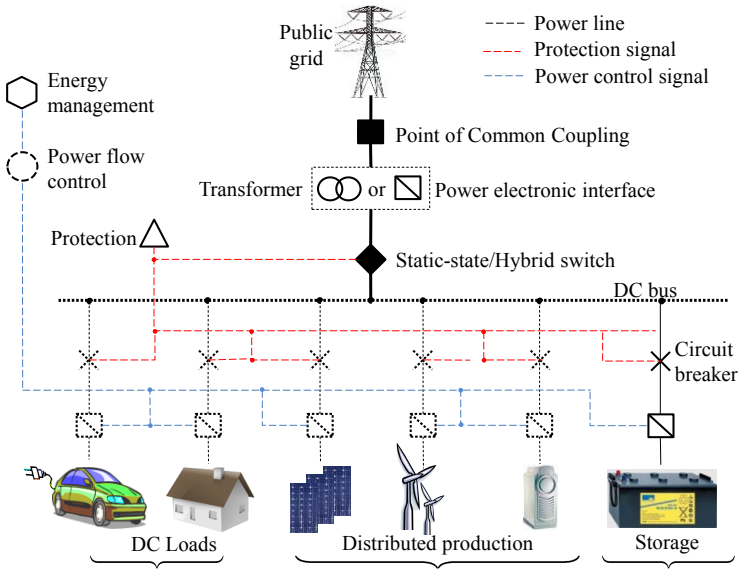

Figure 7. DC microgrid including small scale wind generator overview

Nowadays, small wind turbine, which represents wind generation source with the ability to produce not more than 100kW of electrical power, is often integrated in urban microgrids. Regarding the conceived microgrid, *i.e.* power system and its real time control, to integrate the small scale wind turbine it is necessary:

- to choose and study the electrical machine able to produce energy to the best price;
- to choose and study the topology of the structure which respect to conversion mechanical energy into electrical energy;
- to study and propose the method and algorithm to extract the maximum power and therefore the maximum energy;
- to study and propose the control strategy able to extract the maximum power as well as a required limited power;
- to study and propose the model of the aerodynamic and the electrical power in order to be able to calculate wind power predictions.

To meet these requirements, the small-scale wind turbine study is proposed starting with this thesis.

5. *Main objectives of the thesis*

For small wind turbines, in urban areas, some typically machines are used: asynchronous machine with squirrel cage, double-fed asynchronous machines, and Permanent Magnet Synchronous Machines (PMSM). Due to its easy fabrication, relatively small size and high torque, as well as to avoid the problems of excitation in the ordinary machines, the PMSM is often used and has become more and more widespread.

With respect to conversion mechanical energy into electrical energy with small-scale wind generator, there are two types of structures: the passive structure, *i.e.* non-controllable converter, and the active structure, *i.e.* controllable converter. The advantages of passive structure are its robustness and its attractive price, but on the other hand, the flow of energy cannot be optimized. The active structure allows this optimization.

To extract the maximum power and therefore the maximum energy, an algorithm of maximum power point tracking (MPPT) is required. Thus, the wind generator is driven by a MPPT seeking in real-time the maximum power point. There are two categories of MPPT methods: the first one is a direct process and the second one is an indirect process. The direct MPPT is based on the perturbation of a variable system and the observation of the system in real-time. The complexity arises when the ratio between the values of perturbation and observation time has to be selected, mainly for systems with a lot of noise. The indirect MPPT method is based on iterative search as well as the knowledge of the wind generator parameters.

The accurate knowledge of these parameters can often cause additional problems and also requires the use of mechanical sensors such as a speed sensor. Thus, an incremental encoder or resolver can be used for rotor position measurement. Therefore, this information can be naturally provided by tracking the rotor position at every moment. However, these position sensors have their limitations. For incremental encoder is necessary to determine the initializing position. To overcome this limitation, it is required to use an initializing procedural in each PMSM start-up by tracking an index, which is not desirable in wind turbine applications. Furthermore, the incremental encoder is also sensitive to noise and, unless using of complementary signals, these parasites signals may be taken as useful impulses. Regarding the resolver, it may be able to overcome the incremental encoder limitations, but its speed performances do not permit a widespread use. Also, its fabrication cost is often more expensive than the PMSM itself.

Therefore, to increase the system overall reliability and at the same time to limit the economic cost, for small-scale wind generator the mechanical sensor is eliminated. As a result, in our case, a speed estimator is needed.

Concerning the estimation of PMSM rotational speed, there have been a number of studies that proposed various methods for this aim. While the estimation method based on observer depends to

some extent on the accuracy of the motor model, the extended Kalman filter (EKF) is the most popular model-based estimator allowing sensorless drive control in a wide speed range. The Kalman filter principle introduced by Rudolf Emil Kalman, represents an efficient means for the recursive data processing. Performance of the EKF depends on the correct prior knowledge of the process and measurement noise covariance matrices. In adaptive Kalman filter, the knowledge about the noise covariance values is adjusted according to the difference between the predicted estimates and the current measurements.

This study focuses on a small-scale wind generator based on PMSM with an active structure to maintain the optimum TSR constant. The proposed MPPT is based on the knowledge of the parameters of small scale wind generator as input with EKF-based estimation of mechanical rotation speed. Structured into three chapters, the rest of this thesis is organized as follows.

The **chapter 1**, ***Evolution of renewable energies and the place of wind power generation***, presents a thorough overview of the evolution of renewable energy while paying special attention to the place of wind power generation. A general literature review is conducted presenting previous works on various wind power generation systems as well as the conception and topology of converters.

In **chapter 2**, ***Studied wind turbine – control analyses and energy optimization***, a wind turbine conversion system is detailed by explaining its different structures and all its elements. Static converters are essential in the structure of such a system. They allow not only operating at variable speed but also extracting the maximum amount of produced power. A frequently used structure is one that uses a three-phase diode bridge rectifier associated with a controllable converter. Then, in order to design an MPPT controller not only robust and effective, but also to optimize the all over cost of the system, both methods direct and indirect are taken in consideration. To allow experimental validation in the laboratory, an emulator of the system were constructed. Experimental results are shown to demonstrate the effectiveness of the proposed controller.

Chapter 3, ***Rotational speed and rotor position estimation***, focuses on comparative study about rotational speed and rotor position estimation for synchronous machine. The exact information about rotor position and rotational speed is important for good performance of drive system and to assert control reliability. Many years ago, sensors were used to get this information. With the advancement of technology, methods of estimation started to appear more and more, in order to create a substitute to the physical sensors. This trend of replacing a physical sensor with an estimation procedure has two visible advantages: (i) minimizing the overall cost of the system by economizing the cost of this sensor; (ii) improving the system characteristics by increasing the stability, heightening the robustness, time economizing, decreasing faults probability, etc. In small scale wind turbine systems these advantages can be of great importance considering the relatively high cost of position sensor and adding to it the obstacles posing technically by using it. In case that sensorless tool must rebuild the

system state, then an observer is what can be appropriate tool. Indeed, an observer is a software tool for measurement allowing the estimation of system state from a limited amount of information. The adaptive estimator of the rotation speed is selected and validated in chapter 3, as well as experimental results are given and discussed.

Conclusions and perspectives are presented in the final part of this thesis.

Finally, concerning the PMSM used in the laboratory test, three appendixes are given to present the parameters measurement, its geometrical and mechanical parameters, and the PMSM modeling.

Chapter I. Evolution of renewable energies and the place of wind power generation

I.1. Renewable energies a societal goal

Before the industrial revolution of the 19th century, all energy was almost used from renewable sources. Indeed, 5000 BC the Egyptians used wind energy for moving or displacing objects. Around 2000 BC, it was in Persia that used for the first time wind mills. Not until the 12th century to see them coming to Europe. There are many other examples of the use of renewable energy before the industrial revolution. The current global energy situation is complicated because of the depletion of fossil resources that is difficult to calculate, but also because of the ever increasing energy needs. In fact, it has been consumed in the last 20 years as much as since 1850 and knowing that there are about two billion human beings who do not have access to electricity. To this is added obviously the struggle against the emission of greenhouse gases. Currently renewable energies are therefore used as primary sources when there is no other way, *e.g.* the connection to the existing power grid is difficult, or when their profitability is proven. Therefore, the renewable energies should be feasible from a technical, environmental, and economic point of view.

There are many definitions that characterize a renewable energy:

- Energy that can be reconstituted or is recovering faster than it is used;

- Energy natural renewal is fast enough for it to be considered an inexhaustible at the human time scale;
- An inexhaustible primary energy in the very long term, as it is directly come from natural phenomena.

Renewable energy is often classified into five families: sun, wind, water, geothermal, and biomass. They have an unlimited amount on a human scale; they do not emit greenhouse gases to produce energy and are becoming less and less expensive because they are increasingly used.

Since 2012, renewable energies have a little over 25% of global power capacity with an increase of 8.5% compared to 2011. In terms of electricity, they provide just over 21% of global demand with 16% from hydropower and 5% of other types of renewable energy. Despite the current financial crisis, global investment in the renewable energy sector has increased by 6 during the last 8 years. In addition, a highest future growth should take place in developing countries.

Table 1 summarizes the current situation of renewable electricity production and gives the goals for France in 2020.

Table 1. Current situation and renewable electricity goals for France in 2020 [10]

Category	2020 objectives	Current situation	Remarks
Wind Power	19000 MW	8807 MW end of Sept. 2014	Very uncertain goal. It would take an average additional 1,500 MW per year to achieve the goal
Hydraulic	28300 MW	25700 MW end of 2013	Very uncertain goal. It will depend on the success of the revival of the sector and the renewal of hydropower concessions
Biogas	4230 GWh	1521 GWh in 2013	The goal can be achieved. It will depend on the development of agricultural biogas
Marine energy	6800 MW (including 6,000 MW of offshore wind)	240 MW end of 2013	Very uncertain goal. The offshore wind has been delayed and the progress of projects of other technologies is slow
Photovoltaic	5400 MWp (under standard test condition)	5412 MWp end of Sept. 2014	The goal is already achieved. The sector needs a new direction in order to project itself
Waste and solid biomass	1.2 MTOE (Million Tonnes of Oil Equivalent) produced	0.39 MTOE in 2013	Very uncertain goal. It will depend on the success of projects on solid biomass and energy improvement of existing incineration plants
Geothermal	80 MW	17.2 MW end of 2012	The goal can be achieved. New projects materialize but their advance is slow
Solar thermodynamic	540 MW	1.01 MW	Very uncertain goal. The challenge of the industry is not at the level of national production but export

Hydropower is the second source of electricity in France and the first among the sources of renewable electricity. It represents about 20% of total capacity. The little hydroelectricity represents only 8% of the total production capacity of hydropower. Wind energy is in second place of renewable electricity production. The wind electricity generation have benefited from resumption growth in 2014. This recovery appears to be due to the simplification of administrative procedures started in 2013. Small scale wind generation still show low capacity compared to large scale wind generation. Currently, there is no mapping of the productive capacity of small scale wind turbines. As a final point, even if the photovoltaic sector has already reached its goal, this conceals a lack of ambition in larger scale development. Since 2013, the world market seems to have believed the economic and energetic benefits of this sector. However, facing the current crisis, France resists to this progress. Photovoltaic is found in several forms: small installations for individuals, medium and large installations associated with commercial buildings and high power photovoltaic plants. Since 2013, in France, the consumption has emerged as a possible revival of the sector.

Table 1 also demonstrates that all objectives, except photovoltaic, will have difficulty in being achieved until 2020 in France.

I.2. Wind power generation and wind turbines

As concluded above, increasing depletion of conventional fuels and the induced environmental pollution lead over past decade to implementation growth of renewable energy sources. Therefore, wind energy has gained tremendous attention. As mentioned earlier among all renewable energy, devoid of wood energy, it is the wind energy which was first exploited by man. Since ancient times, it was used for the propulsion of ships and then the flour mills and structures for pumping water. The first known use of wind energy dates back to approximately 2000 years BC. Hammurabi, founder of the Babylon power, had designed an entire irrigation project of Mesopotamia using wind power. The first written description of the use of windmills in India dates from about 400 BC. In Europe the first windmills were introduced in the early middle ages. First used to grind grain, hence the name "mills", they were also used in the Netherlands to dry lakes or flooded land. From the 14th century, windmills are everywhere in Europe and become the main source of energy. Upon arrival of the steam engine, the windmills begin their gradual disappearance. The electricity appearance gives the idea to Poul La Cour in 1891 to associate a wind turbine generator. Thus, the energy from the wind could be "rediscovered" and used again. At the beginning of last century, wind turbines have a massive emergence (6 million manufactured parts) in the U.S.A. where they were the only way to get electricity in the isolated countryside. In the 1960s, it was about 1 million wind turbines working worldwide. The 1973 oil crisis has revived again the search of turbines achievements in the world [11].

Currently, wind turbines are mostly used in two major areas: production for remote sites and production for the power grid injection. For remote sites, the power of a wind turbine is normally from a few tens of watts to tens of kilowatts. For power grid injection, the power of a wind turbine is normally from a few hundred kilowatts to a few megawatts. In the case of power grid injection, the wind turbines can be on land but also at sea, which is called offshore. Since 2001, the worldwide capacity of wind turbines exponentially increases as shown in Figure 8. In five years, it has almost tripled. The leading countries in the world were Denmark, Germany and Spain. More recently, China became the country with the largest installed wind capacity, overtaking the U.S.A. and Germany (in relation to the number of inhabitants). Figure 8 also shows that in 2013 there has been, for the first time since 1997, a reduction in installed capacity.

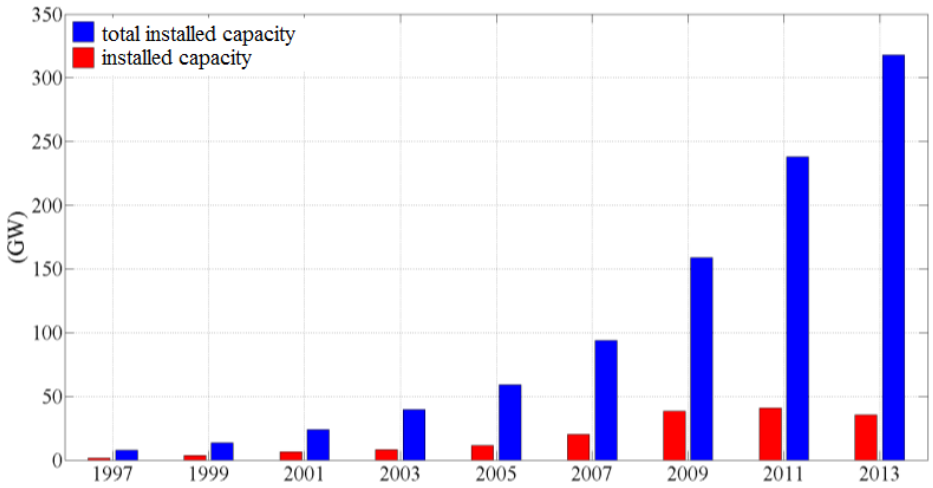

Figure 8. Evolution of the production capacity of wind turbines [12]

By means of a wind turbine associated with the power conversion system, a wind generator converts the wind energy into different forms of electrical energy. To elaborate in more details about wind turbine, the section I.2.1 is presented.

I.2.1. Wind turbine operating types

Wind turbines can revolve about either a horizontal axis or a vertical one, the former is older and more widespread as well. Vertical axis designs produce a smaller amount of power and are not as much widespread [17]. Figure 9 shows why today most of wind turbines are equipped with three blades. Indeed, it is with blades number that power coefficient c_P , which plays a key role in wind power formula, reaches its maximum value.

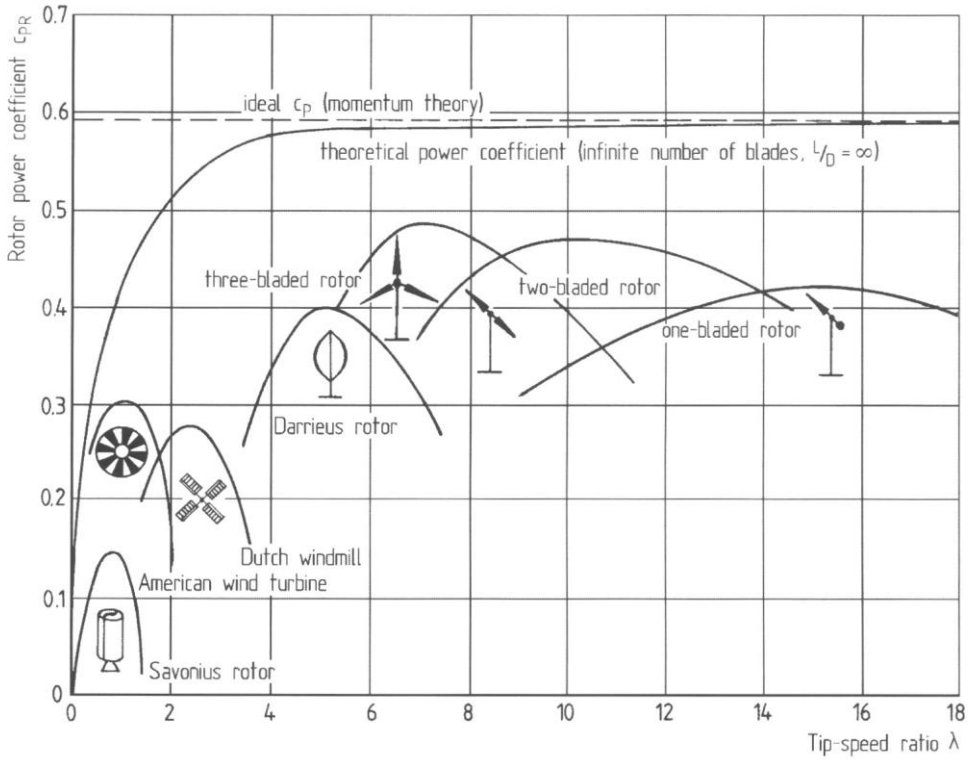

Figure 9. Evolution of the power coefficient c_P as a function of λ and type of wind turbine [13]

Figure 9 also shows that if it is desired to have a maximum power coefficient c_P, then λ must be maintained at a constant value. As wind speed and blade radius after manufacturing both are out of control and it is not possible to change them, so that, the rotational speed Ω must be adapted in real time. This adaptation is called variable speed control and it allows working constantly at the maximum power point (MPP). High power wind turbines, mainly for power grid injection, operate under maximum power point tracking (MPPT) methods like as the nacelle orientation to "capture" the maximum wind power, the pitch system based on wedging action with variable step that inclines the blades, or the stall system leading to aerodynamic standstill. These first MPPT methods are active, while the stall system is a passive one. This system consists on the design of the blades shape and this is achieved by numerical modeling and then by validation by wind tunnel based on a prototype in reduced scale.

I.2.2. Various types of wind turbines

Wind turbines are classified into two types depending on the axis of blades, while depending on the capacity of power production wind turbines can be mainly divided into two categories as well as small scale wind turbines (which are studied in this thesis) and large scale wind turbines. At first glance, the use of large scale wind turbines in urban areas may seem surprising. Nevertheless, as the size and the electric power of urban microgrids are not defined, it is possible for a city to have its periphery near a large scale wind turbine.

I.2.2.1. Large scale wind turbine

Wind turbines from a few kW to 7.5MW are considered large turbines; those which are installed today in France have a power of 1 to 3 MW. In general, they are set together in wind farms 6-210MW. The Danish company Vestas tested in January 2014 its new V164 turbine of 8MW (Figure 10), the mast height of 140 meters and rotor diameter of 164 meters and reached a total height of 220 meters [15]. By using three phase turbine, [18] presented the control strategy of a wind turbine based on a PMSM. It proposed the modeling of the wind turbine system and the control strategy using Matlab/Simulink software in order to analyze the performances of the control strategy.

Figure 10. Vestas turbine V164 of 8MW [14]

In recent years, multiphase large scale wind turbines have been increasingly used. In the literature, an electric machine having at least three distinct stages (3 independent currents) is a multiphase machine. Multiphase machines most frequently encountered are the three-phase machine coupled in star with accessible neutral, the five-phase machine, the six-phase machine called "double star", and the seven-phase machine. Multiphase machines have the following key benefits [19], :

- *Minimization of electromagnetic torque pulsations.* The interactions between the current harmonics and electromotive force can create torque pulsations. For an electrical machine, when the number of phases increases the torque pulsations decrease in amplitude (with higher frequency).
- *Increased functional reliability* (the multiphase machine therefore have a reduced structural reliability). It is quite easy to understand that compared to three-phase, the higher in phase

number is the less harmful will be the loss impact of one (or more) phase(s). For example, the "double star" machine can operate with a single star.

- *Less power per phase* (or current per phase). For a given power, it also seems clear that the more increased phases the less power per phase is. This allows less parallel connection and/or series of components, it is also possible to use simple structures inverters.

The research work in [20], for example, dealt with the generation of optimal current references for multiphase permanent-magnet (PM) synchronous machines. It carried out the study in normal or fault mode and provided experimental results of a five-phase surface-mounted PMSM in order to demonstrate the proposed strategy. Despite these non-negligible advantages, the multiphase machines can raise the following key issues:

- How to connect them to the existing three-phase network?
- Do they have a control model as "simple" as the three-phase machines?
- How to manage and minimize the torque pulsations in degraded mode?

Thus, in the coming years, multiphase machines strategy is a promising approach for the wind turbine system; especially to be integrated in the microgrid system which can operate in grid-connected or off-grid modes [21], [22].

I.2.2.2. Small-scale wind turbine

Small-scale wind generator is the name given to wind generation systems with the capacity to produce less than or equal to 30kW (in Europe) or 100kW (in USA) of electrical power. These wind generators are usually equipped with turbine whose blades are approximately 2m to 7.6m in diameter, and they operate mostly in grid-connected mode, but stand-alone or isolated mode may be also chosen.

In the following section, different types of machines used for wind turbines will be discussed especially for small-scale ones.

I.2.2.2.1 Different types of machines

Various types of electrical machines can be used in small scale wind generator. Permanent magnet synchronous machine (PMSM) is most commonly used; although induction machine may also be used [25]. PMSM is popular for efficiency, reliability, energy density, small size and light weight. For PMSM, in recent years, new topologies such as axial flux appear. These are excellent electrical machines but have large manufacturing constraints [26]. In this thesis, the used machine is a classical radial flux PMSM.

I.2.2.2.1.1 Asynchronous machines

Asynchronous electrical machines are simpler to manufacture and less costly. They fall into two main categories; the first is with a squirreled cage and the other is a double-fed machines.

Asynchronous machines with squirreled cage have the advantage of being standardized and manufactured in large quantities and in a very large scale of power. They are also less demanding in terms of maintenance and have a failure rate very low. In wind turbines with sizable dimensions (high power and large blade radius), the rotation speed is low. However, it is not possible to design an asynchronous generator with a correct slow return. It is therefore necessary to insert between the turbine and the induction machine a mechanical speed multiplier. It is sometimes used as a solution to change the stator winding configuration (poles number) and therefore the use of machinery type Dahlander, [27]; but again the yield is less than optimal over the entire wind range. Another possibility is to use a frequency, but this is generally expensive (variable frequency and speed multiplier) and therefore it is rarely used. The majority of applications in wind power are in constant rotation speed and direct connection to the grid. These machines can be easily used in large wind turbines because of the blades rotational speed and possibility of direct-drive. However, further than lower energy efficiency compared to systems with variable frequency, the rigidity of wind turbine causes sudden changes in power, and the grid problems in case of wind drop are their main disadvantages [13].

Double-fed asynchronous machine is currently one of two competing solutions in variable speed wind applications. In this case, the stator of generator is directly coupled to the grid most often by a transformer. In place of the squirrel-cage rotor, these machines have a wound rotor induction whose electronic control ensures the change in slip. The wind turbine thus allows the rotor set of variable speed operation over a range of speed depending on the type and sizing of the wind turbine rotor [13]. These machines are a bit more complex than induction motors cage with which they share a need for speed multiplier. Their strength is slightly diminished by the presence of system rings and brushes, but the benefits of variable speed operation are an advantage sufficient to numerous manufacturers (Vestas, Gamesa, etc.) to use this type of machine. The nominal rotation speeds of these machines are usually slightly lower compared to machines with squirrel cage then the ratio multiplier speeds may be smaller [27]. An alternative and very interesting solution to obtain a variation in the rotation speed of about 30% around the synchronous speed is to couple the generator rotor to double-fed rotor through two 3-phases converters, one as rectifier mode and the other as an inverter. In general, the design of the wind turbine rotor is limited to 25% of the rated power of the electrical machine stator, which is sufficient for a change about 30% of the speed range. That is its main advantage, while its main drawback is related to interactions with the grid, especially over current caused by voltage dips of grid [13].

As these types of machines are used only for large-scale wind applications, in the next part, synchronous machines will be presented.

I.2.2.2.1.2 Synchronous machines

For several decades the industry has used the DC motor with the main advantage of being easily controllable through the natural decoupling of flux and torque. On the other hand, the presence of the collector brush system has always been a big engine problem which limits the power rating and maximum speed. Also, this presents difficulties in maintaining of continuous operating by predicted interruptions, which limit increasingly its use. It is for these reasons and thanks to advances in power electronics that the industry has moved towards the use of AC machines to take advantage from benefits such as the flexibility of speed changing rate and operation stability. Among the AC machines used in the drives, the PMSM has a number of advantages, namely no losses to the rotor, low inertia, and its high mass torque compared to asynchronous machine and classic synchronous machine. Moreover, PMSM has relatively small inductance, which results in rapid current response and thus of the torque. From technical viewpoint, this machine is more compact and generates less energy losses than separately excited machine. It generally has a low inertial time constant and high massif torque, it is robust and reliable. The two major drawbacks are: the lack of adjustment in the amplitude of the magnetic moment and its high cost [19].

- With external excitation:

  Synchronous machines with external excitation are known to offer very high torque with suitable geometrical dimensions. They can therefore be used in direct drive wind turbines. Systems of this type also have their defects. The wound rotor of synchronous machines requires regular maintenance of the rings and brushes system. The excitation circuit of the inductor requires the presence of a supply network and of reactive power. Isolated sites are adapted to these generators in the presence of capacitors battery or an independent voltage source. By cons, the adjustability of the inducer of these machines provides another means for adjusting the operating point of energy. Power electronics is required for all applications using this type of machine that are of variable speed. However, contrary to asynchronous machines the conversion wind turbine placed on the stator should be sized for the entire power generation system [13].

- With permanent magnets:

  The development of magnetic materials has allowed the construction of permanent magnet synchronous machines by costs which are becoming competitive. The machines of this type are with large number of poles and allow the development of considerable mechanical torques. There are several concepts of synchronous permanent magnet applications dedicated to wind

turbines; they are construction machinery standard (radial magnetization), discoid generators (axial field), and external rotor. The coupling of these machines with power electronics is becoming more economically viable, making it a serious competitor for all types of asynchronous generators. Systems of this type have a failure rate considered miniature by eliminating some sources of defects: deletion of speed multiplier and the rings and brushes system for magnet generators. Maintenance costs are minimized while this is very interesting in wind energy applications, especially in inaccessible sites (*e.g.* offshore). The obligatory presence of power electronics allows finally a simple regulation of the rotation speed and thus an effective energy optimizing [27].

By choosing PMSM for its noticeable advantages, there are various types of control allow connection between the generator and electrical grid. The next part will be dedicated to present these types of connections.

I.2.2.2.2 Converter types and their structures

For small-scale wind generator, there are two types of structures for converting mechanical energy into electrical energy. Passive structure uses a no controllable three-phase AC-DC converter, *e.g.* three-phase diode bridge [25], as in Figure 11 (a).

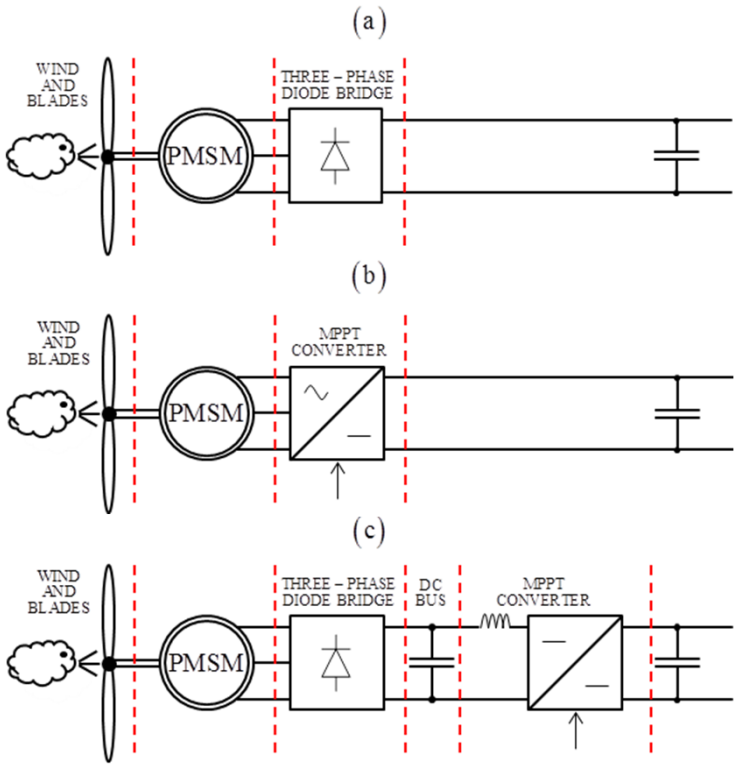

Figure 11. Different small scale wind generator structures [30]

Sometimes it is possible to find an active structure based on controllable three-phase AC-DC converter [25] as in Figure 11 (b). By adding a controllable DC-DC converter to passive structure, it is easy to get an active structure as in Figure 11 (c).

I.2.2.2.2.1 Three-phase diode bridge

This part briefly describes the static converters commonly used in power conversion wind systems. All these topologies are designed for the use in medium and high power scale, while our case study is that of small scale. Converters based on fully controlled components are expensive therefore disadvantageous in a set of small scale. In the effort to reduce costs, the diode bridge, which is inexpensive, seems attractive, provided that the energy performance is not too degraded. Since PMSM produces a voltage at variable frequency and amplitude, additional power electronic devices are required to meet the needs required by the load. When this method is used to provide the output voltage then it will be untreated before it is introduced to the load or the grid. In this study, a three-phase diode bridge is considered to rectify the voltage generated by the PMSM.

In the circuit constituted by a diode bridge, the diodes are assumed ideal (ideal switches) and the output current of the rectifier circuit is continuous (highly inductive load). Each diode thus functions during a third period while the rectified voltage consists of six sinusoidal portions per one period of time. A topology of passive diode rectifier can be used as shown in Figure 11 (a).

Adding a chopper behind the diode bridge is used to control the DC voltage and therefore the output power of the generator as it will be explained later. This structure is used for wind energy of small scale. However, this type of association does not control the machine's power factor and the current is greater than about 20% in the classic topology with fully controlled converter for same power. Similarly without adding the chopper, the voltage of the generator varies, so the DC voltage is also varies and it is necessary that the DC voltage is greater than the AC voltage of the network side, which increases loss. In both cases the topology is less interesting than the combination of two entirely controlled as explained in the following paragraph.

I.2.2.2.2.2 Voltage three-phase inverter

For PMSM in small-scale wind turbines, the general structure to extract power is given in Figure 12. Wind energy is captured by wind turbine blades; it is then converted into electrical energy by PMSM. This energy is sent to the DC bus through an inverter (MPPT inverter). This inverter may either require the torque or rotation speed. Then, DC bus energy is sent to the grid via the grid inverter. As this thesis focuses on small-scale wind turbine integrated into microgrid, the grid connection (grid plus its inverter) is replaced by a programmable electronic load (PEL) and wind and blades are replaced by a wind emulator (as it will be seen in the next chapter).

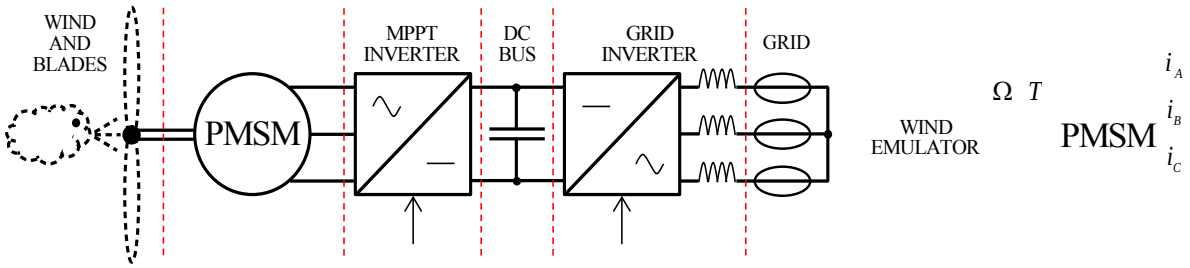

Figure 12. General structure to extract power in case of use three-phase inverter [123]

One of the constraints considered for this work is that the electrical machine used is a synchronous machine with permanent magnets and the topology of the control structure is already determined (which will come later in I.2.2.2.2.3). However to verify this structure, a research work in our laboratory is carried out in [123]. By using vector control based on PMSM model, which is given in Appendix II, this structure is carried out. The direct component of current in *d-q* axis does not contribute to the torque; to get maximum torque per ampere this component (variables with an asterisk are references) must be settled at zero value in vector control. In this type of application, the control is often done using proportional-integral (PI) controllers. In closed loop and for this type of device, PI controllers introduce two poles, but also a zero. The settings are more complex. Integral-proportional (IP) controllers are used to eliminate zero. Figure 13 shows current loops of PMSM in *d-q* axis for given rotational speed with currents reference in rotating frame.

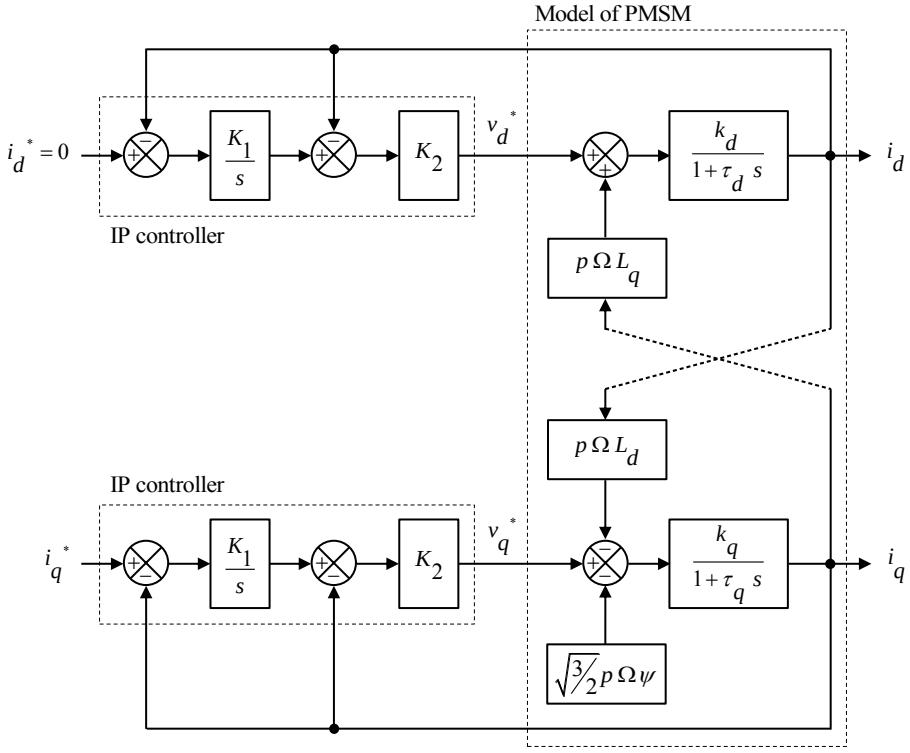

Figure 13. Vector control - PMSM current loops for given value of rotational speed [123]

The closed loop transfer function with IP controller can be written for both axis *d* and *q* respectively as in (1) and in (2), with s as Laplace variable:

$$i_d(s)=\frac{1}{1+\dfrac{1+k_d K_2}{k_d K_1 K_2}s+\dfrac{\tau_d}{k_d K_1 K_2}s^2}i_d^*(s)+\frac{p\Omega L_q k_d s}{k_d K_1 K_2+(1+k_d K_2)s+\tau_d s^2}i_q(s) \tag{1}$$

$$\begin{aligned} i_q(s)=&\frac{1}{1+\dfrac{1+k_q K_2}{k_q K_1 K_2}s+\dfrac{\tau_q}{k_q K_1 K_2}s^2}i_q^*(s)+\frac{p\Omega L_d k_q s}{k_q K_1 K_2+(1+k_q K_2)s+\tau_q s^2}i_d(s)\\ &-\frac{\sqrt{3/2}\,p\Omega\psi k_q s}{k_q K_1 K_2+(1+k_q K_2)s+\tau_q s^2} \end{aligned} \tag{2}$$

Where $k_d=k_q=1/R_S$ and $\tau_d=L_d/R_S=\tau_q=L_q/R_S$ and with K_1 and K_2 as controller parameters. For the regulation part, the determination of K_1 and K_2 is based on (3) and (4).

$$\frac{i_d(s)}{i_d^*(s)}=\frac{1}{1+\dfrac{1+k_d K_2}{k_d K_1 K_2}s+\dfrac{\tau_d}{k_d K_1 K_2}s^2}=\frac{1}{1+2\xi\tau s+(\tau s)^2} \tag{3}$$

$$\frac{i_q(s)}{i_q^*(s)}=\frac{1}{1+\dfrac{1+k_q K_2}{k_q K_1 K_2}s+\dfrac{\tau_q}{k_q K_1 K_2}s^2}=\frac{1}{1+2\xi\tau s+(\tau s)^2} \tag{4}$$

Experimental test is carried out to verify the control performance in this type of structure. Figure 14 shows that for steady state ($\Omega=100$rpm and $i_q^*=6\sqrt{3/2}$A) the currents in the natural base i_A, i_B, and i_C are identical to their references i_A^*, i_B^*, and i_C^*. Thus the vector control operates properly in steady state for this structure.

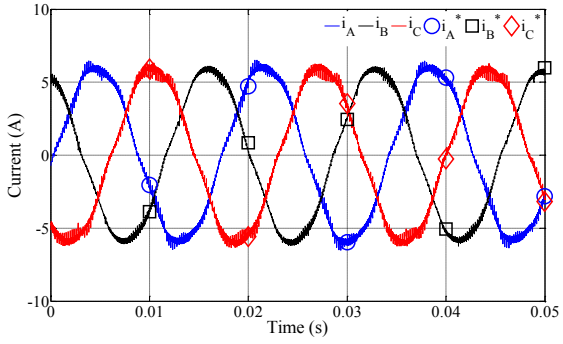

Figure 14. Currents in the natural base and their references [123]

This type of structure and control offers a good performance, yet it is required a high complexity in design and expensive equipment for being carried out. Therefore, in the third structure, the cost will be minimized.

I.2.2.2.2.3 Three-phase diode bridge with chopper

Static converters are essential elements of the wind energy conversion system with variable speed. They allow operating at variable speed and thus extracting the maximum power generated by the turbine. Power can be optimized (the DC side) by a voltage control (accordingly the rotational speed of the generator) with a controlled PWM rectifier as seen in the last part, or by a rectifier of three-phase diode bridge associated with a controllable converter (step-type buck or chopper). As it is presented in the last paragraph, configurations based on a rectifier bridge with six controlled switches are costly and require a rather complex control circuit. The structure of this part requires a simple and less expensive control system. As the output voltage of PMSM is too high, a boost converter (chopper) is chosen to use for a high voltage output.

I.3. Conclusion

A brief description of renewable energy has been presented in this chapter. In this context, some key concepts about wind technology were given as methods of description of wind resources, examples of architectures, used generators, etc. the work of this thesis focuses on a small scale wind power system dedicated to a site concern the urban environment. Examples of practices and industrial achievements of this set are offered. The turbine types of horizontal and vertical axis are described for the various improvements of possible performance. Wind turbine in our case is small scale one of horizontal axis. Types of machines used in the small scale wind turbine were classified to choose the most appropriate for the studied system. PMSM is used in our study case for its known advantages. In terms of control, various structures and control of small scale wind turbine were listed and studied.

Therefore this chapter has helped to build the foundations of our study through the representation of all the elements of wind power system represented by different energy conversion structures. Investigative search has been described and allows to focus on the target for this study in the context of small-scale wind turbine. Several structures and management strategies with regard to cost criteria (simplicity of construction and maintenance) and energy efficiency were discussed. According to this criterion, special attention was paid to the performance in each model.

A major part of this chapter has dealt with wind turbine structure and the insertion of a conversion system to be associated with the small-scale wind turbine. This part has allowed highlighting several key points:

- A brief description of the diode bridge in its environment has been proposed. This structure is sufficiently simple and quick to implement, yet it does not offer any kind of power optimization.
- Fully controlled converter was presented to optimize the power and control the system. It is proved that its performance is good enough but the cost remains the main obstacle for implementation.
- Finally, static conversion structure for DC-DC was presented through a power control adapted to provide voltage control. It is highlighted, under static conditions, the interest of such structure to variable DC bus voltage which offers the opportunity to maximize the power whatever the wind conditions are.

As the last configuration is considered, certain components of wind turbine have to be characterized. Thus, in the next chapter the components characterization will be presented and the wind power will be fully illustrated. Also, the next chapter will focus on performance of the considered structure under various strategies to extract the maximum power, which will conclude on looking for the best cost.

Chapter II. Studied wind turbine – control analyses and energy optimization

A practical approach to energy production is to use wind turbine coupled with a PMSM. PMSMs are reliable, efficient and of low maintenance. In addition, with flexible operation, they may have a direct coupling to the turbine (no gearbox, another mechanical system). Thus, system based on PMSM can operate at variable speed, to extract more energy with less mechanical stress and therefore, less energy variations, which is not the case with a constant speed operation [17].

In this chapter, a wind turbine conversion system will be detailed by explaining its different structures and all its elements. Static converters are essential in the structure of such a system. They allow not only operating at variable speed but also extracting the maximum amount of produced power. The frequently used structure is the three-phase diode bridge rectifier associated with a controllable converter. Then, in order to design an MPPT controller not only robust and effective, but also to optimize the all over cost of the system; both direct and indirect methods are taken in consideration. To allow experimental validation in the laboratory, an emulator of the system was constructed.

Experimental results are shown to demonstrate the effectiveness of the proposed controller.

II.1. Wind turbine emulator

As it is mentioned in chapter I, small-scale wind turbines are wind turbines which have a capacity inferior than or equal to 30kW for Europe and 100kW for USA. These wind turbines are usually equipped with blades having a diameter of between two and eight meters. In the European case, they are generally used in standalone operation for powering remote sites. Small-scale wind turbines use several types of electric machines, like asynchronous machines [28], but the most used is PMSM. The PMSM is popular because it is effective and reliable. It also has a good energy density per given volume and weight. In recent years, the axial flux PMSM appeared; it is of highly performance, but it has strong manufacturing constraints [26]. Thus, this study focuses on a small-scale wind turbine with PMSM of radial flux type. For converting mechanical energy into electrical energy, small-scale wind turbine mainly use two types of structures; passive structure and active structures. Various types of these structures are illustrated in first chapter in Figure 11.

Figure 11 (a) shows the passive structure that uses a static uncontrollable AC-DC converter (three-phase diode bridge). Occasionally, it is also possible to find the active structure of Figure 11 (b). This structure uses a controllable AC-DC converter. Besides, by adding a controllable static DC-DC converter, the first passive structure is easily transformed into active structure as shown in Figure 11 (c). The passive structure is robust and does not have a high cost; however it does not optimize the collected energy. At this time, energy flow optimization becomes focus before considering the financial costs of a system (which is quite debatable). It is for this reason that the passive structure is virtually no longer used. This leaves two types of active structures that are presented in Figure 11 (b) and (c).

To operate the structure presented in Figure 11 (b), it takes 6 transistors and closed loop control (to some extent directed by elaborated control as it is presented in chapter I). However for the structure presented in Figure 11 (c), it takes 7 diodes, one transistor and closed loop control (directed by a simple control). Then, it is readily understood why that in most applications, the structure of Figure 11 (c) is frequently used. Therefore, in this study the structure (c) of the Figure 11 is considered. The scheme of the studied wind emulator principle is illustrated in Figure 15.

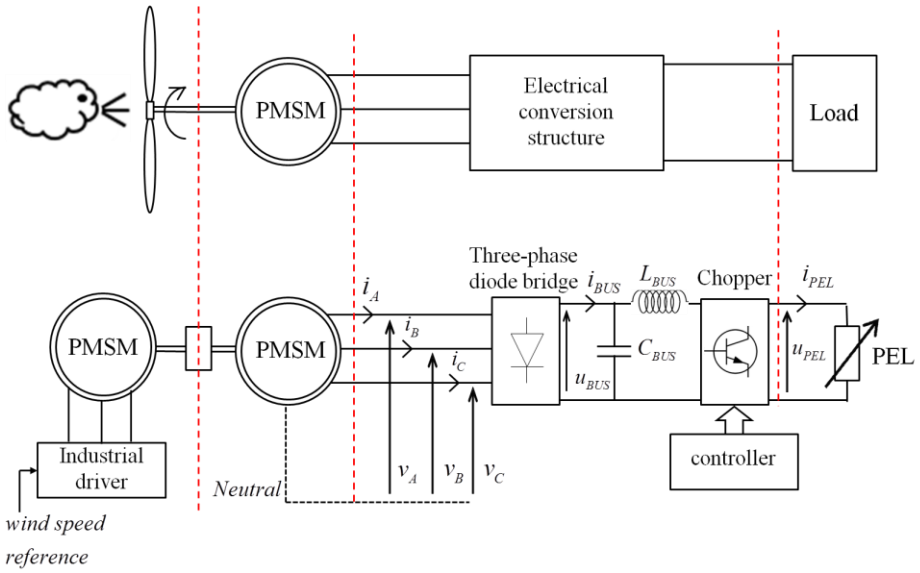

Figure 15. Scheme of studied wind emulator principle

The test bench for the wind turbine emulator consists of various devices shown in Figure 16.

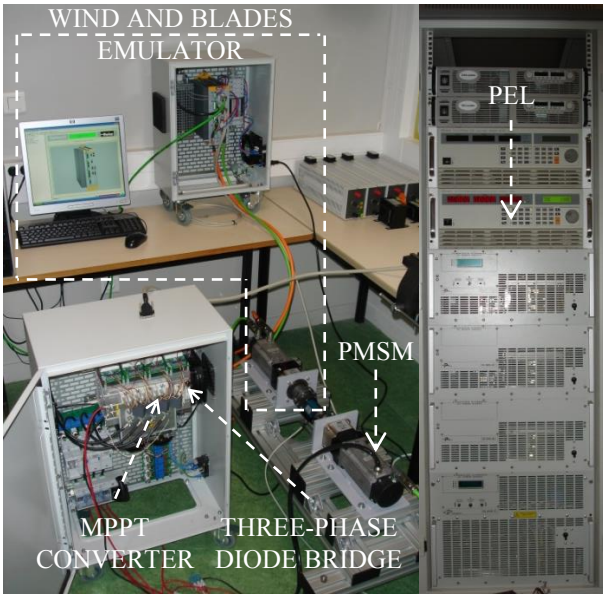

Figure 16. Various devices for the test bench of wind turbine emulator [123]

To emulate wind and blades, it is required a control board for rapid control prototyping (Digital signal processing and control engineering, dSPACE DS1104) to control a three-phase industrial driver (C3S063V2F10 from Parker) to drive a three-phase PMSM (NX430EAJR7000 from Parker) which emulates dynamic characteristics of wind and blades. The parameters of this type of PMSM are given in Appendix III. The generator is a same PMSM as that emulates the wind and the blades. A three-phase diode bridge (SKD 51/14 from SEMIKRON) connects the generator outputs and converts the AC power from the generator into DC form. A DC bus uses a capacitor of 1 mF and an inductance of 50 mH (267.5mΩ) to obtain an acceptable balance between filtering quality and system dynamics. In order to operate the MPPT, it requires that the control board dSPACE DS1104 (sample time of 100μs)

controls another driver (SKHI22A from SEMIKRON) to drive an IGBT module (SKM100GB063D from SEMIKRON). In addition, one programmable electronic load (PEL, PL-6000-A from Puissance+) with a 1.1mF capacitor is used to emulate the power demand. For all operating points of the studied system, the PEL maintains voltage u_{PEL} at constant value (400V).

II.1.1. Aerodynamic and electrical power

The principle of wind turbine operation is based on the formula for the aerodynamic power (p_{AERO}) given in (5):

$$p_{AERO} = \frac{1}{2}\rho\pi R^2 c_P v^3 \tag{5}$$

where ρ, R, c_P, and v are respectively the density (kg/m^3), the radius of the blades of the considered wind turbine (m), the power coefficient, and wind speed (m/s). The power coefficient c_P is not constant but it depends on the normalized wind speed v and wind turbine type *i.e.* Coefficient c_P is a function of tip-speed ratio ($\lambda = R\Omega/v$).

The first step is to create a "wind emulator" that must emulate the aerodynamic power and the inertia moment of the blades which is brought about by the rotational axis. To perform that, one of the two electrical machines mentioned above is controlled as motor with an industrial driver. The latter controls the speed (for its analog input 0-10V). The speed reference is obtained by solving the equation (6):

$$\frac{1}{\Omega}\left(p_{AERO} - p_{EM}\right) = J\frac{d\Omega}{dt} + F\Omega \tag{6}$$

where p_{EM}, J, and F are respectively electromagnetic power (W), moment of inertia of blades (kg.m^2) which is brought about by rotational axis, and the viscous friction coefficient (N.m/rad).

In order that the "wind emulator" is as realistic as possible, in last equation the used parameters are the geometric, aerodynamic, and mechanical parameters of BERGEY EXCEL 1 [30], [31], which are given in Appendix III. In fact, all parameters of small scale wind turbine are difficult to be found. Therefore, these parameters are known for this type of wind turbine which is the same type of that one installed in our site, further more it is well known for performance and reliability. The power coefficient c_P is an approximated polynomial function of the 7th order is given in (7), whose factors are also taken from BERGEY EXCEL 1 [30], [31], given in Appendix III:

$$c_P(\lambda) = \sum_{K=0}^{7} a_K \lambda^K \tag{7}$$

Finally, the electromagnetic power is difficult to measure, an approximation thereof is used as in (8):

$$p_{EM} = v_A i_A + v_B i_B + v_C i_C \tag{8}$$

For various wind speeds, Figure 17 and Figure 18 respectively give the experimental evolution of the aerodynamic power and electric power ($p_{BUS} = u_{BUS}\, i_{BUS}$) as a function of the bus voltage u_{BUS} and the bus current i_{BUS} .

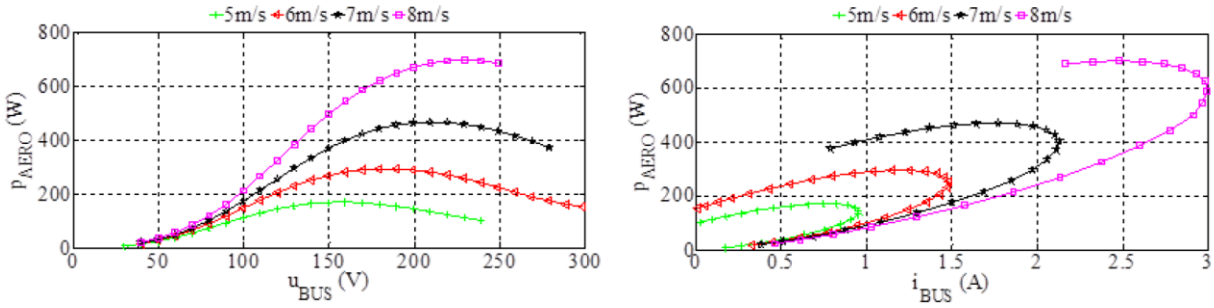

Figure 17. Experimental evolution of the aerodynamic power according to u_{BUS} and i_{BUS} [29]

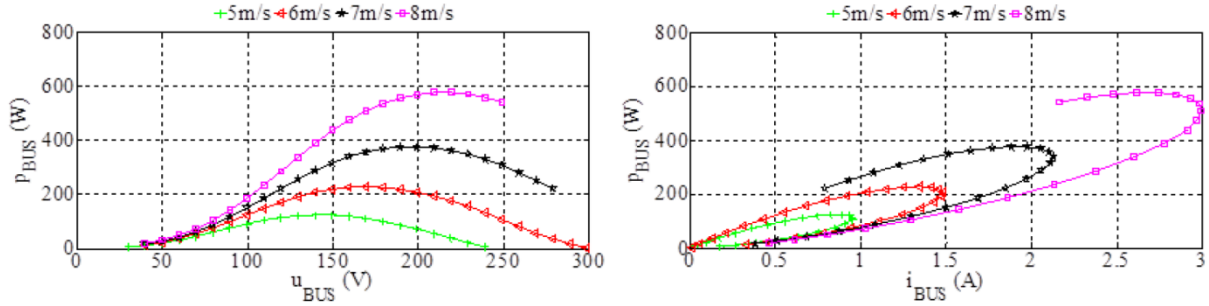

Figure 18. Experimental evolution of the electric power according to u_{BUS} and i_{BUS} [29]

Figure 17 and Figure 18 show that for a given wind speed, the aerodynamic MPP and the electric MPP are different. This difference is mainly due to losses in the PMSM and the three-phase diode bridge. These figures also show that with this system it is much more difficult to control the system with i_{BUS} than with u_{BUS} . Indeed, for a given current there are two points of power: aerodynamic and electrical. The control is therefore carried out always with voltage.

A converter can impose different values of u_{BUS} across three-phase diode bridge. Considering an arbitrary profile of wind speed given in Figure 19, Figure 20 shows the evolution of p_{BUS} for different values of u_{BUS} ranging from 100V to 250V. The respective recovered energies are 1.6Wh for 100V, 4.3Wh for 150V, 5.55Wh for 200V and 4.95Wh for 250V, while potentially recoverable energy is 5.9Wh (Figure 19). For arbitrary wind speed profile, it seems that the optimal value of u_{BUS} is 200V. Figure 19 and Figure 20 show that to get the maximum energy when the wind is random, u_{BUS} must

be varied in real-time. Taking into consideration the MPP shown in Figure 17 for different wind speeds (which depend on u_{BUS}), optimum u_{BUS} for different values of rotational speed ($n = 60\Omega/2\pi$ rpm) is an almost linear function as presented in Figure 21. In this work, as three-phase diode bridge is used, an experimental analysis is carried out instead of analytical study to determine the values of u_{BUS}. In fact, analytical study when it is constructed provides evaluation of parameters under different conditions which is not concerned. So that analytical study is not presented in this thesis.

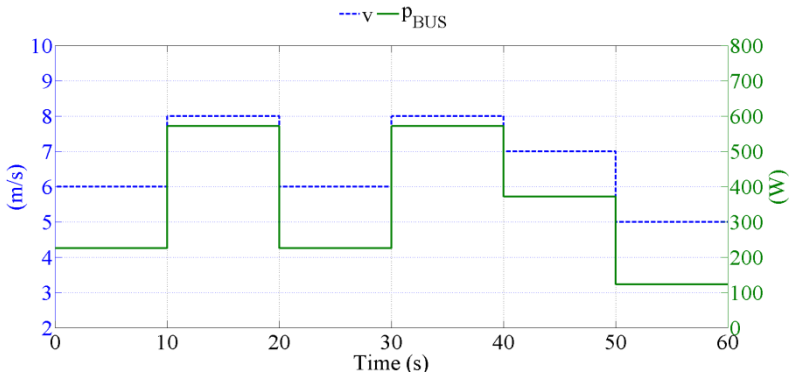

Figure 19. Arbitrary wind speed profile and optimum evolution of p_{BUS} [29]

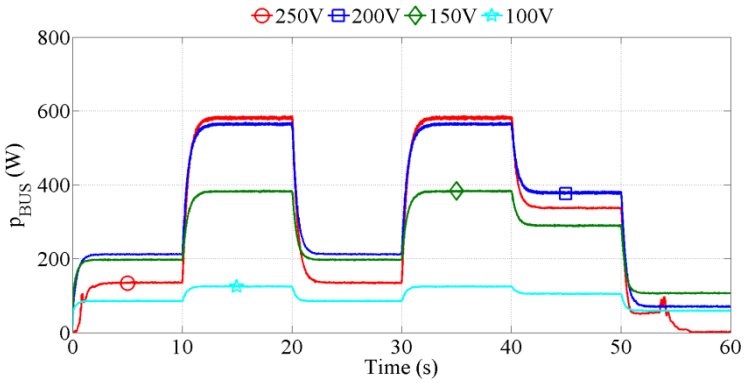

Figure 20. Experimental evolution of p_{BUS} for different values of u_{BUS} [29]

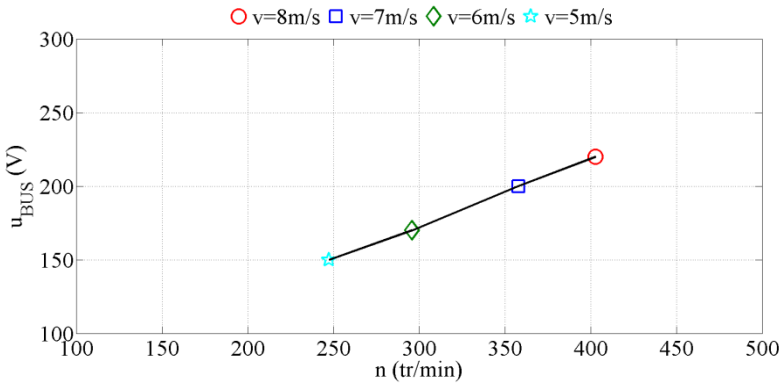

Figure 21. Experimental optimum u_{BUS} for different values of n [29]

II.1.2. PMSM and control system

PMSM plays a key role in the production systems of wind energy to transform mechanical energy into electrical one. A rigorous mathematical modeling of PMSM is a prerequisite for the design of the machine control algorithms as well as features analysis at steady and dynamic states of wind energy conversion systems. Studying the behavior of an electric machine is a difficult task and requires, first and foremost, a good knowledge of its dynamic model in order to predict well by simulation its behavior in the different considered states. For this reason, PMSM modeling in both *A-B-C* and *α-β* references is given in Appendix II. All variables with asterisk are reference values.

The control cooperates with the strategy of MPPT which aims to extract maximum electrical power, *i.e.* the maximum electrical energy. As it is concluded above, the bus voltage is used as the controlled parameter for MPPT algorithm and the reference value of bus voltage u_{BUS}^{*} is the calculation result of this algorithm.

It is absolutely necessary to use a regulator to control the system following the u_{BUS}^{*} calculated by MPPT algorithm. In order not to complicate the task but also to avoid focusing on this, a hysteresis corrector is used. In this study the hysteresis controller (schema with hysteresis controller is given later in Figure 28) is chosen due to its rapid response capability, wide bandwidth and low difficulty of realizing. The bandwidth of the hysteresis correction is set as small as possible to minimize the ripple of the electrical quantities.

Figure 22, Figure 23, Figure 24, Figure 25 and Figure 26 show the dynamic process of system response to bus voltage step input using the hysteresis control. For these figures, experimental conditions are as follows: 8m/s wind speed, 100V initial bus voltage u_{BUS}, and 10V step change of bus voltage are used to obtain a significant difference.

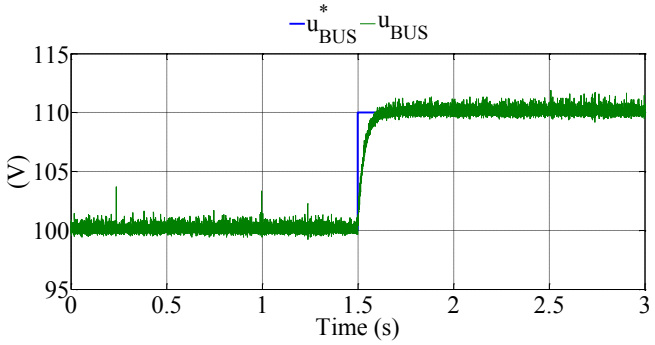

Figure 22. Experimental evolution of u_{BUS}^{*} and u_{BUS} [29]

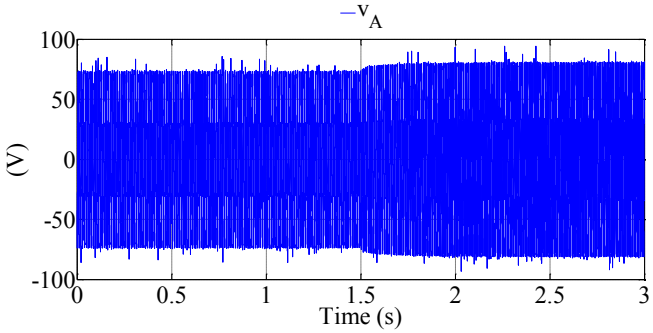

Figure 23. Experimental evolution of v_A [29]

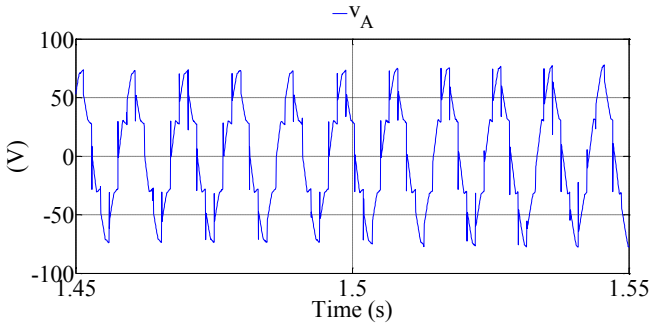

Figure 24. Experimental evolution enlarged of v_A [29]

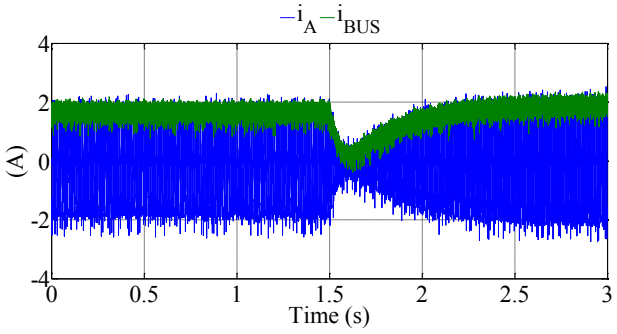

Figure 25. Experimental evolution of i_A and i_{BUS} [29]

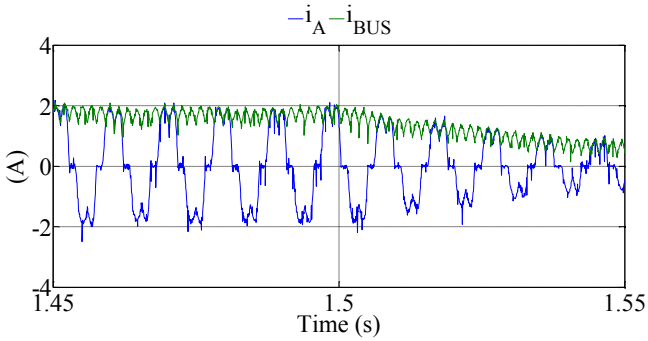

Figure 26. Experimental evolution enlarged of i_A and i_{BUS} [29]

Experiment evolutions shown in Figure 22 suggest that u_{BUS} can properly track the reference of bus voltage u_{BUS}^* under the control of the hysteresis method. Given the fact that all three-phase voltages

(v_A, v_B, and v_C) and three-phase currents (i_A, i_B, and i_C) are balanced, thus the same behavior is expectable, just evolutions of single phase voltage (v_A) and current (i_A) are presented in the following figures (Figure 23, Figure 24, Figure 25 and Figure 26) aiming to highlight the signal changes before and after u_{BUS} changing.

Figure 23, Figure 24, Figure 25 and Figure 26 present the whole dynamic response of v_A, i_A, and i_{BUS}, while Figure 24 and Figure 26 display the enlarged evolution for each variable. It is obvious that, comparing with three-phase current, three-phase voltage respond to the reference of bus voltage more rapidly, meanwhile wave forms of v_A and i_A do not transform significantly. This means that hysteresis control meets the requirement of rapid response, without the distortion of system operating mode.

II.2. Maximum Power Point Tracking

As explained in the last section, that it becomes possible to impose reference value of voltage bus u_{BUS}^* into the system. So, to maintain the bus voltage at a constant reference value, which permits to ensure the management of the energy transferred toward the grid properly, it is necessary to use a MPPT procedure.

To extract the maximum power and therefore the maximum of energy, it is essential to use a MPPT algorithm. For small-scale wind turbines (as for other nonlinear energy systems), there are two types of MPPT methods. The first is so-called direct method and the second is called indirect method.

The first method is based on the perturbation and observation (P&O) of system variables in real time. The complexity of this type of method is the choice of disturbance ratio and the observation time value especially when the studied system is very noisy. A great value of this ratio means faster response, but more oscillations around the MPP. A small value improves accuracy but also reduces the rate of convergence [32], [33]. In both cases, there is a loss of efficiency.

The second method is based on the knowledge of the wind turbine model [34]. Exact knowledge of the wind turbine model can sometimes cause problems and demand above all using a mechanical sensor (for a speed or wind speed). To save the cost of buying a mechanical sensor and not to reduce the overall system reliability, mechanical sensor may not be used. So, the speed of wind turbine must be estimated. Indeed, the price of a mechanical sensor can be up to 20% of the total price of a small-scale wind turbine. In the case of large-scale wind turbines, there is no mechanical sensor problem because the purchase price is small compared to the total investment. An estimator, however, could afford to have redundancy in case of failure of the mechanical sensor.

In recent years, a number of very good works related to the MPPT algorithms for small-scale wind turbines have been presented [35]-[46]. The most encountered works are based on direct method and using P&O [35]-[40]. These studies can be classical works or improvements with fixed or variable pitch. There are also some indirect methods [41]-[44] and non-standard methods [45], [46]. Indirect methods are less frequently used. In addition, there are very few works that give experimental results with real wind profile [37], [41], [44], and [45].

II.2.1. Direct MPPT

Direct methods are independent from the knowledge of the power curves and speed of wind. They are based on methods like P&O, Hill Climb Searching, etc, which were successfully applied in photovoltaic systems. Yet the wind energy conversion process is more complicated because of the stochastic nature of wind, the complex aerodynamic and non-linear behavior of the generator and of the electrical system, the application of these methods into a conversion small-scale wind system require changes and adaptations.

The MPPT algorithm proposed in [47] exploits the fact that the optimum power curve of a wind turbine is characterized by a single constant k_{opt}. Hence, if the maximum can be detected and successfully achieved, then k_{opt} can be extracted by measuring the power and rotation speed. Once k_{opt} is known, it can serve as specific reference to the size and direction of the next disturbance.

In [48], the authors proposed an MPPT controller based on the current at wind turbine input and wind speed. The controller generates the appropriate duty cycle for the boost converter, and hence the maximum power point is tracked. The optimized reference current is used to obtain the maximum output power generated from wind for different wind speeds. However, in the methods described above, they require the measurement of the rotor speed which requires a speed sensor that costs still expensive and not easily measured accurately.

Therefore, a MPP continuation method was proposed in [49]; it is based on the equation $\Delta P/\Delta T = 0$, with ΔP the step of power between two successive points and ΔT the step of the time values, that calculates the new duty cycle to check the MPP when the wind speed changes. Authors of [50] proposed a method based on the same equation, but using a fuzzy controller to check the MPP. Both show that they do not need neither knowledge of wind turbine power curve or wind speed. However, these methods only work for a constant load. If the load changes when the wind speed is constant, the current and voltage will change but $\Delta P/\Delta T$ remains at the same value, then the controller cannot identify this change to move the system to the new MPP; in this case the extracted power is no longer maximized. Accordingly, these methods cannot be applied in this manner for microgrids whose loads vary with time.

The basic principle of the direct MPPT algorithm is shown in Figure 27 [51], [52]. Δu , k and $k-1$ in Figure 27 means respectively the perturbation step size, the iteration for the actual case and the iteration for previous case.

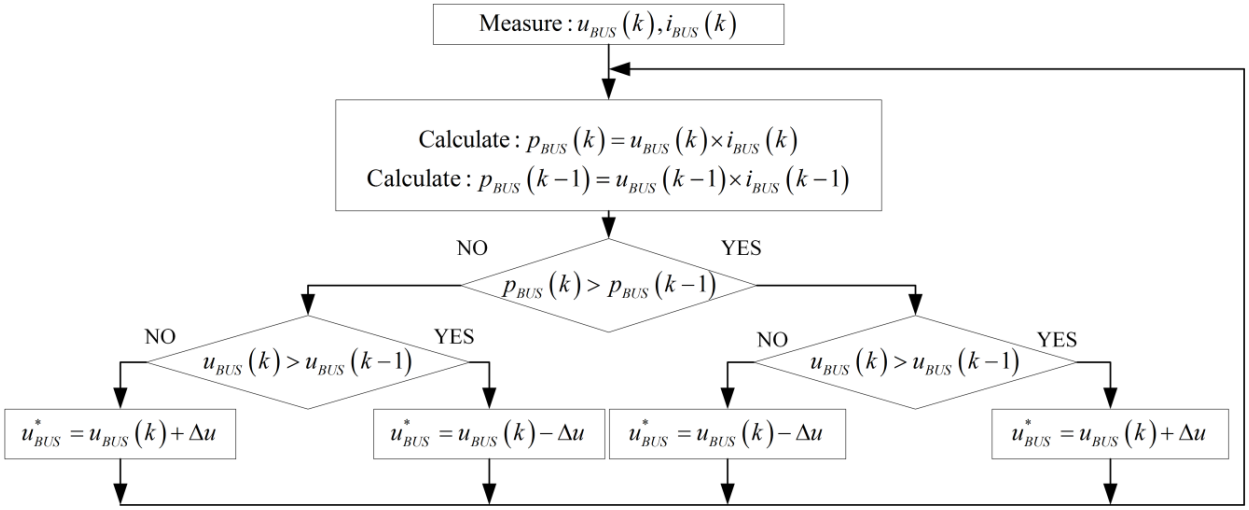

Figure 27. Principle of P&O method [29]

In the context of this research work, the three direct methods chosen are the P&O not fixed step, the P&O variable step based on the Newton-Raphson method, and P&O with variable step based on fuzzy logic.

The reference value of bus voltage u^*_{BUS} is the calculation result, while Δu in Figure 27 means the perturbation step size. To make sure that the combination of the values of the perturbation facing on the observation time, the dynamic characteristics of bus power responding to the bus voltage should be investigated. For this, several groups of experiments with different step inputs of bus voltage have been carried out and are presented in section II.2.3.

II.2.2. Indirect MPPT

Indirect MPPT methods are based on the wind turbine power curve. From this curve the optimal speed can be determined according to each wind speed and then controlling the rotor to follow this optimal speed [53], or by feed-forward controller [54]. In [55] MPPT algorithm based on the use of the memories and the initial value of reduced speed is proposed. The proposed algorithm adapts itself and accurately performs the automatic update setting of the reference speed data as the wind speed changes based on the characteristics of the generator. In indirect method, there is also the torque control: from the optimal speed, optimal torque is calculated for each wind speed and this reference is then followed by a control, sliding mode [56] or by a fuzzy controller [57].

A drawback of indirect methods is that the power curve of a wind turbine is not available with high precision and will change according to the rotor aging. Another disadvantage is that it requires the

measurement of the rotational speed of the rotor. The price of anemometers or speed/position sensors is a barrier to the application of indirect methods in isolated sites [58]. Therefore, it is necessary to measure or estimate the speed rotation to know the voltage u_{BUS} to be imposed across three-phase diode bridge. Consequently, the next section presents the model of PMSM prepared to the estimation of rotational speed and position.

II.2.3. Experimental validation using rotational speed sensor and hysteresis controllers

Figure 28 shows the structure used for this experimental validation in case of direct method, knowing that in the case of the indirect method the speed becomes the entry of "MPPT" block. In this experimental test, the speed is obtained by a mechanical sensor.

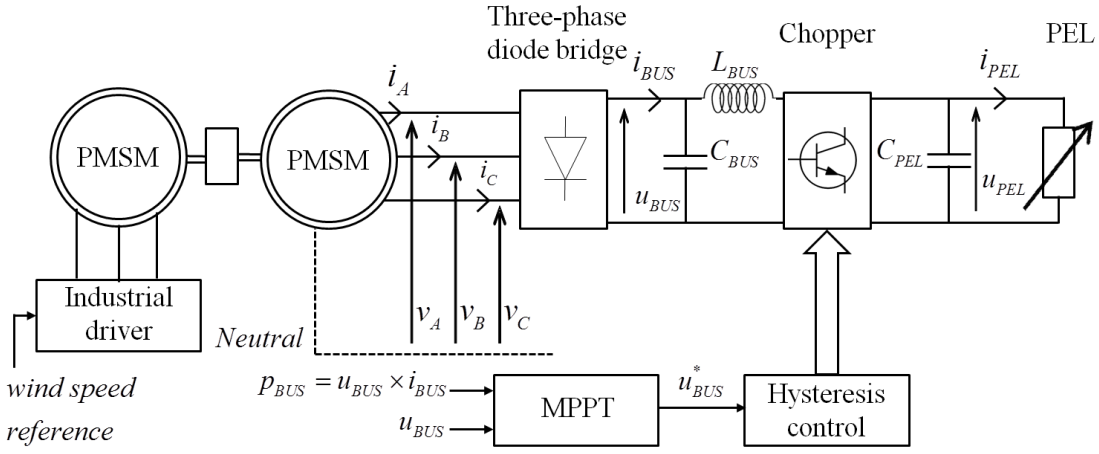

Figure 28. Structure used for experimental comparison of MPPTs

The components of test bench of studied emulator are illustrated in Figure 28. Wind and blades are emulated by three-phase brushless servomotor (NX430EAJR7000 from Parker) driven by three-phase industrial inverter (C3S063V2F10 from Parker). This industrial driver is controlled in speed by a dSPACE DS1103 (controller board for rapid control prototyping). The measurement of the real speed rotation is effected by a rotating speed sensor (DR2513 from SCAIME) and also verified through a resolver (TS2620N861E11 from Tamagawa). The PMSM, which is used, is the same as that emulates the wind and the blades. The three-phase diode bridge is classical (SKD 51/14 from SEMIKRON). Capacitor C_{BUS}=1mF and inductance L_{BUS}=10mH (22.5mΩ) were utilized to obtain a good compromise between filtering and system dynamics. Indeed, large values are filtered heavily but will limit the system dynamics. IGBT module (SKM100GB063D from SEMIKRON) is used as a MPPT converter. It is controlled at 5kHz with step of time up to 0.2ms by the dSPACE DS1103 via a driver (SKHI22A from SEMIKRON). The power demanded by the DC microgrid is emulated by a programmable electronic load (PEL, 63202 from Chroma). The capacitor C_{PEL}=1.1mF is the bus

capacitor of DC microgrid (which is the capacitor connected in parallel to the PEL). Generally, DC microgrid can use multiple voltages including 400V. PEL maintains voltage u_{PEL} equal to 400V whatever the operating point of the small scale wind generator.

II.2.3.1. Direct method

This section presents experimental results for both fixed and variable step size for the proposed MPPT algorithm. As input for whole system, an arbitrary wind speed profile is used (Figure 29, Figure 30, Figure 31 and Figure 32).

According to the analysis presented in Section II.2.1, MPPT algorithm must work discontinuously in time domain. The observation time step is chosen as 2 seconds. For the fixed step size method, the perturbation step size Δu, as defined by (11), is fixed as 5V, which is considered as a compromise between the stability and the tracking speed. To improve the efficiency and the accuracy of the conventional P&O method, variable step size algorithms have been proposed.

In this study, the method used for modifying perturbation step size Δu depends on the slope of the power with respect to the input voltage, as expressed by the equations (9), (10) and (11):

$$slope(k) = \frac{p_{BUS}(k) - p_{BUS}(k-1)}{u_{BUS}(k) - u_{BUS}(k-1)} \tag{9}$$

$$\Delta slope(k) = slope(k) - slope(k-1) \tag{10}$$

$$\Delta u = \frac{\Delta p_{BUS}(\mathrm{k})}{\Delta slope(k)}, \Delta u \in [-5,5] \tag{11}$$

The experimental results are presented as follows. Figure 29 shows the potential available bus power p^*_{BUS} and the evolution of bus power respectively for step size fixed (p_{BUS-F}) and variable (p_{BUS-V}). Figure 30 displays the experimental evolution of bus voltage for step size fixed (u_{BUS-F}) and variable (u_{BUS-V}).

Figure 31 presents the experimental evolution of Δu which is fixed at 5V for fixed step size method (Δu_F) and calculated by equations (9), (10) and (11) for variable step size method (Δu_V).

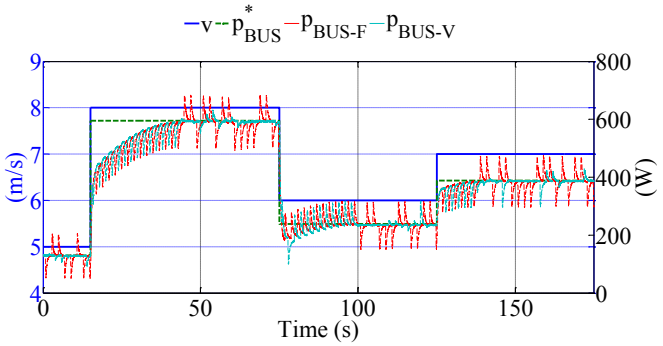

Figure 29. Potential bus power p_{BUS}^{*} and experimental evolution of p_{BUS-F} and p_{BUS-V} [29]

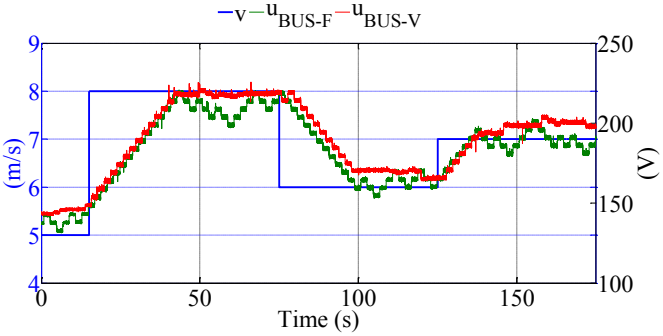

Figure 30. Experimental evolution of u_{BUS} [29]

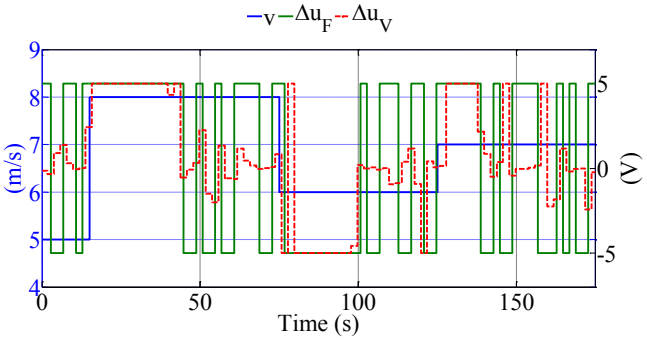

Figure 31. Experimental evolution of Δu for both cases [29]

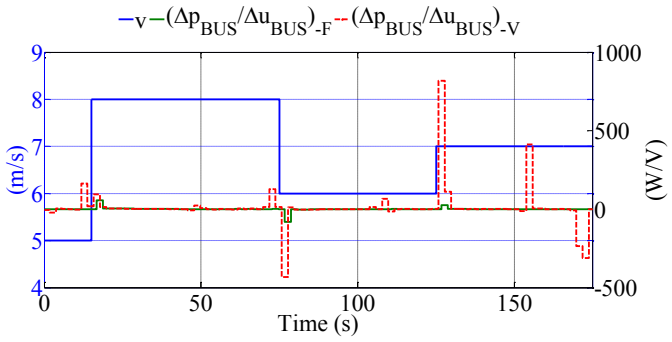

Figure 32. Experimental evolution of $\Delta p_{BUS} / \Delta u_{BUS}$ [29]

Due to the presence of noise in real signals of p_{BUS} and u_{BUS}, operating points of both fixed step size MPPT and variable step size MPPT drift around each MPP. Under the condition of bus power steady-state value changing insignificant, the different behavior of bus voltage (as presented in Figure 30) is

important to identify the distinction between these two algorithms. Results of observation ($\Delta p_{BUS} / \Delta u_{BUS}$) are very sensitive to the noise from p_{BUS} and u_{BUS} (see in Figure 32). But, since the variable step size algorithm calculates Δu with the $\Delta p_{BUS}(k)/\Delta slope(k)$ instead of directly $\Delta p_{BUS} / \Delta u_{BUS}$, it could suppress this interference. Therefore, even sometimes certain undesired results of $\Delta p_{BUS} / \Delta u_{BUS}$ emerged, the algorithm will not result in a divergence. Thus, experimental results show a good quality of power signal, *i.e.* less power fluctuations on DC link bus.

II.2.3.2. Indirect method

Based on the results presented in Figure 21, it is possible to set the reference voltage u_{BUS}*. Figure 33 shows that the reference voltage u_{BUS}* and the real voltage u_{BUS} on the system are the same. In addition, Figure 33 illustrates that the control of MPPT converter work properly.

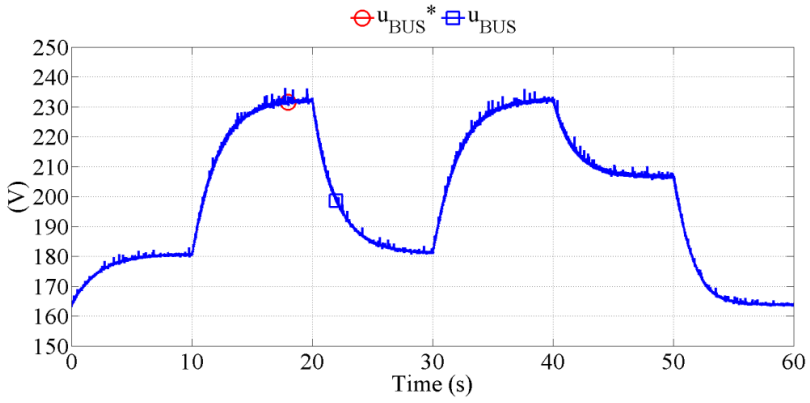

Figure 33. Experimental evolution of u_{BUS}* and u_{BUS} [30]

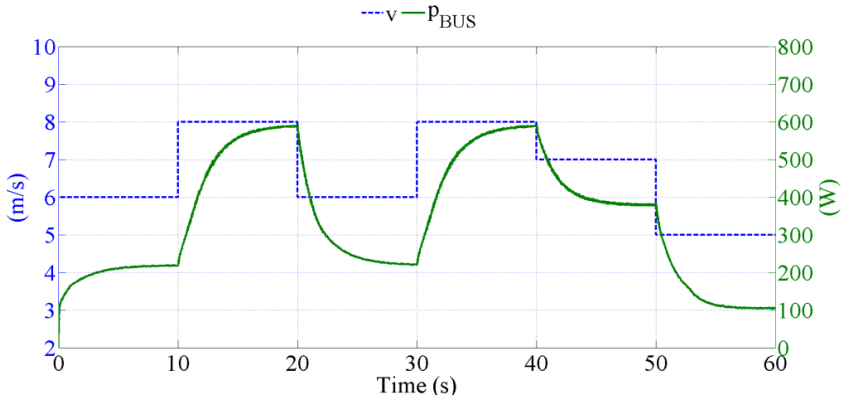

Figure 34. Arbitrary wind speed profile and experimental evolution of p_{BUS} [30]

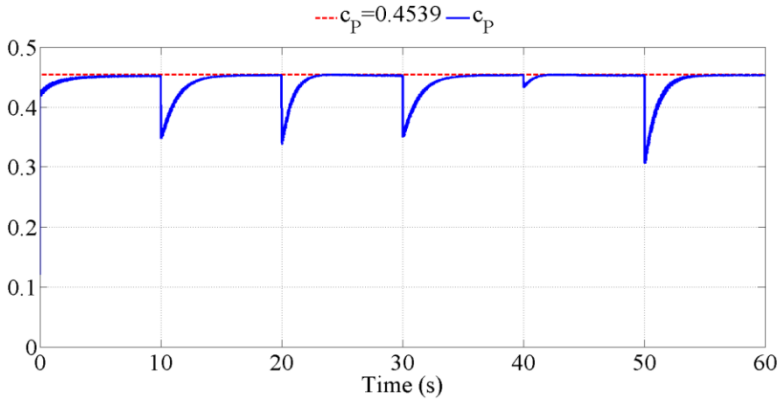

Figure 35. Evolution of wind turbine power coefficient c_P [30]

Figure 34 shows the arbitrary wind speed profile and the power recovered p_{BUS}. The corresponding energy is 5.8kWh while potentially recoverable energy is 5.9kWh which equivalent to a relative error of about 1.7%. With interpolation factors used, the optimum TSR is equal to 7 giving the optimum wind turbine power coefficient equal to 0.4539.

Figure 35 shows that the real wind turbine power coefficient is not always equal to 0.4539. However, being the use of the electrical MPP and the absence of the use of the aerodynamic MPP, this coefficient is close to 0.4539.

The results obtained in this context are given only by a single algorithm; there is no comparison between several algorithms. Yet in the context of this research, an experimental comparison was performed for three direct methods and indirect method based on an actual wind profile. The selected wind profile is given in Figure 36. The variation of this profile is actual wind Compiegne on 15 January 2015.

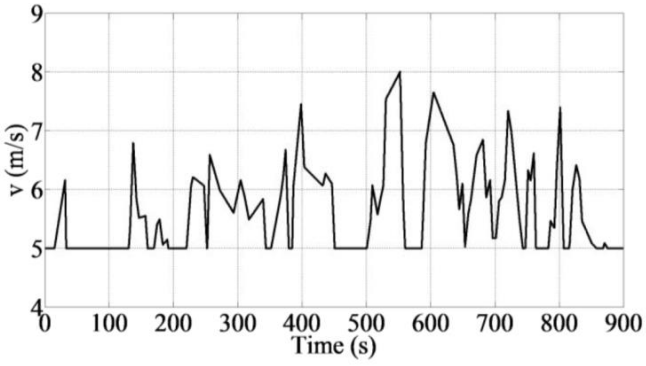

Figure 36. Selected wind profiles

Figure 37 shows the experimental results obtained for the actual wind profile. In order to get the results for other profiles, some time must be taken to adjust iteratively the three direct methods to obtain the best results in terms of recovered energy. Without expertise, it is not

easy to get good results. In the indirect method, a quick and simple reversal of Figure 18 is enough. For Figure 37, the results of different MPPT methods are distinguished by:

- Subscript '-p' means the potential value for optimal condition which are based on the prior experimental data shown in [29];

- Subscript '-f' means P&O fixed step-size method;

- Subscript '-v' means P&O with variable step-size based on Newton-Raphson method;

- Subscript '-vf' means P&O with variable step-size based on fuzzy logic method;

- Subscript '-lt' means look-up table method (indirect method).

This case, which presents a real wind speed profile based on real data, contains many rapid changes. Consequently, values of energy for different MPPT methods are distributed. Comparing with P&O method with variable step-size based on Newton-Raphson method, P&O method combining fuzzy logic method can significantly increase the harvested energy.

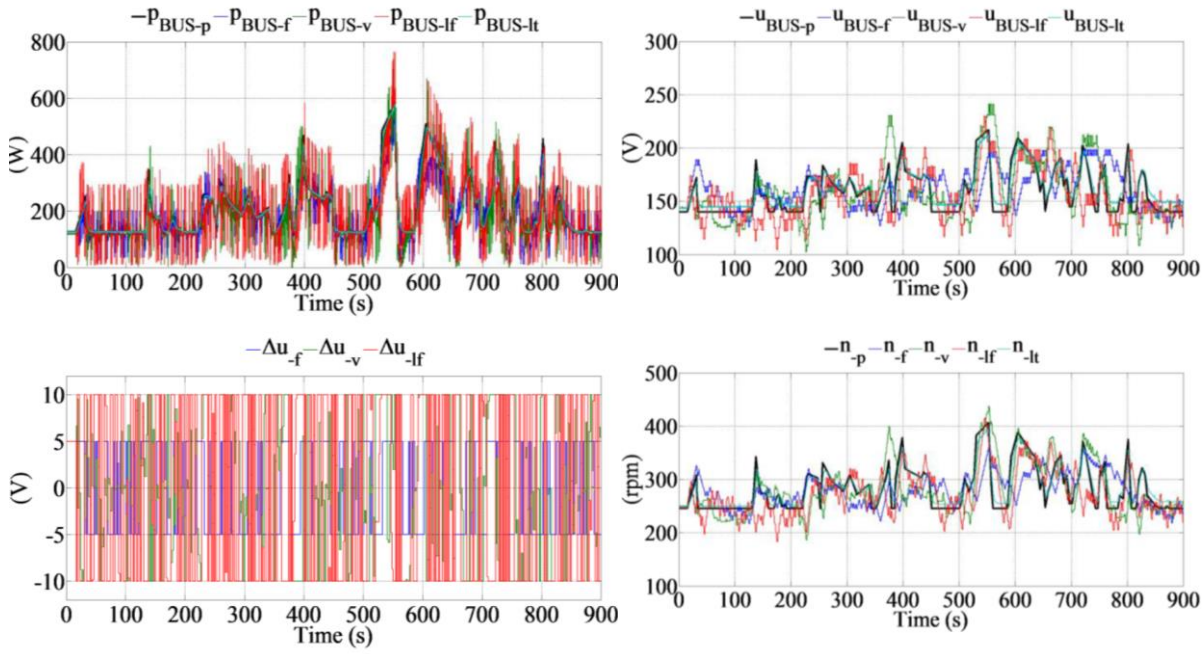

Figure 37. Experimental results for the actual wind profile [10]

Table 2. Energies and their differences from potential value

Method	-f	-v	-vf	-lt
Energy (Wh) (potential 52.28)	46.22	46.69	48.95	51.66
Difference (%)	11.59	10.68	6.36	1.18

From these results, under complex wind speed variation, it can be concluded that direct methods are disadvantageous: P&O is of less efficiency under rapid variation of wind speed, knowing that mechanical inertia cannot be ignored. Concerning the production, energies extracted by direct methods are significantly affected by how fast the wind speed varies. On the other hand, look-up table method

extracts about 98.82% of potential energy, even though evolutions of u_{BUS} did not match the optimal theoretical curve at 100% (Figure 37); it is significantly better than the others. Thus, for different wind profiles, the indirect method extracts more than 98% of the theoretical potential energy through proper monitoring of the MPP and without power oscillations around the MPP.

II.3. Conclusion

In this chapter, the model of small-scale wind turbine emulator, which is considered to study, is presented along with the experimental validation. Small-scale wind turbines as large-scale ones are now well integrated into electrical power grids. The small-scale wind turbines are most often used as stand-alone systems, seen as substitutes for the connection to national grid, or integrated in an electrical microgrid. On the other hand, large-scale wind turbines are often used as systems connected to the national grid, with an injection of total and permanent power. For small wind turbines, experimental validation shows that this is a tool that has become essential in order to demonstrate concepts and/or theoretical approaches.

In this chapter, firstly a direct MPPT algorithm is introduced with two strategies, *i.e.* fixed and variable step. According to the characteristic of the small scale wind generator, the classical fixed step P&O method and a variable step P&O method are implemented to achieve MPPT. Experiments results suggest that both algorithms correctly find out the MPP no matter the wind speed increases or decreases. With the physical restrictions, extracted energies for two methods are not significantly different, but the variable step MPPT clearly suppresses the oscillation amplitude when generator system operates close to the MPP.

Then a simple and robust MPPT indirect method was validated. For small-scale wind turbines with a high mechanical time constant, the indirect method of MPPT gives the best results. Moreover, this method is not only for experts of MPPT methods, it is fast to implement given its simplicity. As mentioned above, the price of a mechanical sensor can be up to 20% of the total price of a small-scale wind turbine. To use an indirect MPPT of less cost, estimating the speed becomes a vital matter.

In the next chapter, the sensorless approach in PMSM case will be focused on. A state of the art will be presented to illustrate the methods that the most used in literature. The most commonly used methods will be tested for speed/position estimation for PMSM. Best estimation will be developed for the studied system to achieve balance between estimation accuracy and overall cost.

Chapter III. Rotational speed and rotor position estimation

In this chapter, comparative study about rotational speed and rotor position estimation for synchronous machine is focused on.

The exact information about rotor position and rotational speed is important for good performance of drive system and asserting control reliability. Many years ago, sensors were used to get this information. With the advancement of technology, methods of estimation started to appear more and more, in order to create a substitute to the physical sensors. This trend of replacing a physical sensor with an estimation procedure has two visible advantages: (i) minimizing the overall cost of the system by economizing the cost of this sensor; (ii) improving the system characteristics by increasing the stability, heightening the robustness, time economizing, decreasing faults probability, etc.

In small-scale wind turbine systems these advantages can be of great importance considering the relatively high cost of position sensor and adding to it the obstacles posing technically by using it. In case that sensorless tool must rebuild the system state, then an observer is what can be an appropriate tool. Indeed, an observer is a software tool for measurement allowing the estimation of system state from a limited amount of information, *i.e.* the inputs and outputs of the system.

III.1. State estimator

The dynamic behavior of many physical systems can be described using a mathematical model that involves a set of differential equations relating a finite number of internal variables, also called state variables. The temporal evolution of the system is characterized by its changing state variables, which depends on the applied drive signals and initial conditions. This system state representation is particularly well adapted to the synthesis of many control laws (*e.g.* state feedback control). The implementation of these control techniques requires knowledge of the evolution of all state variables. However, on a practical level, the state variables do not always correspond to system measures, or they are devoid of any physical sense, because their direct measurement is subject to technical as well as technological or economic constraints (*e.g.* difficult instrumentation system, unavailable or very expensive sensor…). For these reasons, the complete state of the system may be difficult or quite impossible to measure. The value of one or more variable(s) of system state should be estimated or rebuilt in a rule through an observer, also said software sensor. The estimation of the system state also plays a central role in the context of systems monitoring and diagnostic. It serves, in fact, to generate system failure symptoms established from the comparison between the estimated signals and those measured. The reconstruction of a system of state variables is therefore a fundamental problem in the engineering sciences.

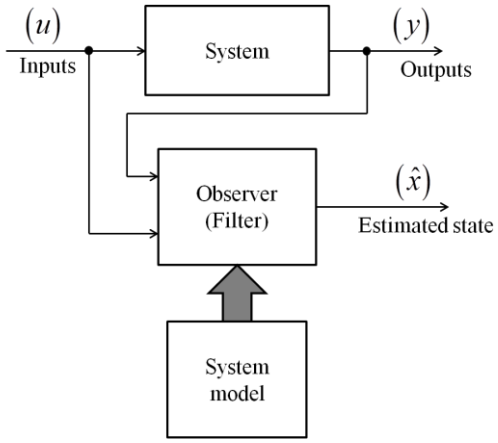

Figure 38. Principle of state estimation

The reconstruction of state proposes to provide estimates of the state variables ($\hat{x}$) from the known variables, *i.e.* the system inputs (u) and outputs (y), as illustrated in Figure 38. A solution to the problem of estimating the system state, based on knowledge of a mathematical model of the linear time-invariant (LTI) system, was introduced by Kalman and Luenberger [62] in the 1960s.

The estimate of the variables of concern is accomplished through the Kalman filter in the stochastic case or through Luenberger observer, also said proportional gain observer, in the deterministic case. An observer (or filter) is a dynamic system that outputs an estimate of the process state from the

inputs, outputs and the system model and, using a correction proportional to the difference between the measured and the estimated output. The correction gain for the Luenberger observer is obtained by imposing a convergence speed of the estimation error. As for the Kalman filter, it uses the statistical properties and noise of the system to obtain the optimal correction gain minimizing the variance of the estimation error. The reconstruction of state for systems characterized by LTI model seems to have reached a certain maturity and there are many synthesis algorithms available.

However, different approaches, leading to a state estimation for specific classes of nonlinear models, have been proposed in the literature. Most of these approaches are extensions of concepts introduced by Kalman or Luenberger. The most widespread are undoubtedly the extended Kalman filter (EKF) and the observer of extended Luenberger. Under these approaches, estimating the state of the system is carried out from a linearization at every moment of the nonlinear pattern along the estimated trajectories. This approach is valid only for models locally differentiable and estimation error convergence is guaranteed only locally. The nonlinear function is linearized around current estimate. Other techniques allow obtaining an auxiliary linear system from a transformation (change of coordinates) of the nonlinear system state. It is thus possible, using conventional techniques, to design an observer in the new coordinate of system. An inverse transformation then leads to obtain a nonlinear observer for the origin nonlinear system. The main drawback of this approach is due to the restrictive conditions of appropriate transformation availability [63].

The high gain observers are applicable for systems that cannot be linearized by a change of coordinates, but provided that the system is globally Lipschitz. These observers have a structure similar to Luenberger observer. As its name refers, this observer uses a large gain which increases according to constants of Lipschitz of the system. This gain compensates the effects of non-linear part of the system on the estimation error. The literature provides various syntheses of high gain observer techniques. The adaptive gain observers proposed in [64], combines high-gain type observer with extended Kalman filter to allow the benefit from advantages of each structure. This behavior type of observer has an initial large gain type whose global convergence is proved and an asymptotic behavior close to that of extended Kalman filter with remarkable strength properties. More recently, so-called algebraic methods applied to early state estimate closed loop delivered in this direction are encouraging [65]. All these methods require precise knowledge of a nonlinear mathematical model of the system over the entire operating range. However, obtaining such a model is far from being easy because of the complex nature of nonlinear systems. Black-box identification techniques are often relied on to represent mathematically the system dynamic behavior. The choice of the internal structure of the model is the keystone of these identification techniques. Indeed, the model structure must, firstly, be general enough so as to take into account a diverse number of modeling situations and, secondly, be able to promote further exploitation. Using the multi-model it is allowed to achieve an excellent compromise between the two.

In this section, we will present some methods among the most used in the case of the sensorless control of PMSM. But before addressing this issue, a study of PMSM observability is presented.

III.1.1. Observability study of PMSM

As already mentioned, in case of sensorless approach, if the system state must be rebuilt, an observer then is needed. Indeed, an observer is a mathematical means of measurement allowing the estimation of a system state from a limited amount of information (the inputs and outputs of the system). Definitely, before trying to reconstruct the system state, there is a necessity to know if the state variables are observable or not. The concept of observability is whether the state can be reconstructed from the input and output signals. In the case of linear systems, observability is determined, conventionally, by an order condition. In the case of nonlinear systems, which is the case of PMSM, the notion of observability depends on both inputs and the initial conditions [66].

To study the observability of synchronous machine, the model given by equations in (α-β) is considered whose differential writing can be deduced by (12):

$$L_S \frac{d}{dt}\begin{bmatrix} i_\alpha \\ i_\beta \end{bmatrix} = \begin{bmatrix} v_\alpha \\ v_\beta \end{bmatrix} - R_S \begin{bmatrix} i_\alpha \\ i_\beta \end{bmatrix} + K\,\omega \begin{bmatrix} \sin\theta \\ -\cos\theta \end{bmatrix} \tag{12}$$

with v_α, v_β voltages in α-β reference (V), i_α, i_β currents in α-β reference (A), K flux magnets constant, ω electrical speed of the rotor ($\omega = p\Omega$ with p number of pole pairs) and θ ($\theta = \omega t$) electrical position.

It is assumed that the variation of machine parameters, the stator resistance, the stator inductor and the flux of magnets, is so slow compared to that of the currents and speed. Thus, it can be assumed that $d/dt\, R_S = d/dt\, L_S = d/dt\, \psi = 0$ and that R_S and L_S are known (ψ is the induced flux by the permanent magnets).

Let ψ_α and ψ_β the two-phase stator flux of PMSM given by (13):

$$\frac{d}{dt}\begin{bmatrix} \psi_\alpha \\ \psi_\beta \end{bmatrix} = \begin{bmatrix} v_\alpha \\ v_\beta \end{bmatrix} - R_S \begin{bmatrix} i_\alpha \\ i_\beta \end{bmatrix} \tag{13}$$

Therefore, that results in (14):

$$\left(\psi_\alpha - L_S i_\alpha\right)^2 + \left(\psi_\beta - L_S i_\beta\right)^2 = \varphi_F^2 \cos^2\theta + \varphi_F^2 \sin^2\theta = \varphi_F^2 \tag{14}$$

It is defined in (15) that:

$$\psi_\alpha^2+\psi_\beta^2+\left(L_S i_\alpha\right)^2+\left(L_S i_\beta\right)^2-2\left(\psi_\alpha L_S i_\alpha+\psi_\beta L_S i_\beta\right)-\varphi_F^2=0 \tag{15}$$

A measurable output y must be defined and ψ_α and ψ_β must be reconstructed to build the function of observability $H_{Obs}=\left(y,\frac{dy}{dt},\frac{d^2y}{dt^2}\right)^T$. Hence, it is possible to calculate the instantaneous observability of ψ_α and ψ_β, *i.e.* φ_f and θ by illustrating the injectivity of observability function H_{Obs} for every *t*.

After defining y, the calculation of $\frac{dy}{dt}$ and $\frac{d^2y}{dt^2}$ are carried out respectively in (16) and (17):

$$\left.\begin{aligned}
&y=\left(L_S i_\alpha\right)^2+\left(L_S i_\beta\right)^2-\varphi_F^2=\psi_\alpha^2+\psi_\beta^2-2\left(L_S\psi_\alpha i_\alpha+L_S\psi_\beta i_\beta\right)\\
&\frac{dy}{dt}=2\frac{d\psi_\alpha}{dt}\psi_\alpha+2\frac{d\psi_\beta}{dt}\psi_\beta-2L_S\psi_\alpha\frac{di_\alpha}{dt}-2L_S i_\alpha\frac{d\psi_\alpha}{dt}-2L_S\psi_\beta\frac{di_\beta}{dt}-2L_S i_\beta\frac{d\psi_\beta}{dt}\\
&\frac{dy}{dt}+2L_S i_\alpha\frac{d\psi_\alpha}{dt}+2L_S i_\beta\frac{d\psi_\beta}{dt}=2\frac{d\psi_\alpha}{dt}\psi_\alpha+2\frac{d\psi_\beta}{dt}\psi_\beta-2L_S\psi_\alpha\frac{di_\alpha}{dt}-2L_S\psi_\beta\frac{di_\beta}{dt}\\
&\frac{dy}{dt}+2L_S i_\alpha\left(v_\alpha-R_S i_\alpha\right)+2L_S i_\beta\left(v_\beta-R_S i_\beta\right)=2\frac{d\psi_\alpha}{dt}\psi_\alpha+2\frac{d\psi_\beta}{dt}\psi_\beta-2L_S\psi_\alpha\frac{di_\alpha}{dt}-2L_S\psi_\beta\frac{di_\beta}{dt}\\
&\frac{dy}{dt}+2L_S i_\alpha\left(v_\alpha-R_S i_\alpha\right)+2L_S i_\beta\left(v_\beta-R_S i_\beta\right)=2\psi_\alpha\left(\frac{d\psi_\alpha}{dt}-L_S\frac{di_\alpha}{dt}\right)+2\psi_\beta\left(\frac{d\psi_\beta}{dt}-L_S\frac{di_\beta}{dt}\right)
\end{aligned}\right\} \tag{16}$$

$$\left.\begin{aligned}
&\frac{d^2y}{dt^2}+\frac{d\left(2L_S i_\alpha\left(v_\alpha-R_S i_\alpha\right)+2L_S i_\beta\left(v_\beta-R_S i_\beta\right)\right)}{dt}\\
&=2\frac{d\psi_\alpha}{dt}\left(\frac{d\psi_\alpha}{dt}-L_S\frac{di_\alpha}{dt}\right)+2\psi_\alpha\left(\frac{d^2\psi_\alpha}{dt^2}-L_S\frac{d^2i_\alpha}{dt^2}\right)\\
&\quad+2\frac{d\psi_\beta}{dt}\left(\frac{d\psi_\beta}{dt}-L_S\frac{di_\beta}{dt}\right)+2\psi_\beta\left(\frac{d^2\psi_\beta}{dt^2}-L_S\frac{d^2i_\beta}{dt^2}\right)\\
&\frac{d^2y}{dt^2}-2\frac{d\psi_\alpha}{dt}\left(\frac{d\psi_\alpha}{dt}-L_S\frac{di_\alpha}{dt}\right)-2\frac{d\psi_\beta}{dt}\left(\frac{d\psi_\beta}{dt}-L_S\frac{di_\beta}{dt}\right)\\
&\quad+\frac{d\left(2L_S i_\alpha\left(v_\alpha-R_S i_\alpha\right)+2L_S i_\beta\left(v_\beta-R_S i_\beta\right)\right)}{dt}\\
&=2\psi_\alpha\left(\frac{d^2\psi_\alpha}{dt^2}-L_S\frac{d^2i_\alpha}{dt^2}\right)+2\psi_\beta\left(\frac{d^2\psi_\beta}{dt^2}-L_S\frac{d^2i_\beta}{dt^2}\right)
\end{aligned}\right\} \tag{17}$$

Now, by defining the following changing in structure of variables in matrices form as in (18):

$$
\begin{aligned}
D_1 &= y \\
D_2 &= \frac{dy}{dt} + 2L_S i^T C_v \\
D_3 &= \frac{d^2 y}{dt^2} - 2\frac{d\left(\psi - L_S i\right)}{dt} C_v + \frac{d\left(2L_S i^T C_v\right)}{dt}
\end{aligned} \tag{18}
$$

where: $i = \begin{bmatrix} i_\alpha & i_\beta \end{bmatrix}^T$ and $C_v = \frac{d}{dt}\begin{bmatrix} \psi_\alpha \\ \psi_\beta \end{bmatrix} = \begin{bmatrix} v_\alpha \\ v_\beta \end{bmatrix} - R_S \begin{bmatrix} i_\alpha \\ i_\beta \end{bmatrix}$.

These three new variables, D_1, D_2 and D_3 are measurable. For the system to be observable, it is necessary that from $\left(D_1, D_2, D_3\right)$ must be calculated only one ψ. It is proceed by contradiction assuming that there are ψ_1 and ψ_2. Then, in this case, gives the equivalent (19):

$$
\left\{\begin{aligned}
D_1 &= |\psi_1|^2 - 2L_S i^T \psi_1 = |\psi_2|^2 - 2L_S i^T \psi_2 \\
D_2 &= 2\frac{d\left(\psi_1 - L_S i\right)}{dt}\psi_1 = 2\frac{d\left(\psi_2 - L_S i\right)}{dt}\psi_2 \\
D_3 &= 2\frac{d^2\left(\psi_1 - L_S i\right)}{dt^2}\psi_1 = 2\frac{d^2\left(\psi_2 - L_S i\right)}{dt^2}\psi_2
\end{aligned}\right\} \Leftrightarrow \left\{\begin{aligned}
&|\psi_1|^2 - 2L_S i^T \psi_1 - |\psi_2|^2 + 2L_S i^T \psi_2 = 0 \\
&2\frac{d\left(\psi_1 - L_S i\right)}{dt}\psi_1 - 2\frac{d\left(\psi_2 - L_S i\right)}{dt}\psi_2 = 0 \\
&2\frac{d^2\left(\psi_1 - L_S i\right)}{dt^2}\psi_1 - 2\frac{d^2\left(\psi_2 - L_S i\right)}{dt^2}\psi_2 = 0
\end{aligned}\right\} \tag{19}
$$

Therefore, by rewriting equation (19) and considering that $\lambda_1 = \left(\psi_1 - \psi_2\right)/2$ and $\lambda_2 = \left(\psi_1 + \psi_2\right)/2$, it becomes as in (20) and (21):

$$
\left\{\begin{aligned}
&4\left(\lambda_2 - L_S i^T\right)\lambda_1 = 0 \\
&\left(2\frac{d\left(\psi_1 - L_S i\right)}{dt} - 2\frac{d\left(\psi_2 - L_S i\right)}{dt}\right)2\lambda_1 = 0 \\
&\left(2\frac{d^2\left(\psi_1 - L_S i\right)}{dt^2} - 2\frac{d^2\left(\psi_2 - L_S i\right)}{dt^2}\right)2\lambda_1 = 0
\end{aligned}\right\} \Leftrightarrow \left\{\left[\begin{array}{c}
4\left(\psi_1 - L_S i^T + \psi_2 - L_S i^T\right) \\
\left(\frac{d\left(\psi_1 - L_S i\right)}{dt} - \frac{d\left(\psi_2 - L_S i\right)}{dt}\right)^T \\
\left(\frac{d^2\left(\psi_1 - L_S i\right)}{dt^2} - \frac{d^2\left(\psi_2 - L_S i\right)}{dt^2}\right)^T
\end{array}\right]\lambda_1 = 0\right\} \tag{20}
$$

$$
\left[\begin{array}{cc}
2\varphi_f \cos\theta & 2\varphi_f \sin\theta \\
-\varphi_f\, \omega \sin\theta & \varphi_f\, \omega \cos\theta \\
-\varphi_f \frac{d\omega}{dt}\sin\theta - \varphi_f\, \omega\cos\theta & \varphi_f \frac{d\omega}{dt}\cos\theta - \varphi_f\, \omega \sin\theta
\end{array}\right]\lambda_1 = A_1\lambda_1 = 0 \tag{21}
$$

To have a unique solution, *i.e.* $\psi_1 = \psi_2$, the matrix A_1 must be invertible. Based on (21), it can be proved that if $\omega \neq 0$, the matrix A_1 is invertible, which makes it necessary that $\psi_1 = \psi_2$. Otherwise, at standstill, the matrix A_1 is reversible and in this case of $\psi_1 \neq \psi_2$ the instantaneous observability of ψ

is not guaranteed. Thus, it is demonstrated that for a non-zero speed, the position and the machine flux can be observed if the stator resistance and inductance are well-known.

III.2. Various types of estimators

To classify the methods of position estimation, the principle and the used technique have to be differentiated. So, as principle, there are two methods, one depends on estimating the EMF or extended EMF, and another depends on rotor flux estimation or saliency phenomenon.

Several works based on the first approach, either by using observers [67] and [71], or a voltage model compares between the calculated and detected variables [72]-[77], or fuzzy logic technique [78]. In the case of techniques using a model of voltages and currents, the measured phase parameters (voltages and/or currents) are used to estimate the position based on the equations of machine. For machines with intern magnets, the approach of extended EMF (EEMF) is used because of the approximations of normal method of EMF, which can lead to estimation errors and therefore instability in the system [79]-[81]. However, the parameters variation due to temperature and saturation affects the accuracy of the estimate. In methods using technique of a state observer or the Kalman filter, the effect of parameters variation is not as critical as in the case of methods of voltage model. However, the common problem to this class of techniques is the direct association between the accuracy of the estimated rotor position and amplitude of the EMF which is proportional to the rotational speed. Indeed, in the range of low speeds, where the EMF is very low, the estimate is significantly degraded. To resolve this problem, an injection of a high frequency current is considered to detect small changes in EMF in the machine phases. The use of this strategy allowed obtaining a maximum torque at PMSM start-up. Some algorithms, as given in [82], using EKF, model reference adaptive system (MRAS) or other methods based on sophisticated identification procedures, allow, under certain conditions, the operation from zero speed; but they need a complex mathematical model and they are expensive to use in commercial systems [83]. In this approach, a system model with the same real inputs is involved to produce an estimate of the output, which is supplied as a feedback to the model to correct the estimate. EKF is used for this estimate and shows high performance [60], [83]-[86].

In the second approach, using the flux linkage is best known for several years. The basic idea is simple, based on the phase-voltage equation that can be written as in (22):

$$\left.\begin{aligned} v &= R_S i + d\varphi/dt \\ \varphi &= \int \left(v - R_S i\right) dt \end{aligned}\right\} \tag{22}$$

Hence, it is possible to still obtain an estimate of flux linkage phase by the previous integrating [3]. Anyway, due to issues of isolation, this is not practical to measure the voltage at the phase's terminals.

In addition, that is due to the dead time of the switching signals of voltage commutation, because of the large error. On other hand, to achieve this estimate, an observer with mechanical model or non-mechanical model can also be used. All types of machines use frequently the principle of closed-loop observer [94]-[104]. Techniques that exploit magnetic saliency phenomenon are mainly based on the injection voltage or current signals at high frequency (HF) in the phases of the synchronous machine and utilize signals that are induced to detect the rotor position. Another technique known as INFORM (indirect flux detection by on-line reactance measurement) is injected to the machine phase voltage vector rotating at a high frequency and uses a tracking algorithm of current response. However, it is used only in the case of interior permanent magnet (IPM) synchronous machine. It is applied in several jobs [75], [87]-[93]. Moreover, it is used as a complementary technique to estimate the initial position and in the region of low speed [79], [94]-[97]. The use of this class of methods in high speeds is not desirable because the injected HF signal superimposed on the machine power generates a couple parasite that can degrade the performance of the drive [79].

Various position estimation techniques have been developed for brushless machines, and many are still developing. Concerning rotor position information, sensorless control techniques can be divided into two classes [105]. The first one, well-known since several years, uses the flux linkage variation; it is based on high frequency signal injection to extract the rotor position [106], [107]. This method explores the rotor anisotropies from HF signals that are injected into the machine, and so it allows operation at low speed and at standstill. However, the injected signals can produce harmonic currents, which increase electrical losses and induce torque oscillations. Furthermore, it is quite complex and requires special development both in control design and signal conditioning to extract the rotor position [105]. Therefore, the most highlight advantage of this technique that it can be used in the whole region of speed including standstill and low speed. But, on the other hand, it generates extra losses and torque ripples and consequently a lot of noise. For that reason it is often used just for zero and low speed [119].

The second method is based on motional EMF or fundamental excitation [108], [109], either by using an observer, a voltage model comparing between calculated and detected variables or by fuzzy logic and other intelligent techniques. So, in general, this method depends on the machine model to estimate its EMF, which in turn, can provide the information of the rotor position and speed. This method is suitable for medium and high speed range and remains the standard industrial solution [105]. One major problem in back-EMF based methods is their poor performance in low speeds due to low signal to noise ratio in the sampled back-EMF [118]. Thus, for both machine starting and steady state, the fundamental excitation and the signal injection methods can sometimes work together. In [118], both of them were combined using an observer by model reference adaptive system. This solution improved the operation at low speed range; however, torque ripple can come out due to the injected signals. It is carried out with high performance in [120]; it is proposed for surface mounted PMSM an

field-programmable gate array (FPGA) based hybrid sensorless controller combining a linearly compensated flux observer and the alternating voltage HF injection method. The main idea is that model-based observers cannot work well at low speed; therefore, the signal injection method is used. A hybrid observer is used to perform a smooth transition between both strategies, in which the estimated flux angle is obtained with the linear combination of both observers. As in [120], also [121] presented sensorless PMSM control employing the HF injection algorithm and combined it with the extended Kalman filter for estimation of rotor position and speed in the whole range. Both algorithms have partial usage. The former one can be used in standstill and in very low speeds whilst EKF can be employed in higher speeds. A proper transition between the two strategies is achieved by a hybrid estimator which is based on probabilities calculation for each particular estimation algorithm. In [122], to extract the rotor position information, HF signal injection was used at very low speeds below 100rpm, while to obtain it at speeds superior than 500rpm a sliding mode observer (SMO) was used. A weighting algorithm was performed as a handover between these two processes and it takes place when the drive is operating between 100 and 500rpm. It showed that the proposed sensorless drive system is able to estimate the rotor position and speed accurately at very low speeds including standstill during both steady-state and dynamic operations under both loaded and unloaded conditions.

In addition, as mentioned above, due to current advanced microprocessor technology, some applications of classical state observers of modern control theory arise: optimal state observers, Luenberger observer and EKF [123].

The next parts present the most frequent used types of estimation methods to conclude which is the most appropriate for the studied system. Firstly, in the next part, EMF method is applied in this work by using an observer, the SMO and a study of this observer based on EMF estimation is carried out. Then, a study of speed and position estimation by phase locked loop (PLL) is carried out using second method of rotor flux estimation. Subsequently, MRAS algorithm is applied in the rotor reference frame and speed and position estimation is obtained. Finally, EKF approach is applied in both stator and rotor reference frames to examine its performance in estimating rotor speed and position.

III.2.1. EMF (Electromotive-Force)

Regarding the fundamental excitation method, there are various techniques and strategies to employ this method. The back-EMF can be calculated based on the voltage and current measurements using the machine model or by some technique such as the model reference adaptive systems and the observers. Authors of [108] and [124] estimated the EMF using voltage and current measures. In the former, it is done through operational amplifiers by integration, which can degrade the accuracy of the estimation, where in the latter voltage transducers built around isolation operational amplifiers to achieve more accurate estimation. A nonlinear position observer was proposed in [125], where

stability analysis is carried out in continuous-time domain and it is shown that, depending on the load condition, the system performance degrades when the speed approaches zero. This is the main drawback of this technique.

III.2.1.1. SMO (Sliding Mode Observer)

SMO has attracted the attention of researchers for its robustness, speed of convergence, good performance and low sensitivity to parameter uncertainty. In [66], the author presents two types of SMO: one SMO of first order using EMF and complete model of the machine and another SMO of higher order. These methods are based on the estimation of the EMF which is proportional to the rotor speed. The principle of the SMO is to force the dynamics of an *n*-order system using discontinuous functions to converge to a range S of dimension (n-n_1) called sliding surface (where n_1 is the dimension of the measurement vector). Thus, the sliding mode control is a nonlinear concept which is to "bring the state trajectory to the sliding surface and to change it with some momentum to the point of balance" [66].

Three steps are therefore essential to develop a SMO. First, it requires a switching surface given by $S(x)=0$. Then, it must define the convergence condition. Finally, it determines the control law.

An observer in classical sliding mode whose correction term is a sign function was used in [110], [111]. In [110], a SMO is presented for the PMSM. This observer allows the estimation of the rotor position and speed from the measurements of voltages and stator currents. The effectiveness of this observer has been tested in simulation. In [111], a sensorless control scheme have been proposed based on the sliding mode technique to estimate the position and speed of the PMSM. They integrated the Lyapunov algorithm to determine the law of adaptation of speed and stator resistance. Despite the effectiveness of this observer, the chattering phenomenon caused by the sign function, used as a switching function in the classic SMO, is still a major drawback. This causes oscillations, degradation of performance and even system instability. Indeed, the magnitude of EMF is very small at low speed, which affects the accuracy of estimation of the rotor position. To overcome this problem, a low-pass filter and an additional compensation of the rotor position are used. However, by adopting this solution, the delay caused by the filter is still an issue.

To reduce this phenomenon and to increase the accuracy of rotor position estimation at low speed and stability of the high-speed system, some improvements were made by replacing the sign function with softer features. Some researchers have proposed replacing the sign function with saturation function [112]. Using this function greatly reduces the chattering, but the presence of a low-pass filter cannot be avoided.

Other solutions proposed in the literature have replaced the sign function by a sigmoid function [113], [114]. The latter allows a smooth transition and therefore a considerable reduction of the chattering

phenomenon to the two other switching functions. A comparative study of the three switching functions was carried out in [115]. Based on simulation results, it has been found that the use of the sigmoid function allows a greater improvement relative to the two other switching functions.

In [116], a hybrid SMO has been developed combining two types of SMO. The first is non-singular terminal sliding mode which enables rapid convergence with good accuracy. The second, a SMO of high order guarantees stability and solves the chattering problem.

The difference between SMO and more traditional observers, ***e.g.*** Luenberger observers, is that there is a non-linear term injected into the observer depending on the output estimation error. The concept of sliding mode was originally applied to control system design and later applied for estimating system states [118]. In [118], a method of designing a sliding mode linear functional observer has been illustrated for a system with unknown inputs. It presented the existence conditions for the observer and proposed a structure and design algorithm for the SMO. The proposed algorithm was then applied for sensorless control of PMSM.

In this approach, system has robust properties in opposition to parameters uncertainties and external disturbances. Thus, it can be applied in critical environment like wind energy conversion system. However, it is important to indicate that the observers design and stability analysis are usually carried out in continuous-time domain, while their implementations are in discrete-time domain. Hence, the continuous-time sliding mode conditions can fail to predict stability performance of the system [130], [131]. Alternatively, [132]-[134] suggest sensorless control by means of sliding mode approach. The most important reasons to use sliding mode are: easy implementation, reduced order and inherent robustness in the presence of parameter uncertainties and of perturbations, which are attractive advantages [135].

In this section, a SMO based on [117] is presented. This observer is chosen due to its following advantages:

- It is based on EEMF which involves simple equations, generic and applicable to all types of synchronous machines.
- It uses only two of machine parameters: the stator resistance R_S and inductance of the transverse axis L_q.
- It does not use the machine speed as input.

All variables with an asterisk (*e.g.* i^*) are reference values, with a hat (*e.g.* $\hat{i}$) are estimated values and with a tidemark (*e.g.* $\tilde{i}_\alpha$) are error estimation values.

Electrical equations of PMSM in the fixed reference (α-β) are given by (23) (see Appendix II):

$$\begin{bmatrix} v_\alpha \\ v_\beta \end{bmatrix} = R_S \begin{bmatrix} i_\alpha \\ i_\beta \end{bmatrix} + L_S \frac{d}{dt}\begin{bmatrix} i_\alpha \\ i_\beta \end{bmatrix} + K\,\omega \begin{bmatrix} \sin\theta \\ -\cos\theta \end{bmatrix} \tag{23}$$

The electrical equations of synchronous machine in α-β reference may be formulated as in (24) using the equivalent of EMF:

$$\frac{d}{dt}\begin{bmatrix} i_\alpha \\ i_\beta \end{bmatrix} = \frac{1}{L_S}\begin{bmatrix} v_\alpha \\ v_\beta \end{bmatrix} - \frac{R_S}{L_S}\begin{bmatrix} i_\alpha \\ i_\beta \end{bmatrix} - \frac{1}{L_S}\begin{bmatrix} e_\alpha \\ e_\beta \end{bmatrix} \tag{24}$$

A SMO can be defined as in (25):

$$\frac{d}{dt}\begin{bmatrix} \hat{i}_\alpha \\ \hat{i}_\beta \end{bmatrix} = \frac{1}{L_S}\begin{bmatrix} v_\alpha \\ v_\beta \end{bmatrix} - \frac{R_S}{L_S}\begin{bmatrix} \hat{i}_\alpha \\ \hat{i}_\beta \end{bmatrix} - \frac{K_{SMO}}{L_S}\begin{bmatrix} \text{sign}(\hat{i}_\alpha - i_\alpha) \\ \text{sign}(\hat{i}_\beta - i_\beta) \end{bmatrix} \tag{25}$$

with K_{SMO} the observer gain and $\text{sign}(\hat{i}_\alpha - i_\alpha)$ given by (26):

$$\text{sign}(\hat{i}_\alpha - i_\alpha) = \begin{cases} 1 & if \quad (\hat{i}_\alpha - i_\alpha) > 0 \\ 0 & if \quad (\hat{i}_\alpha - i_\alpha) = 0 \\ -1 & if \quad (\hat{i}_\alpha - i_\alpha) < 0 \end{cases} \tag{26}$$

The dynamics of the error along the sliding surface are defined by (27), as the difference between the equation (24) and equation (25):

$$\frac{d}{dt}\begin{bmatrix} \tilde{i}_\alpha \\ \tilde{i}_\beta \end{bmatrix} = -\frac{R_S}{L_S}\begin{bmatrix} \tilde{i}_\alpha \\ \tilde{i}_\beta \end{bmatrix} - \frac{1}{L_S}\begin{bmatrix} e_\alpha \\ e_\beta \end{bmatrix} - \frac{K_{SMO}}{L_S}\begin{bmatrix} \text{sign}(\tilde{i}_\alpha) \\ \text{sign}(\tilde{i}_\beta) \end{bmatrix} \tag{27}$$

with $\tilde{i}_\alpha$ and $\tilde{i}_\beta$ given in (28) observation errors of current i_α and i_β respectively:

$$\begin{bmatrix} \tilde{i}_\alpha \\ \tilde{i}_\beta \end{bmatrix} = \begin{bmatrix} \hat{i}_\alpha - i_\alpha \\ \hat{i}_\beta - i_\beta \end{bmatrix} \tag{28}$$

The stability analysis of this observer is carried out by considering a Lyapunov function V given by (29):

$$V = \frac{1}{2}(\tilde{i}_\alpha^2 + \tilde{i}_\beta^2) \tag{29}$$

The derivative of this function relative to time is given by (30):

$$\frac{d}{dt}V = \left(\frac{d}{dt}\tilde{i}_\alpha\right)\tilde{i}_\beta + \left(\frac{d}{dt}\tilde{i}_\beta\right)\tilde{i}_\alpha = -\frac{R_S}{L_S}(\tilde{i}_\alpha^2 + \tilde{i}_\beta^2) + \frac{1}{L_S}(e_\alpha\tilde{i}_\alpha + e_\beta\tilde{i}_\beta) - \frac{K_{SMO}}{L_S}(|\tilde{i}_\alpha| + |\tilde{i}_\beta|) \tag{30}$$

The observer is stable if $\frac{d}{dt}V < 0$. Therefore, it is obtained $-\frac{R_S}{L_S}\tilde{i}_\alpha^2 < 0$ and $-\frac{R_S}{L_S}\tilde{i}_\beta^2 < 0$.

Hence, it is sufficient to check the inequality (31):

$$\frac{1}{L_S} e_\alpha \tilde{i}_\alpha - \frac{K_{SMO}}{L_S} |\tilde{i}_\alpha| + \frac{1}{L_S} e_\beta \tilde{i}_\beta - \frac{K_{SMO}}{L_S} |\tilde{i}_\beta| < 0 \tag{31}$$

In other words, it is necessary that (32) to be checked:

$$K_{SMO} > \max(|e_\alpha|, |e_\beta|) \tag{32}$$

The estimated currents tend toward actual currents as soon the observer reaches the sliding surface. In this case, $\tilde{i}_\alpha = 0$ and $\tilde{i}_\beta = 0$. In order to force the convergence $\hat{i}_\alpha$ to i_α and $\hat{i}_\beta$ to i_β, a desired value of the observation error is set equal to zero. Then, the estimation scheme given in Figure 39 is applied. Once the sliding surface is reached and the observation error tends to zero, EMF is given by the equation (33):

$$\begin{bmatrix} e_\alpha \\ e_\beta \end{bmatrix} = K_{SMO} \begin{bmatrix} \text{sign}_S(\tilde{i}_\alpha) \\ \text{sign}_S(\tilde{i}_\beta) \end{bmatrix} \tag{33}$$

where sign_S is the equivalent function to the sign function in the sliding surface.

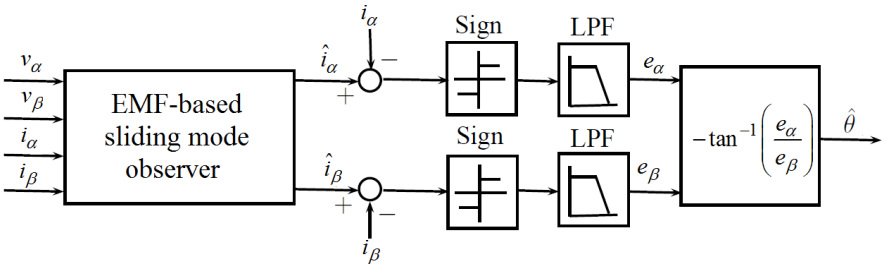

Figure 39. Block diagram of the SMO based on EME

Low-pass filters (LPF) are used to extract e_α and e_β. The estimated rotor position is then given by (34):

$$\hat{\theta} = -\tan^{-1}\left(\frac{e_\alpha}{e_\beta}\right) = -\tan^{-1}\left(\frac{K_{SMO}\,\text{sign}_S(\tilde{i}_\alpha)}{K_{SMO}\,\text{sign}_S(\tilde{i}_\beta)}\right) \tag{34}$$

In the ideal case, *i.e.* for a stable system, the trajectory given by the estimation errors of the currents slides on the sliding surface. However in this case, because of the delay due to the switching time, the estimated currents fluctuate around the true value. This phenomenon, chattering, will affect the control accuracy by causing oscillation or instability and degrading system performance. That is why the sign function used in [117] is replaced by the sigmoid function to reduce the effect of chattering.

In this case, the observer's equations become as in (35):

$$\frac{d}{dt}\begin{bmatrix}\hat{i}_\alpha \\ \hat{i}_\beta\end{bmatrix}=\frac{1}{L_S}\begin{bmatrix}v_\alpha \\ v_\beta\end{bmatrix}-\frac{R_S}{L_S}\begin{bmatrix}\hat{i}_\alpha \\ \hat{i}_\beta\end{bmatrix}-\frac{K_{SMO}}{L_S}\begin{bmatrix}H(\hat{i}_\alpha - i_\alpha) \\ H(\hat{i}_\beta - i_\beta)\end{bmatrix} \tag{35}$$

where H is the sigmoid function given by (36) and a in (36) is a positive constant used to adjust the slope of sigmoid function. It acts on the reaching mode:

$$\begin{bmatrix}H(\tilde{i}_\alpha) \\ H(\tilde{i}_\beta)\end{bmatrix}=\begin{bmatrix}\left(\frac{2}{1+\exp(-a\,\tilde{i}_\alpha)}\right)-1 \\ \left(\frac{2}{1+\exp(-a\,\tilde{i}_\beta)}\right)-1\end{bmatrix} \tag{36}$$

This is the first step of the estimation by sliding mode where the state vector must reach the sliding surface. The sliding surface may be defined by the estimation error of the currents i_α and i_β as (37):

$$S_n=\begin{bmatrix}S_\alpha \\ S_\beta\end{bmatrix}=\begin{bmatrix}\tilde{i}_\alpha \\ \tilde{i}_\beta\end{bmatrix}=0 \tag{37}$$

After sliding mode reaches the observer becomes robust vis-a-vis the parameter variations. This is the second step in the sliding mode estimation where the state vector must slide on the sliding surface, given by $S_n=0$ to reach the point of equilibrium.

To investigate the stability of this observer, the Lyapunov function given by (38) is considered. The derivative of this function relative to time is:

$$\frac{d}{dt}V=-\frac{R_S}{L_S}(\tilde{i}_\alpha^2+\tilde{i}_\beta^2)+\frac{1}{L_S}(e_\alpha\tilde{i}_\alpha-K_{SMO}\,\tilde{i}_\alpha\,H(\tilde{i}_\alpha))+\frac{1}{L_S}(e_\beta\tilde{i}_\beta-K_{SMO}\,\tilde{i}_\beta\,H(\tilde{i}_\beta)) \tag{38}$$

In this case, it must be:

$$K_{SMO}>\max(|e_\alpha|,|e_\beta|) \tag{39}$$

After reaching the sliding mode, the EMF may be given by (40):

$$\begin{bmatrix}e_\alpha \\ e_\beta\end{bmatrix}=K_{SMO}\begin{bmatrix}H_S(\tilde{i}_\alpha) \\ H_S(\tilde{i}_\beta)\end{bmatrix} \tag{40}$$

where $H_S(\tilde{i}_\alpha)$ and $H_S(\tilde{i}_\beta)$ are the EMF on the sliding surface.

The chattering problem is solved using the observer proposed above, which uses the sigmoid function as switching function. This function is characterized by a range of operation, *i.e.* $-1<H(\tilde{i}_\alpha)<1$ and $-1<H(\tilde{i}_\beta)<1$ unlike the sign function which is equal to either 1 or -1.

Using the equations given in (40), the rotor position can be derived by (41):

$$\hat{\theta} = -\tan^{-1}\left(\frac{e_\alpha}{e_\beta}\right) = -\tan^{-1}\left(\frac{K_{SMO}\,\mathrm{H}_S(\tilde{i}_\alpha)}{K_{SMO}\,\mathrm{H}_S(\tilde{i}_\beta)}\right) \tag{41}$$

III.2.1.2. Experimental results of SMO method

This method is verified experimentally using the dSPACE 1104 and MATLAB environment. Three phase diode bridge is used to extract and convert the AC power generated by PMSM into DC power which is supplied to the programmable electronic load (PEL) as shown in Figure 40. An encoder (TS2620N861E11 from Tamagawa) is used to extract the real position of machine rotor. This position is shown in results to compare the estimated one with it.

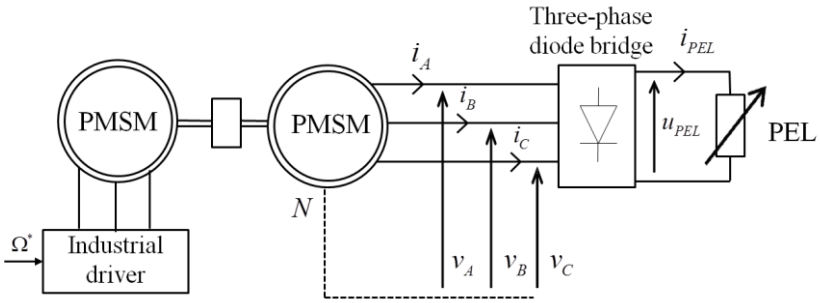

Figure 40. Experimental configuration for position estimation test

The estimated position uses only the measurements of stator voltages and currents which are illustrated in Figure 41 at wind speed of 8m/s where DC voltage bus is equal to its reference. The test of position estimation is carried out at two limit value of wind speed slowest 4m/s and highest 8m/s at the point which is corresponding to its maximum power point. This is done by varying the nominal value of speed to its upper and lower neighborhood. To achieve this variation test and to verify the performance of estimation, the DC bus voltage, which is in our case the same as load voltage, is varied by value of ±10V.

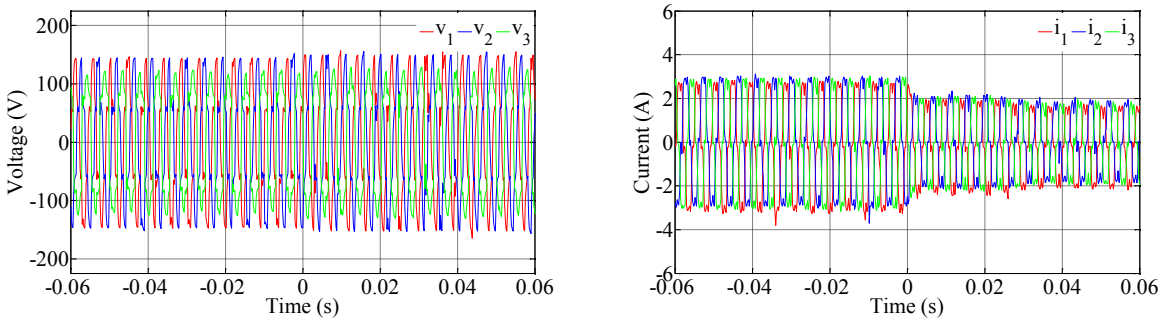

Figure 41. Stator voltages and currents at wind speed 8m/s – SMO method

SMO has good performance in transient case for the two values of wind speed (Figure 42 and Figure 43). Thus, the robustness of the observer is tested vis-a-vis the speed variations, where the value of the DC bus voltage is varied ± 10V for each point.

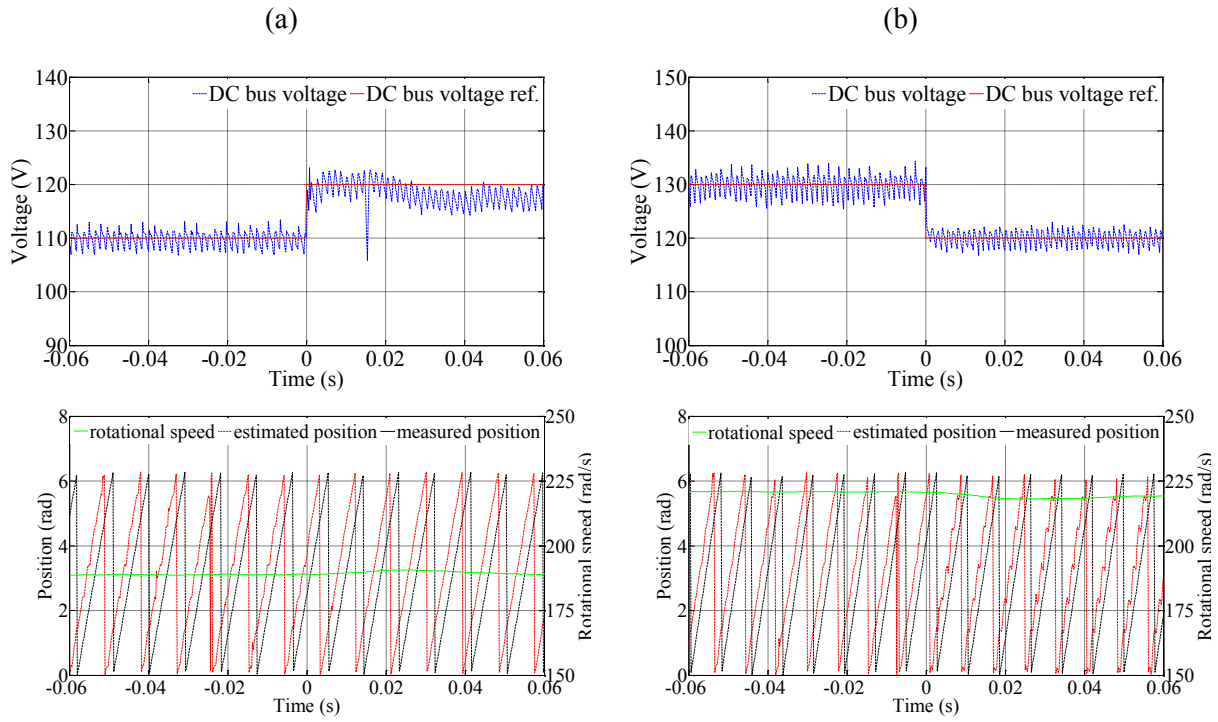

Figure 42. Position estimation by SMO method at wind speed value of 4m/s

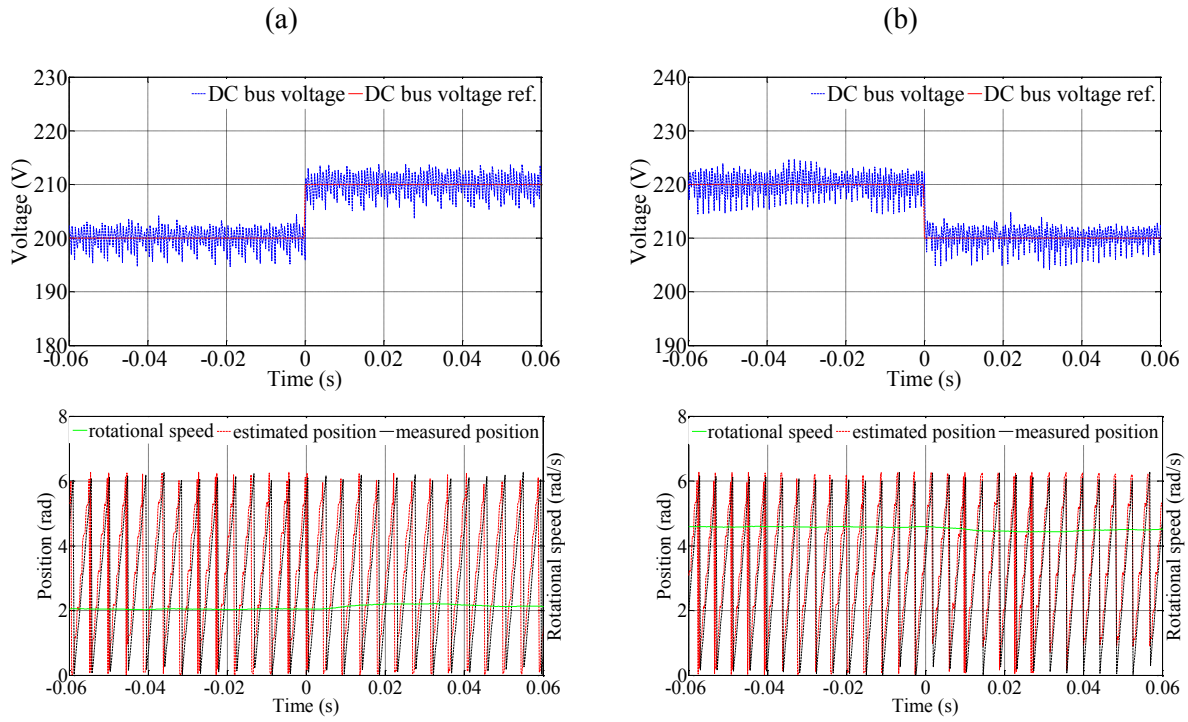

Figure 43. Position estimation by SMO method at wind speed value of 8m/s

In tuning this observer, it is noted that the estimation accuracy is directly related to two quantities; the first is the gain of SMO and the second is time constant of the low pass filter that is used to get the estimated state. It is preferred experimentally to select a small value of SMO gain but enough to induce sliding motion. On the other hand, the time constant must be selected small for higher estimation accuracy but must be enough larger for large value of observer gain.

Figure 42 (a) and Figure 43 (a) correspond to the variation in DC bus voltage of -10V whereas in Figure 42 (b) and Figure 43 (b) correspond to the variation of +10V. In the case of a variation of the speed above the nominal value *i.e.* case (b), it is more accurate but affected much more by the discontinuous phenomenon which is reduced greatly grace to the use of sigmoid function instead of sign function as explained earlier.

The results of using SMO with sign function are not shown here as it is noisier and less accurate. Nevertheless by using SMO showed good estimation yet with fluctuation and error at low speed. So in this method, the need for complementary strategy is still a necessity. The next part will deal with flux estimation method accompanied with a phased locked loop (PLL).

III.2.2. Flux estimation plus PLL (Phased Locked Loop)

A PLL is a system for detecting the instantaneous phase and the direct, negative, zero sequences of any three-phase electric system [126]. These variables are necessary in the step of identifying the harmonic currents. The instantaneous phase is an important and indispensable parameter for

identification methods. Some methods are very sensitive to frequency changes. It is therefore necessary to have a robust PLL to improve the quality of the compensation.

This method is well known as it is simple, the design process is quite easy and its implementation is so suitable. In [127], sensorless control using PLL was realized with vector control and it demonstrated that practical solutions can be provided through this strategy for grid-connected PMSG wind turbine. Anyway, the main drawback of it, is that it is susceptible to be influenced by machine parameters variety and different measurement errors [119].

The design of a PLL system using conventional method is studied in this section.

In three-phase electrical network, the PLL is used to detect the symmetrical components (direct, inverse and homopolar) and also the instantaneous phase (frequency) of voltage. In [128] and [129], three-phase PLL is presented. The three voltages in the reference frame *A-B-C* are transformed into the reference Park where the direct component of voltage is zero if a good estimate of the instantaneous phase is guaranteed.

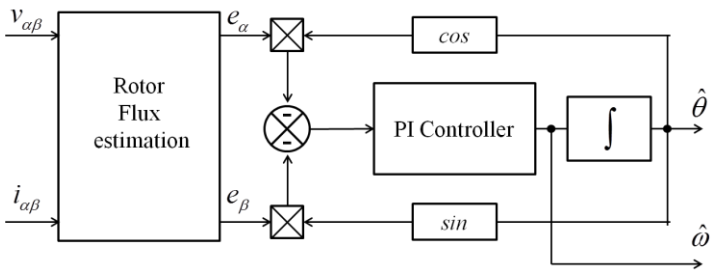

Figure 44. PLL standard schema

So, in this work, a PLL is used to determine the speed and position from the measured voltages and currents. Figure 44 shows the general schema of PLL in stator reference. The two stator voltage and current phases are used as inputs of rotor flux estimation block to estimate the two components of rotor flux. A PLL is used to extract the position and speed information with two components of estimated rotor flux as input variables.

The rotor flux quantity in α-β reference frame could be calculated through equation (42) as follows:

$$\begin{aligned} e_\alpha &= \int \left(v_\alpha - R_S i_\alpha \right) dt - L_S i_\alpha \\ e_\beta &= \int \left(v_\beta - R_S i_\beta \right) dt - L_S i_\beta \end{aligned} \tag{42}$$

The rotor angle can be estimated based on the relationship between flux quantity e_α and e_β and the rotor electrical angle θ.

III.2.2.1. Experimental results of method of flux estimation plus PLL

This method is verified in experimentation using the dSPACE 1104 and MATLAB environment. The same last configuration in Figure 40 is used whereas the estimator of SMO is replaced by PLL estimator. Figure 45 shows the stator voltages and currents which is used as inputs of this estimator to get the rotor position estimation. The test is carried out at the points of maximum power which corresponding to each value of wind speed. DC bus voltage is varied by ±10V.

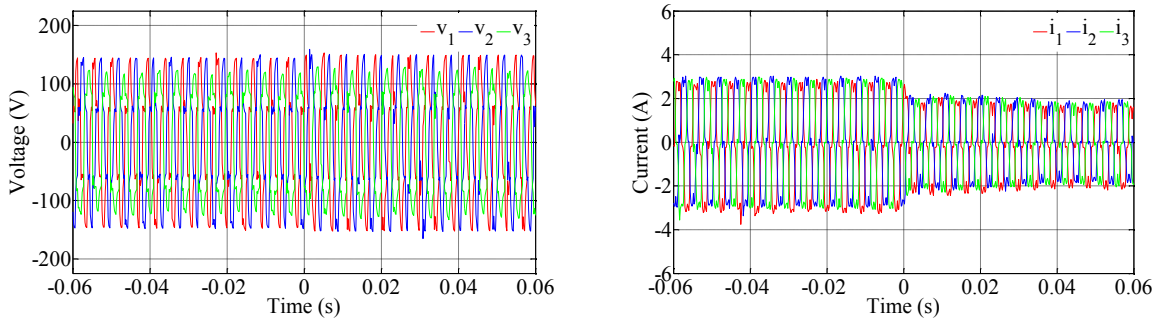

Figure 45. Stator voltages and currents at wind speed 8m/s - PLL method

In this strategy a high pass filter (HPF) is utilized to cascade with the traditional flux integrator and compensates relative phase leading, which could successfully respond to the problems of DC drift and initial value. From Figure 46 and Figure 47, the estimated rotor position and real rotor position are demonstrated respectively at wind speed values of 4 and 8m/s.

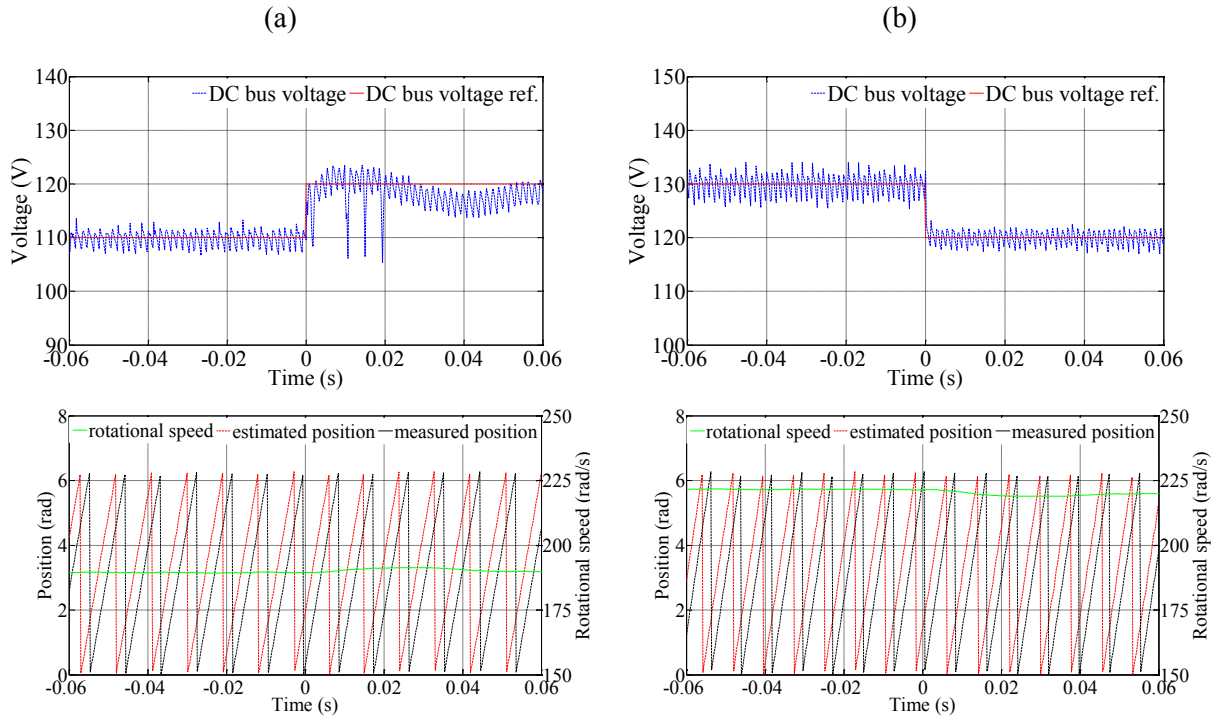

Figure 46. Position estimation by PLL method at wind speed value of 4m/s

The real rotor position is directly measured at the machine shaft using an encoder as mentioned earlier.

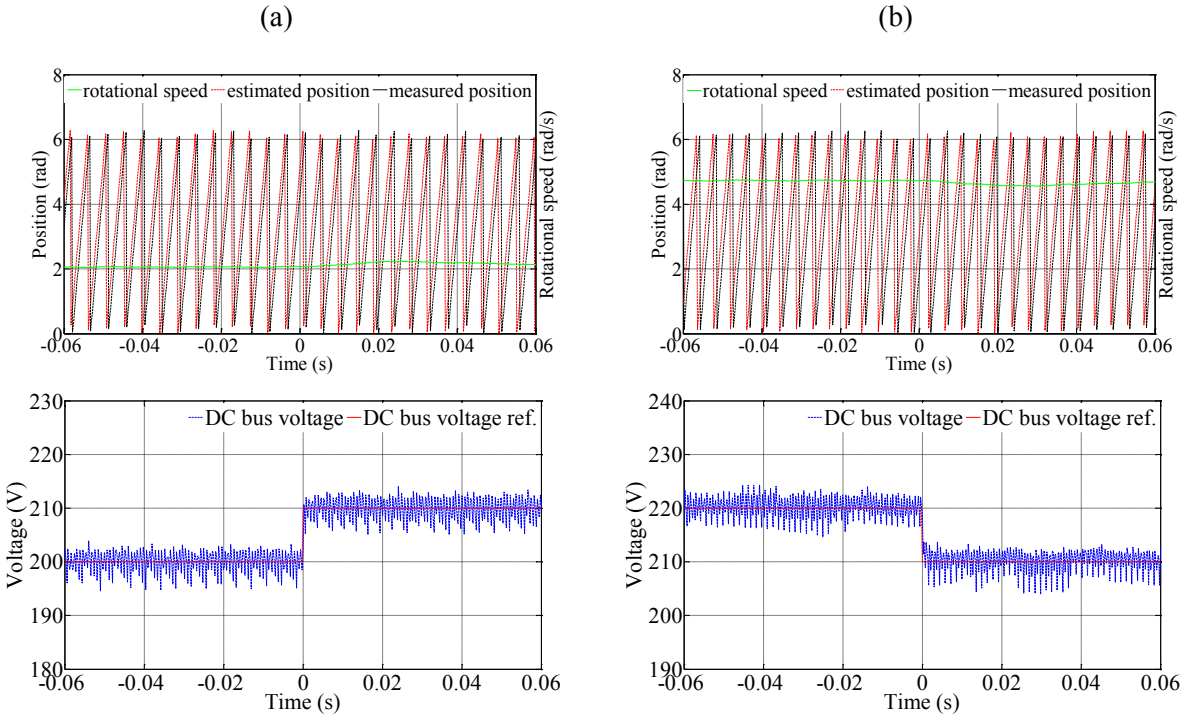

Figure 47. position estimation by PLL method at wind speed value of 8m/s

Figure 46 (a) and Figure 47 (a) correspond to the variation in DC bus voltage of -10V whereas in Figure 46 (b) and Figure 47 (b) correspond to the variation of +10V. In both cases, the estimation is robust and not affected by changes while estimation error is relatively of high value.

The comparison between the results concerning the estimated position and the real measured position demonstrate that position estimation flux estimation plus PLL strategy gives a reasonable precision but it needs a manual starting or adaptive PID tuning.

In the next paragraph, Luenberger observer is presented. Reduced order of this order will be achieved to get the rotor position estimation.

III.2.3. Luenberger observer of reduced order

In this part, the technique of calculating a Luenberger observer is used to reconstruct the position of the PMSM assuming that only the currents are accessible to measurement. The main principles of Luenberger observers are proposed in [136] and [137]. The state presentation is of the equation (43):

$$\begin{aligned} \frac{dx}{dt} &= A.x + B.u \\ y &= C.x \end{aligned} \tag{43}$$

where: x, u, y, A, B and C are respectively state vector, control vector, output vector, matrix of transition, matrix of control and matrix of measurement.

The system to be observed in our case is the model of PMSM; the machine model in *d-q* reference, which is used for dealing with continues variables, is given by the equations (44):

$$\begin{bmatrix} v_d \\ v_q \end{bmatrix} = \begin{bmatrix} R_S & -L_q\,\omega \\ L_d\,\omega & R_S \end{bmatrix} \begin{bmatrix} i_d \\ i_q \end{bmatrix} + \begin{bmatrix} L_d & 0 \\ 0 & L_q \end{bmatrix} \begin{bmatrix} \frac{d}{dt} i_d \\ \frac{d}{dt} i_q \end{bmatrix} + \begin{bmatrix} 0 \\ K\,\omega \end{bmatrix} \tag{44}$$

with L_d and L_q are cyclic stator inductance respectively in direct axis '*d*' and transverse axis '*q*'. In this case, a third equation in addition to these two equations which corresponds to a usual approximation is adopted. This approximation is to assume that the dynamics of the speed is much slower than the stator currents. Let $x = \begin{bmatrix} i_d & i_q & \omega \end{bmatrix}^T$ be a state vector, $u = \begin{bmatrix} v_d & v_q \end{bmatrix}^T$ a control vector and $y = \omega$ is an output vector. The state representation of the PMSM is then as in (45):

$$\left\{ \begin{aligned} \frac{d}{dt} x &= \begin{bmatrix} -\frac{R_S}{L_d} & \frac{L_q}{L_d}\omega & 0 \\ -\frac{L_d}{L_q}\omega & -\frac{R_S}{L_q} & -\frac{K}{L_q} \\ 0 & 0 & 0 \end{bmatrix} x + \begin{bmatrix} \frac{1}{L_d} & 0 \\ 0 & \frac{1}{L_q} \\ 0 & 0 \end{bmatrix} u \\ y &= \begin{bmatrix} 0 & 0 & 1 \end{bmatrix} x \end{aligned} \right. \tag{45}$$

Considering that in the studied machine $L_d = L_q = L_{dq}$ and to simplify the writing of equations by using $\tau_{dq} = R_S / L_{dq}$, the last model can be rewritten as in (46):

$$\begin{cases} \dfrac{d}{dt}x = \begin{bmatrix} -\tau_{dq} & \omega & 0 \\ -\omega & -\tau_{dq} & -\dfrac{K}{L_{dq}} \\ 0 & 0 & 0 \end{bmatrix} x + \begin{bmatrix} \dfrac{1}{L_{dq}} & 0 \\ 0 & \dfrac{1}{L_{dq}} \\ 0 & 0 \end{bmatrix} u \\ y = \begin{bmatrix} 0 & 0 & 1 \end{bmatrix} x \end{cases} \tag{46}$$

In this model, the machine speed ω plays simultaneously the role of state variable and a parameter appearing in the dynamic matrix. In the case of the mechanical sensorless approach, the machine speed is not measured and only the stator currents are accessible to measurement. Then the state vector can be divided into two sub vectors $x_1 = \begin{bmatrix} i_d & i_q \end{bmatrix}^T$ and $x_2 = \omega$. Thus the dynamic matrix and control matrix become as given in (47):

$$\begin{cases} A_{11} = \begin{bmatrix} -\tau_{dq} & \omega \\ -\omega & -\tau_{dq} \end{bmatrix}, A_{12} = \begin{bmatrix} 0 \\ -\dfrac{K}{L_{dq}} \end{bmatrix} \\ B_1 = \begin{bmatrix} \dfrac{1}{L_{dq}} & 0 \\ 0 & \dfrac{1}{L_{dq}} \end{bmatrix} \end{cases} \tag{47}$$

It is evident that the pair (A_{11}, A_{12}) is observable. Therefore, by using the formulas given in [136] and [137] and considering that the real speed as the estimated one, a reduced identity observer is determined for estimating the machine speed so that the rotor position. Let K_L be the gain of the observer, which is can be expressed by $K_L = \begin{bmatrix} k_1 & k_2 \end{bmatrix}$ and thus an equation showing the physical parameters of the machine is constructed as in (48), [136]:

$$\hat{\omega} = Z - k_1 i_d - k_2 i_q \tag{48}$$

with:

$$\frac{d}{dt}Z = \left(-k_1 \tau_{dq} - k_2 + k_1 k_2 \frac{K}{L_{dq}} \right) i_d + \left(k_1 \omega - k_2 \tau_{dq} + k_2^2 \frac{K}{L_{dq}} \right) i_q + \frac{k_1}{L_{dq}} v_d + \frac{k_2}{L_{dq}} v_q - k_2 \frac{K}{L_{dq}} Z \tag{49}$$

Thus, the calculation of the observer is reduced to the calculation of the vector Z, which must ensure the stability under Hurwitz [136], [137]. Yet the observability of the pair (A_{11}, A_{12}) makes this calculation possible.

It is noteworthy that the determined observer depends on the value of speed ω which is not measured. To implement this observer, ω should be replaced by $\hat{\omega}$ in the observer's model, which is a

reasonable approximation since the observer has already begun to converge. For that, the gain k_2 must be chosen such that the convergence is guaranteed.

III.2.3.1. Experimental results of Luenberger method

Using dSPACE 1104 and MATLAB environment, this observer is tested experimentally. The configuration in Figure 40 is used. The estimator which is used is Luenberger of a reduced order. Figure 48 shows the stator voltages and currents which is used as inputs of this observer to estimate the rotor position. The test is carried out at the points of maximum power which corresponding to each value of wind speed Figure 49 and Figure 50.

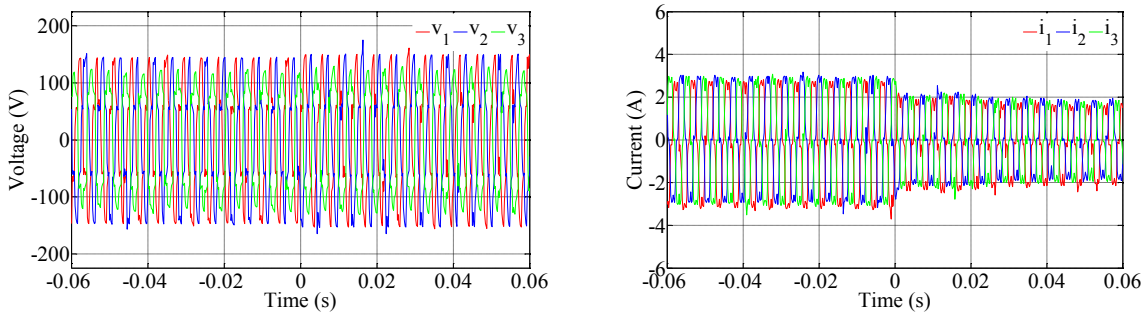

Figure 48. Stator voltages and currents at wind speed 8m/s – Luenberger method

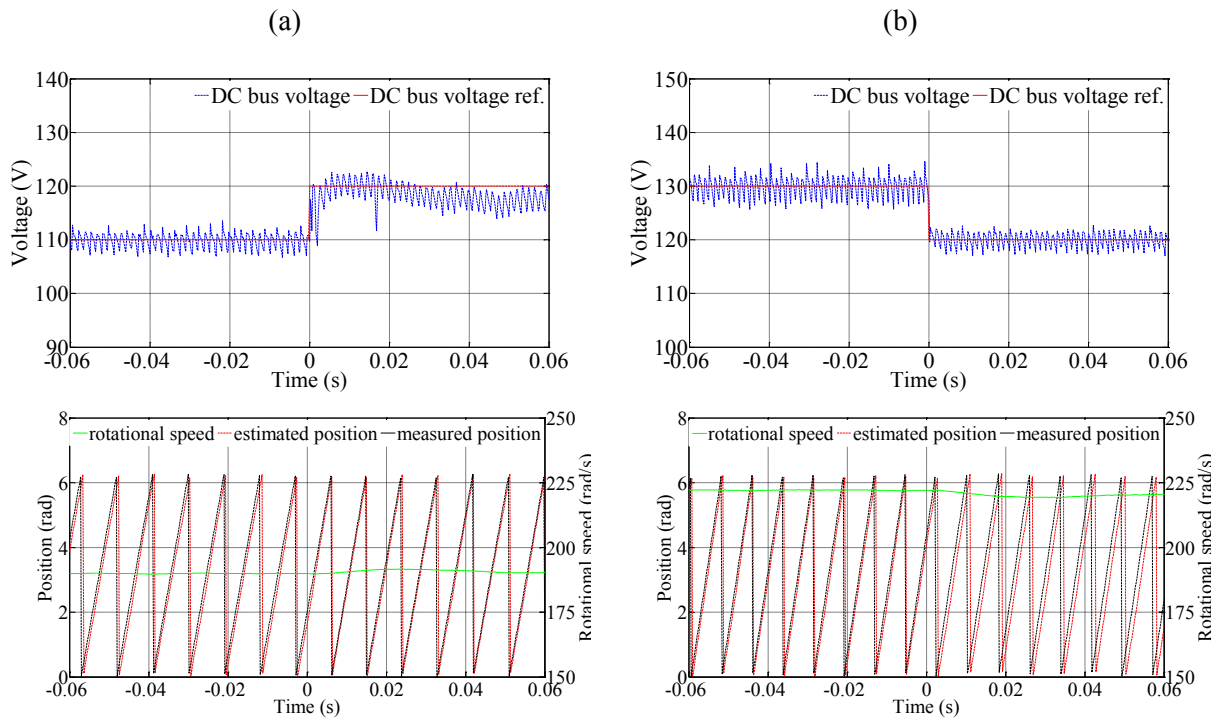

Figure 49. Position estimation by Luenberger method at wind speed value of 4m/s

At each point of maximum power the nominal value of speed is varied to its upper and lower neighborhood. To achieve this changing, the DC bus voltage is varied by value of ±10V to verify the performance of estimation.

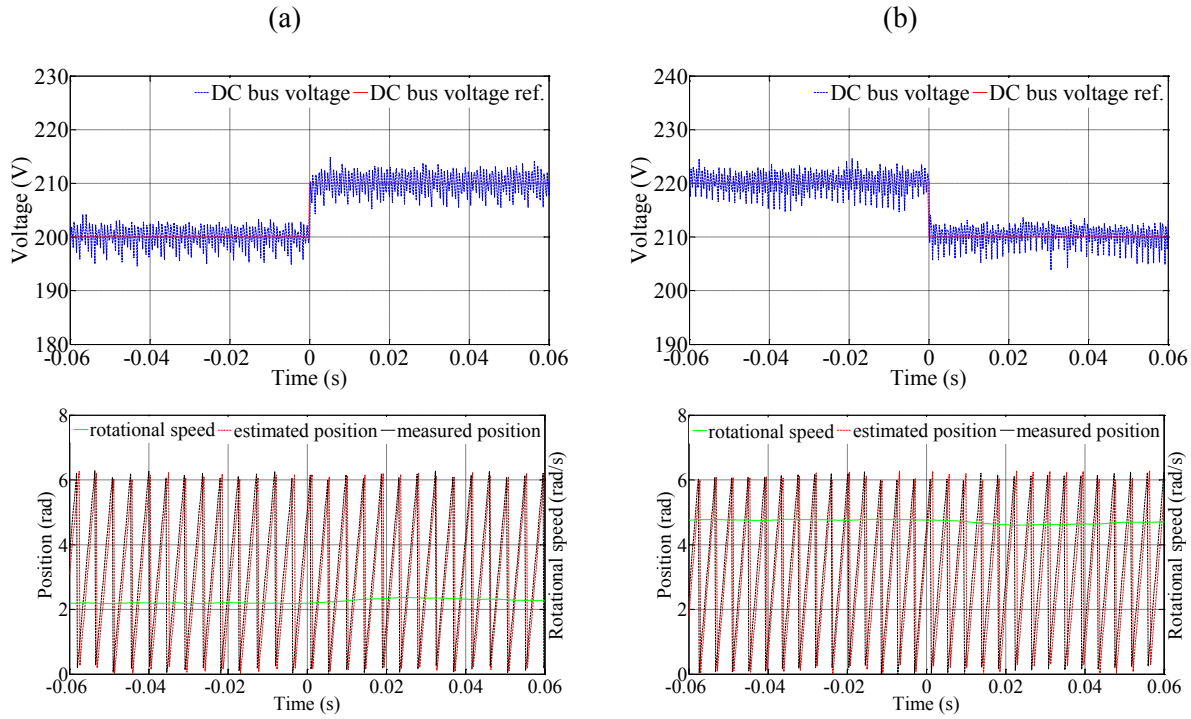

Figure 50. Position estimation by Luenberger method at wind speed value of 8m/s

Figure 49 (a) and Figure 50 (a) correspond to the variation in DC bus voltage of -10V whereas in Figure 49 (b) and Figure 50 (b) correspond to the variation of +10V. In both cases, the estimation is robust and not affected by changes while estimation error is relatively of high value. As shown in Figure 49 and Figure 50, the estimation error of position, which is corresponding to high wind speed (value of 8m/s), is getting smaller in high speed than it is at low wind speed (value of 4m/s). Figure 49 shows that estimation error get bigger when the power shift from its maximum value.

This observer is noted that it is sensitive to the variation of stator resistance parameter than other setting of parameters where the error of estimation is corresponding. A comparison between three tested methods shows that all three methods give in nominal state almost acceptable estimation but all need a complement tool as manual starter. Therefore, a more accurate observer is needed.

The next part will deal in detail with Kalman filtering to get a good estimation of rotor position.

III.3. Extended Kalman filtering

III.3.1. Kalman filtering

The Kalman filter principle introduced by Rudolf Emil Kalman represents an efficient means for the recursive data processing. Concerning the estimation of the PMSM rotational speed, there have been a number of studies that proposed various methods for this aim. While the estimation method based on observer depends to some extent on the accuracy of the motor model; the EKF is the most popular model-based estimator allowing sensorless drive control in a wide speed range [156].

Using the Kalman filter, the control without mechanical sensor can be implemented, because it allows observing and predicting the position and speed from the measurement of currents and supply voltages. Moreover, since the studied system is nonlinear, the algorithm of EKF [138] must be used. This will give optimal recursive states estimation from the measurement of other variables.

In the early 1960s, the Hungarian Kalman published the algorithm of optimal observer [139]. This observer was first used in the domain of space and especially in Apollo program. It is found in the field of electrical engineering for the sensorless control and diagnosis process [145], [146]. Kalman filtering is based on the principle of total observation (Figure 51) that estimates the outputs y from its model (inputs u), then correct the quantities of estimated state $\hat{x}$ using a negative feedback of error estimation [149]. The correction is performed by a gain vector that allows the filter performance to be settled (such as dynamic). This vector gain K is sometimes determined offline for specific performance (*e.g.* pole placement). For the Kalman filter, the gain vector is calculated for each iteration from the error predictions and uncertainties (noise) on the state quantities and measurements, in order to minimize the error between the model and the real system [149].

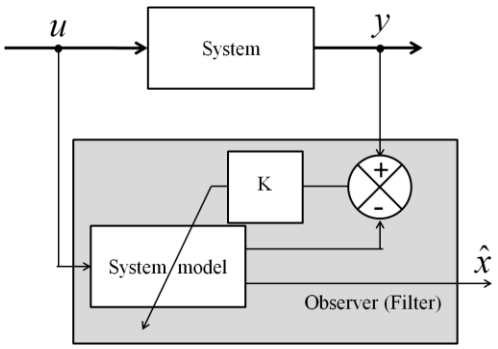

Figure 51. Principle of observation

This technique has the disadvantage of complexity and high degree of difficulty in designing of the estimator gain [19], but on other hand it increases position detection accuracy especially in low speed range and improve noise suppression effectively [119].

In [147], author studies the influence of the use of mechanical equation in the model of the EKF. It then presents the influence of parameter variations on the behavior of the observer. Simulation results are presented without experimental validation. It uses the control signals of inverter and the measurement of the DC bus voltage in order to reconstruct the phase voltages. The author concludes that using a simplified model has the advantage of being light in computational time, but it introduces estimation errors. In addition, it does not allow estimation of the load torque.

In [138] a vector control is provided without position and speed sensor of a salient pole PMSM. The algorithm allowing EKF to estimate the position and speed from the currents and voltages measured in a reference related to the stator. The estimate of the initial position is determined from the measured stator currents after the application of test signals to terminals of PMSM. It presents experimental results in transient and steady state on a machine of 1.4kW. It is highlighted the good performance of the order without mechanical sensor. Finally, the author stressed the need for filtering the measured signals (current and voltage) with the aim of improving the performance of the proposed algorithm. Another technique developed in [148] is to reduce the order of the system and reduce the computational time. This method is based on the choice of EMF and rotor speed as state variables in *d-q* coordinates. Indeed, the author reduces the order of the system to 3, which allows it to minimize matrix operations to reduce the computational time. The author proposes to use the trigonometric arc tangent function to estimate the rotor position from the estimated EMF. Simulation results and experimental results are shown to confirm the robustness of reduced-order Kalman filter concerning the change of stator resistance.

In [150] the authors used an EKF with online tuning of the rotor flux. Although this solution provides wide speed range and has been shown to be capable of delivering full torque at standstill, it requires a high computational effort to compute the optimum state estimation gain matrix from the covariance matrix at every control cycle. A vector controlled PMSM drive has been implemented in [151] by using a low cost digital signal controller. The PMSM drives with sensored and sensorless operations have been performed at various speed and load conditions to demonstrate the performance of the drive at four-quadrant regions. Moreover, the details of voltage and current transitions corresponding to speed transitions have been presented for the sensored and sensorless operations. The speed estimation has been performed by using EKF which estimates the speed and rotor position with the knowledge of the stator currents and voltages.

To sum up, the Kalman filter shows good estimation performance and also robustness to noise and parameter variations. It also has good robustness performance to load changes, particularly when extended to the couple. However, the calculation time of this filter is higher than other observers since it has high mathematical operations.

III.3.2. Principle and functioning

EKF algorithm consists of two main parts which are prediction and correction, where the calculation of the prediction step depends on the estimated state from the previous iteration. The correction step depends on both prediction step and calculation of K, the observer gain; so, to start the process, an initial state is needed. To apply Kalman filter, one must first and foremost model the problem in function to the parameters to be estimated and sensors measurement. The discrete extended Kalman filter model is represented by the equations (50) (where indexes z and z+1 represent respectively the estimated and predicted states):

$$\begin{aligned} x_{z+1} &= Ax_z + Bu_z + v_z = f\left(x_z, u_z, v_z\right) \\ y_{z+1} &= Cx_z + w_z = h\left(x_z, w_z\right) \end{aligned} \tag{50}$$

with x, y, u, v, w, A, B, and C are respectively state vector, output vector, control vector, state noise, measurement noise, matrix of transition, matrix of control and matrix of measurement. The noise v and w are assumed as temporally uncorrelated, zero-mean random sequences with known covariance Q (state noise) and R (measurement noise).

Filtering steps can be illustrated as given in [123]:

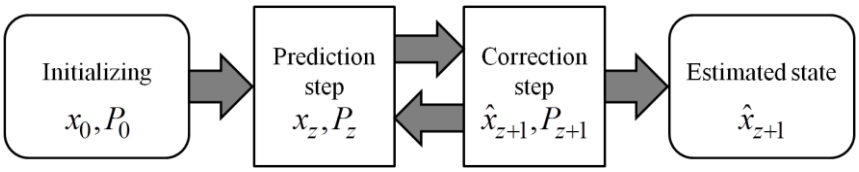

Figure 52. Steps of Kalman filtering

The algorithm EKF is given in Table 3, where the index z-1 represents previous states.

Table 3. The two stages of Kalman filter operating

Prediction stage:	
Prior state vector	$\hat{x}_z = f(\hat{x}_{z-1}, u_{z-1})$
Covariance matrix of prior state	$P_z = A_z\, P_{z-1}\, A_z^T + v_z\, Q_{z-1}\, v_z^T$
Correction stage:	
Optimal gain	$K_{z+1} = P_z\, C_z^T \left(C_z\, P_z\, C_z^T + R_z\right)^{-1}$
Estimated state vector	$\hat{x}_{z+1} = \hat{x}_z + K_{z+1}\left(y_{z+1} - h(\hat{x}_z)\right)$
Covariance matrix of estimated state	$P_{z+1} = P_z - K_z \left(C_z\, P_k\, C_z^T + R_z\right) K_z^T$

When the model of the system is well defined, the two matrices Q and R must be chosen which allows the establishment of the uncertainty degree between the model and the real system. Then, the initial state vector and the initial error covariance matrix P_0 is initialized which is based on supposed

errors on each state. When these steps are carried out and in each sampling period, an estimation phase and then a correction phase are performed. In this context it is worth noting that:

- If Q is small, it reflects a greater confidence in the estimates and less in the measurements; the filter gain tends to decrease. The observations have a very slow convergence dynamics.
- If R is small, it reflects great confidence in the measurements; the filter gain tends to increase. The estimated output will be almost identical to the measures: since the filter will not be correct the observations will also not be.

The understanding and implementation of EKF are not most complicated; the main difficulty lies in selecting Q and R matrices. After defining these two matrices, steps of Kalman filter calculation can be applied, as in Table 3. Thus, it is clear that x_{z+1} is the estimate of new state vector and P_{z+1} is the new matrix of estimated state covariance. The latter matrix can provide information about the accuracy of the estimate of each parameter. These two phases of calculation have to be applied whenever new samples from the sensors are available.

To implement EKF in the small scale wind turbine, the model of the electric machine used must be defined. The mathematical model of the PMSM in the reference related to stator is used and it is given by (51) (Appendix II):

$$\begin{bmatrix} v_\alpha \\ v_\beta \end{bmatrix} = R_S \begin{bmatrix} i_\alpha \\ i_\beta \end{bmatrix} + L_S \frac{d}{dt}\begin{bmatrix} i_\alpha \\ i_\beta \end{bmatrix} + K\omega \begin{bmatrix} \sin\theta \\ -\cos\theta \end{bmatrix} \tag{51}$$

Table 4 demonstrates for this case state vector, control vector, transition matrix and control matrix. To observe the current and to estimate speed and position, the output of this system is chosen as the current. The observation matrix *C* is also set in this table.

Table 4. Components of equations for Kalman filtering in a reference relation to the rotor

state vector	$x = \begin{bmatrix} i_\alpha & i_\beta & \omega & \theta \end{bmatrix}^T$
control vector	$u = \begin{bmatrix} v_\alpha & v_\beta \end{bmatrix}^T$
output vector	$y = \begin{bmatrix} i_\alpha & i_\beta \end{bmatrix}^T$
observation matrix	$C = \begin{bmatrix} 1 & 0 & 0 & 0 \\ 0 & 1 & 0 & 0 \end{bmatrix}$

From equation (51) and Table 4, the observer in (52) can be built:

$$f(x)=\begin{pmatrix} f_1(x_1)=\dfrac{di_\alpha}{dt} \\ f_2(x_2)=\dfrac{di_\beta}{dt} \\ f_3(x_3)=\dfrac{d\omega}{dt} \\ f_4(x_4)=\dfrac{d\theta}{dt} \end{pmatrix}=\begin{pmatrix} \dfrac{1}{L_S}\left(v_\alpha-R_S i_\alpha-K\omega\sin\theta\right) \\ \dfrac{1}{L_S}\left(v_\beta-R_S i_\beta+K\omega\cos\theta\right) \\ 0 \\ \omega \end{pmatrix} \tag{52}$$

The use of EKF involves linearization of state equations around the operating point. The transition matrix A which is the Jacobean of (52) is expressed by (53):

$$A=\frac{df}{dx}=\begin{bmatrix} \dfrac{\partial f_1}{\partial x_1} & \dfrac{\partial f_1}{\partial x_2} & \dfrac{\partial f_1}{\partial x_3} & \dfrac{\partial f_1}{\partial x_4} \\ \dfrac{\partial f_2}{\partial x_1} & \dfrac{\partial f_2}{\partial x_2} & \dfrac{\partial f_2}{\partial x_3} & \dfrac{\partial f_2}{\partial x_4} \\ \dfrac{\partial f_3}{\partial x_1} & \dfrac{\partial f_3}{\partial x_2} & \dfrac{\partial f_3}{\partial x_3} & \dfrac{\partial f_3}{\partial x_4} \\ \dfrac{\partial f_4}{\partial x_1} & \dfrac{\partial f_4}{\partial x_2} & \dfrac{\partial f_4}{\partial x_3} & \dfrac{\partial f_4}{\partial x_4} \end{bmatrix}=\begin{bmatrix} -\dfrac{R_S}{L_S} & 0 & -\dfrac{K\sin\theta}{L_S} & -\dfrac{K\omega\cos\theta}{L_S} \\ 0 & -\dfrac{R_S}{L_S} & \dfrac{K\cos\theta}{L_S} & -\dfrac{K\omega\sin\theta}{L_S} \\ 0 & 0 & 0 & 0 \\ 0 & 0 & 1 & 0 \end{bmatrix} \tag{53}$$

After the system is fully modeled and the construction of EKF observer is done, two matrices appearing in the calculations are required, namely the matrix of measurement noise covariance R and the matrix of state noise covariance Q.

Consider having a sensor with Gaussian noise, the matrix of measurement noise covariance is a matrix with two dimensions, and of value terms, the square of the standard deviation of noise for each sensor. The simple matrix of R is shown in (54) with σ_a, σ_b the standard deviation of current noise.

The matrix of state noise covariance Q represents the system modeling error. This matrix is a diagonal matrix of four dimensions (the size of state vector), shown in (54) with q_a, q_b, q_s and q_p are respectively the maximum permissible error variance of modeling on the current, speed and position. The terms on the diagonal correspond to the square of the maximum standard deviation of error that is allowed for each parameter to estimate. This matrix is determined empirically based on the data of the problem.

To well understand these terms, it is useful to notice that if the terms of error is set too small compared to the reality, then the Kalman filter will fail to rectify the errors of the model and make biased estimates. Contrariwise, if the error terms are too large in relation to reality, then the model will not be biased, but the resulting estimates are of poor quality that is to say, the covariance of the error will be

large. The difficulty of the Kalman filter is to estimate properly this matrix of state noise covariance in order to have the most accurate estimate without bias.

$$\begin{cases} R = \begin{bmatrix} \sigma_a^2 & 0 \\ 0 & \sigma_b^2 \end{bmatrix} \\ Q = \begin{bmatrix} q_a & 0 & 0 & 0 \\ 0 & q_b & 0 & 0 \\ 0 & 0 & q_s & 0 \\ 0 & 0 & 0 & q_p \end{bmatrix} \end{cases} \tag{54}$$

Once implemented in MATLAB and compiled under dSPACE, the EKF produces results fairly quickly. However, for best results, setting the Q and R matrices is done empirically and may take time, depending on the level of expertise of the user. Since the characteristic stochastic noises are generally not known, the tuning of this matrix can be obtained by simulation. After determining the noise of the measures to build R matrix, and after obtaining the optimal value of Q and P_0 matrix by simulation to get best convergence, the values in (55) are chosen by trial and error method:

$$\begin{cases} R = 10^{-8} \begin{bmatrix} 1 & 0 \\ 0 & 1 \end{bmatrix} \\ Q = 10^{-8} \begin{bmatrix} 1 & 0 & 0 & 0 \\ 0 & 1 & 0 & 0 \\ 0 & 0 & 100 & 0 \\ 0 & 0 & 0 & 10^{-6} \end{bmatrix} \end{cases} \tag{55}$$

Figure 53, Figure 54 and Figure 55 show that the results obtained using EKF with non-sinusoidal variables are of good quality where it is performed by using EKF based on model with reference relating to the stator.

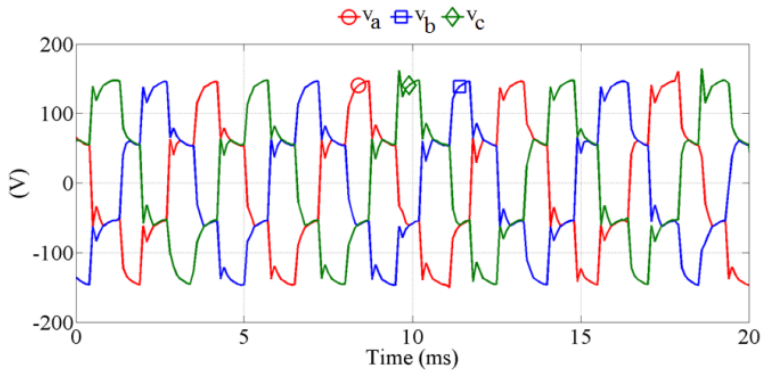

Figure 53. Results obtained for EKF with non-sinusoidal variables (experimental stator voltages at wind speed 8m/s) [30]

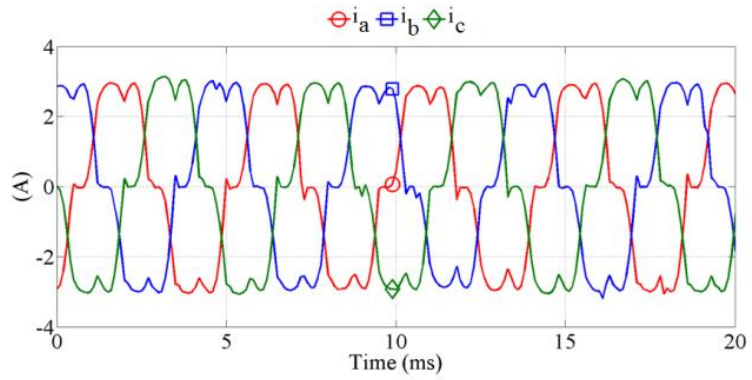

Figure 54. Results obtained for EKF with non-sinusoidal variables (experimental stator currents at wind speed 8m/s) [30]

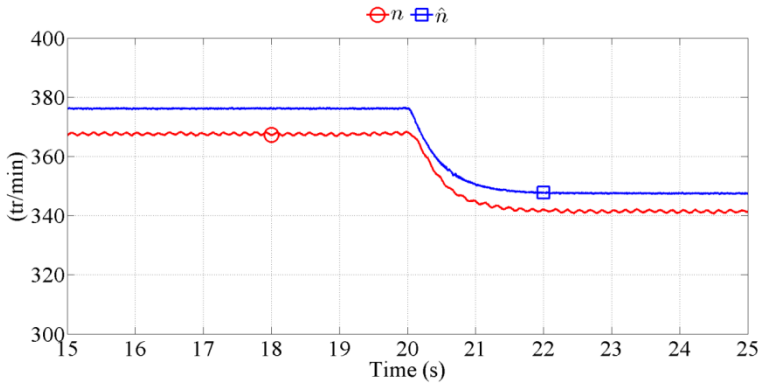

Figure 55. Results obtained for EKF with non-sinusoidal variables (evolution of speed estimation when wind speed change from 8m/s to 6m/s) [30]

By decreasing speed, Figure 55 shows that the estimation response is high enough to follow the measured value (a maximum relative error of about -2.4%, where speed sensor has already average measurement error of this value). Also, in case of increasing speed, the estimated value gets rapidly to the new one. Therefore, good performance of EKF estimator is proved at different cases of PMSM working states.

III.3.3. Highlighting the problem related to EKF use

Performance of the EKF, depends on the correct prior knowledge of the process and measurement noise covariance matrices (Q and R, respectively) [157]. In order to increase the performance and the reliability of the EKF several studies already have tried to develop an adaptive version. Using innovation and state estimation, it seems possible to estimate parameters that characterize the state of the process. These parameters can then be used to adapt the gain matrix by online automatic tuning of some of the covariance matrices used in the computation of the gain matrix. This kind of adaptive EKF is empirical but seems to have good behavior compared to the EKF.

Because of the complexity to ensure robustness when adaptive measure is continuously updated, some authors used an adaptive algorithm based on switching between several models. For example, in [152], authors have developed an application on a highly critical process from robustness point of view. They have proposed two matrices of covariance to switch between them depending on the state of the process. There exist a large number of papers dealing with adaptive observers and adaptive extended Kalman filtering [153] especially in the GPS and DGPS community [154]. In [154] for instance, authors present an adaptive extended Kalman filter using innovation in order to adapt matrices of Q and R, exactly in the same spirit than in the present As obtained in the results of last section, EKF approved a good estimation in various speed ranges and in the two types of machine variables, sinusoidal and non-sinusoidal. Anyway, the main problem of this method is the difficulty of choosing the components of matrices. In [155], the high-gain extended Kalman filter (HG-EKF), which is also an exponentially converging observer, is introduced, but with the property that it is more efficient in the presence of noise. Indeed, the high sensitivity of high-gain observers is a well-known drawback: the high gain ensures convergence but also increases noise effects.

The next part of this chapter focuses on the use of EKF with adaptive auto-tuning for a small scale wind generator based on PMSM with an active structure. The used MPPT, which was presented in chapter II, is based on the knowledge of the parameters of small scale wind generator as input with EKF-based estimation of mechanical rotation speed.

III.4. Extended Kalman filter with adaptive auto-tuning

In adaptive Kalman filter, the knowledge about the noise covariance values is adjusted according to the difference between the predicted estimates and the current measurements. Several ways for this purpose have been developed in [157]-[159] which can be classified into four categories: Bayesian, maximum likelihood, correlation (autocorrelation), and covariance matching. Few studies have introduced methods either offline or non-adaptive to decide metrics of measurement and state noise covariance for the rotor speed estimation. Authors of [156] gave a comparison between three variants of the square-root implementation for the EKF with the standard implementation that consider the full matrix representation in sensorless control of AC motor drive. The benefits of square-root EKF were discussed for every method and they referred that such methods improved accuracy and robustness in critical operating conditions of the drive whereas its computational cost is higher than the conventional algorithm.

III.4.1. Principle and functioning

Every moment z the optimal gain of EKF is calculated so as to minimize the error covariance according to the algorithm of Figure 56, which is more detailed than in Figure 52. Since it is very difficult to access the error covariance of states, then the two matrices Q and R are often used for setting the observer performance and provide a large number of possible parameter settings using simple principle: the more trusted the model (respectively measures) the less the values of (resp. R) must be. In order to handle all these settings at once, De Larminat proposed a method that allows the user to place the poles of the permanent regime of the observer using a single high level parameter T_0 [161], called observability horizon.

Such an approach has already been tried for the adaptive adjustment of an observer for the state of charge of lithium-ion batteries [162].

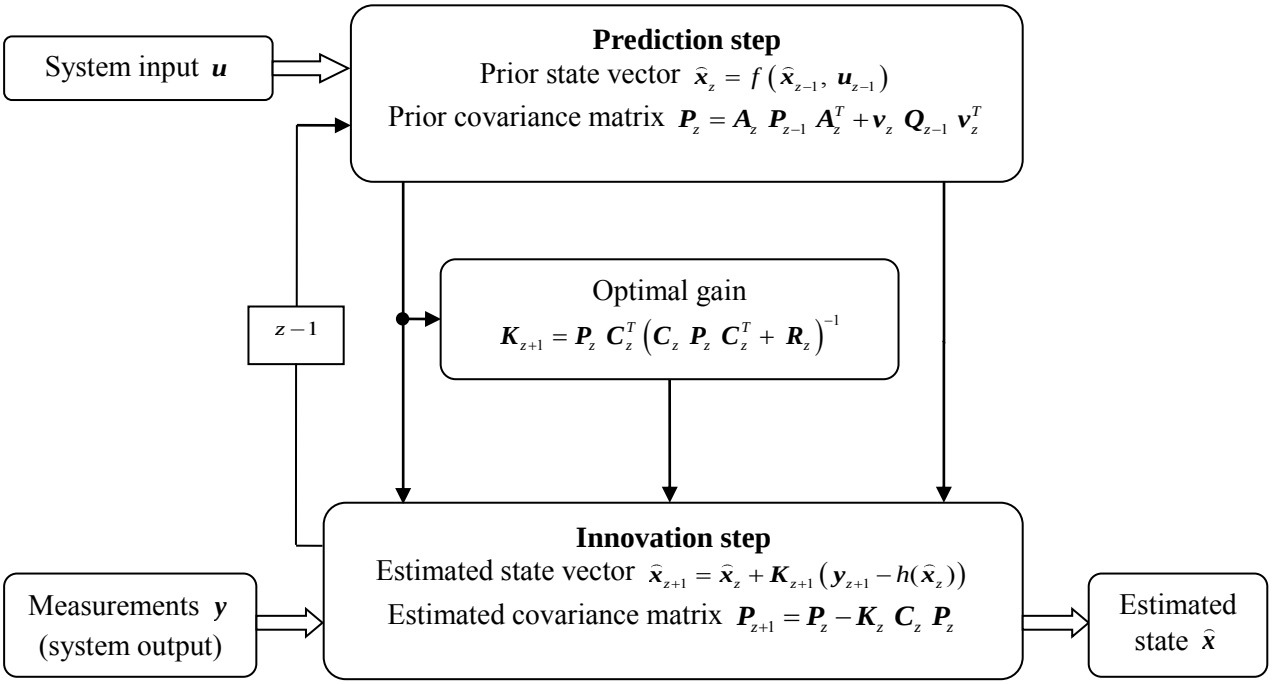

Figure 56. Detailed algorithm of the extended Kalman filter

The observability horizon T_0 is used to compute the partial observability gramian $G_0(T_0)$ given in (56):

$$G_0(T_0) = \int_0^{T_0} e^{A^T t} C^T C e^{At} dt \qquad (56)$$

To write the gramian formula for the studied system, it must, on the first hand, formulate the function $\boldsymbol{H}(\mathrm{t}) = e^{A^T t}\boldsymbol{C}^T\boldsymbol{C}e^{At}$ that is calculated based on its components as follows:

Exponential of the matrix *A* in (57):

$$e^{At} = \begin{bmatrix} e^{-\frac{R_S}{L_S}t} & 0 & \frac{-K\sin\theta}{L_S}t.e^{-\frac{R_S}{L_S}t} & \frac{-K\omega\cos\theta}{L_S}t.e^{-\frac{R_S}{L_S}t} \\ 0 & e^{-\frac{R_S}{L_S}t} & \frac{K\cos\theta}{L_S}t.e^{-\frac{R_S}{L_S}t} & \frac{-K\omega\sin\theta}{L_S}t.e^{-\frac{R_S}{L_S}t} \\ 0 & 0 & 1 & 0 \\ 0 & 0 & t & 1 \end{bmatrix} \tag{57}$$

Exponential of the transpose of the matrix *A* in (58):

$$e^{A^T t} = \begin{bmatrix} e^{-\frac{R_S}{L_S}t} & 0 & 0 & 0 \\ 0 & e^{-\frac{R_S}{L_S}t} & 0 & 0 \\ \frac{-K\sin\theta}{L_S}t + \frac{-K\omega\cos\theta}{L_S}t^2 & \frac{K\cos\theta}{L_S}t + \frac{-K\omega\sin\theta}{L_S}t^2 & 1 & t \\ \frac{-K\omega\cos\theta}{L_S}t & \frac{-K\omega\sin\theta}{L_S}t & 0 & 1 \end{bmatrix} \tag{58}$$

From (57) and (58) the function H can be then built in the result as in (59):

$$H(t) = \begin{bmatrix} e^{-2\frac{R_S}{L_S}t} & 0 & \frac{-K\sin\theta}{L_S}t.e^{-2\frac{R_S}{L_S}t} & \frac{-K\omega\cos\theta}{L_S}t.e^{-2\frac{R_S}{L_S}t} \\ 0 & e^{-2\frac{R_S}{L_S}t} & \frac{K\cos\theta}{L_S}t.e^{-2\frac{R_S}{L_S}t} & \frac{-K\omega\sin\theta}{L_S}t.e^{-2\frac{R_S}{L_S}t} \\ A_{31} & A_{32} & A_{33} & A_{34} \\ A_{41} & A_{42} & A_{43} & A_{44} \end{bmatrix} \tag{59}$$

with:

$$\left.\begin{aligned}
A_{31} &= \frac{-K}{L_S}\left(t\sin\theta + t^2\omega\cos\theta\right)e^{-\frac{R_S}{L_S}t} \\
A_{32} &= \frac{-K}{L_S}\left(-t\cos\theta + t^2\omega\sin\theta\right)e^{-\frac{R_S}{L_S}t} \\
A_{33} &= \left(\frac{K}{L_S}\right)^2 t^2 e^{-\frac{R_S}{L_S}t} \\
A_{34} &= \left(\frac{K}{L_S}\right)^2 t^3.e^{-\frac{R_S}{L_S}t}\omega^2 \\
A_{41} &= \frac{-K}{L_S}t.e^{-\frac{R_S}{L_S}t}\omega\cos\theta \\
A_{42} &= \frac{-K}{L_S}t.e^{-\frac{R_S}{L_S}t}\omega\sin\theta \\
A_{43} &= 0 \\
A_{44} &= \left(\frac{K}{L_S}\right)^2 t^2 e^{-\frac{R_S}{L_S}t}\omega^2
\end{aligned}\right\} \qquad (60)$$

Once $\boldsymbol{G_0}(\mathrm{T}_0)$ has been calculated, $\boldsymbol{Q}$ is deduced and $\boldsymbol{R}$ is normalized to the identity matrix in (61):

$$\begin{cases} \boldsymbol{Q} = \left(\mathrm{T}_0\, \boldsymbol{G_0}(\mathrm{T}_0)\right)^{-1} \\ \boldsymbol{R} = \boldsymbol{I} \end{cases} \qquad (61)$$

Moreover, as it will be illustrated through the experimental results, long observation horizons lead to slow the convergence speed of the estimation. Another important point is that for short observation horizons the steady state Kalman gain is high. This results in considering the smallest modeling error and therefore leads to a "noisy" estimate. On the contrary, long observation horizons induce low steady state Kalman gain and the modeling errors are filtered. The trade-off between speed of convergence and "noisy" estimation is achieved thanks to the influence of the observability horizon. The minimal value chosen for T_0 must be greater than the smallest time constant of the system. In order to be able to deduce on-line the state error covariance matrix $\boldsymbol{Q}$, one has to calculate the analytical expression of the partial observability gramian $\boldsymbol{G_0}(\mathrm{T}_0)$. For the real time implementation of the proposed adaptive tuning observer, the values of $\boldsymbol{G_0}(\mathrm{T}_0)$ have been stored in tables for various observability horizon values and mechanical machine speed values.

Theoretically, the matrix $\boldsymbol{Q}$ is expected to be diagonal. In order to reduce the real time calculation, only the diagonal elements of $\boldsymbol{G_0}(\mathrm{T}_0)$ have been previously calculated off line in relation of T_0 and the speed n. The results of this calculation have been implemented into look up tables (Figure 57) in a

real time calculator. Moreover, since the observability horizon variation acts as a low pass filter, the computation of $\boldsymbol{G_0}(\mathrm{T_0})$ may have a low sampling period in order to reduce the computational effort.

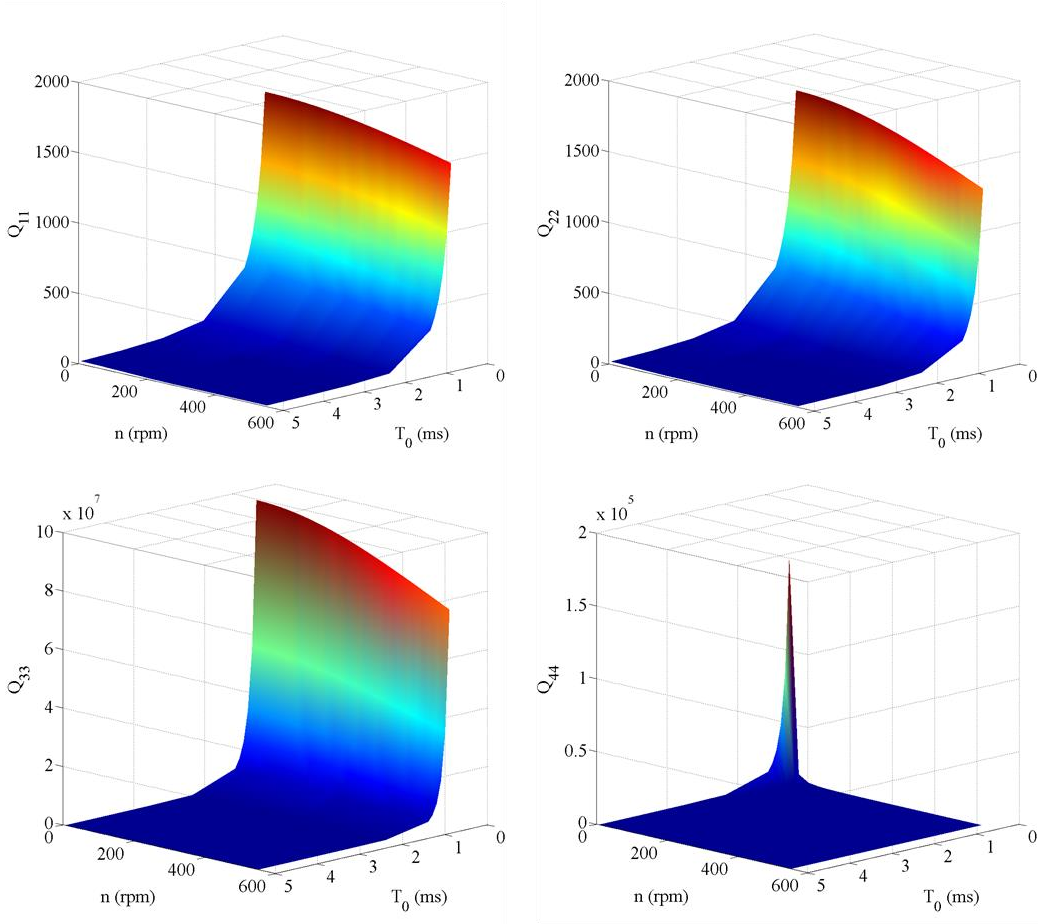

Figure 57. Values of the diagonal of Q [160]

In Figure 57, it can be noticed that for the first three elements $\mathrm{Q_{11}}, \mathrm{Q_{22}}$, and $\mathrm{Q_{33}}$ their values affected primarily by observability horizon variation. Whereas during the speed variation, the values of these three elements stay almost the same. So, by finding the appropriate value of observability horizon, that makes the difference in accurate estimation.

III.4.2. Results and conclusions

Figure 58 (a) shows the evolution of the measured (real n) and the estimated speeds during a step response. During this test the speed increases from 100 to 400rpm, the generated power p_{BUS} varies from 0 to 800W (with the reference bus voltage $u_{BUS}* = 200\mathrm{V}$).

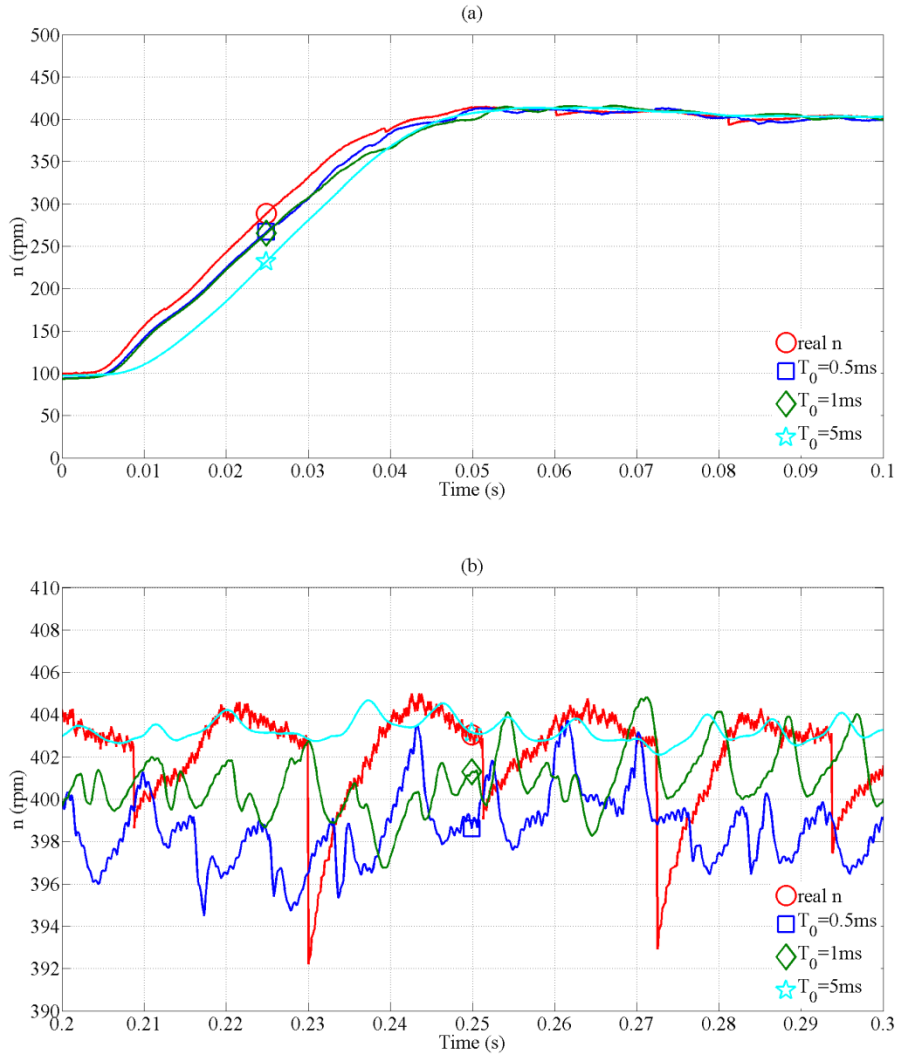

Figure 58. Evolution of measured (real n) and estimated speeds during a step response (a) and on steady state (b).[160]

Different values of T_0 have been tested into the range 0.1ms to 6ms. The lowest value may be greater than the sampling period and the highest one correspond to the time constant L_S/R_S. As it is illustrated on Figure 58 (a), with a small observation horizon, the estimation converges quickly. As it is illustrated on Figure 58 (b), whatever the value of T_0, the estimation errors do not exceed 1%. As one can see, for $T_0 = 5\text{ms}$ the speed estimation filters the high frequencies fluctuations of the real speed induced by eventual perturbations due to the electrical drive system.

In the studied case, the highest value of T_0 seems to be the most convenient for the parametrization of the Kalman filter.

A second test has been experimented to implement the speed observer with the MPPT as shown in Figure 60. A wind speed profile has been emulated as illustrated in Figure 59. It can be seen that short

observation horizons T_0 influence significantly the speed estimation while this one is used inside a MPPT control and consequently influence the performances of the MPPT.

The best performance is obtained for large observation horizon T_0 ($e_{BUS} = 1.7\text{Wh}$ for $T_0 = 5\text{ms}$ versus $e_{BUS} = 1.63\text{Wh}$ for $T_0 = 0.5\text{ms}$). For values of T_0 strongly inferior to the electrical time constant L_S/R_S, the speed observer does not filter the high frequencies perturbations. On the contrary, for large time constant, the speed estimation acts as a low pass filter and rejects the perturbations on the speed. To complete this experimental validation, Figure 61 shows the appropriate use of extended Kalman filter with adaptive control for a real wind profile (of 10 minutes for the 15th of January in Compiegne). As a conclusion, the observation horizons T_0 must be close without being higher than the electrical time constant L_S/R_S in order to warrant the best performances.

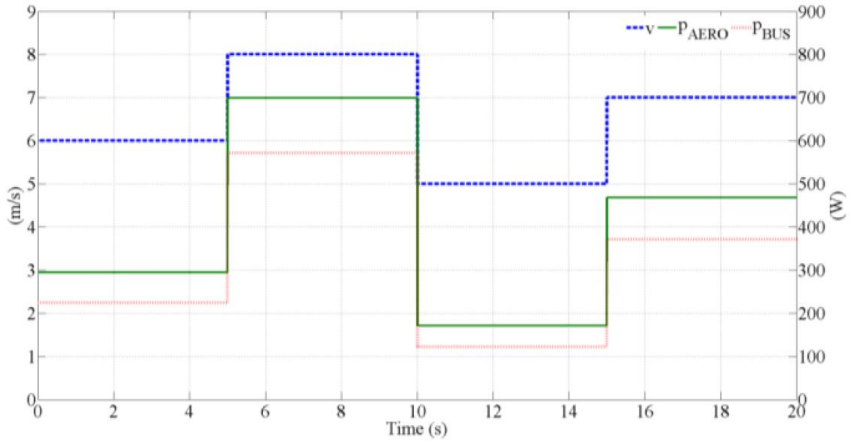

Figure 59. Arbitrary wind speed profile v and optimum evolution of p_{BUS} and p_{AERO} [160]

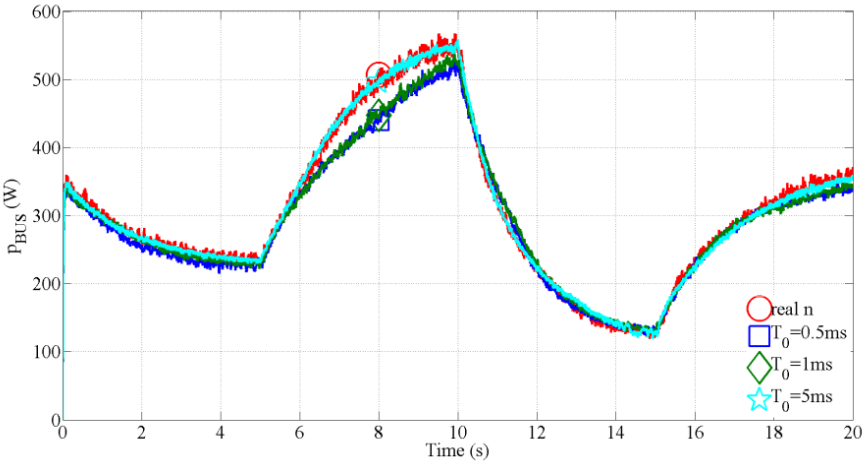

Figure 60. Evolution of the generated power p_{BUS} for a wind speed profile.[160]

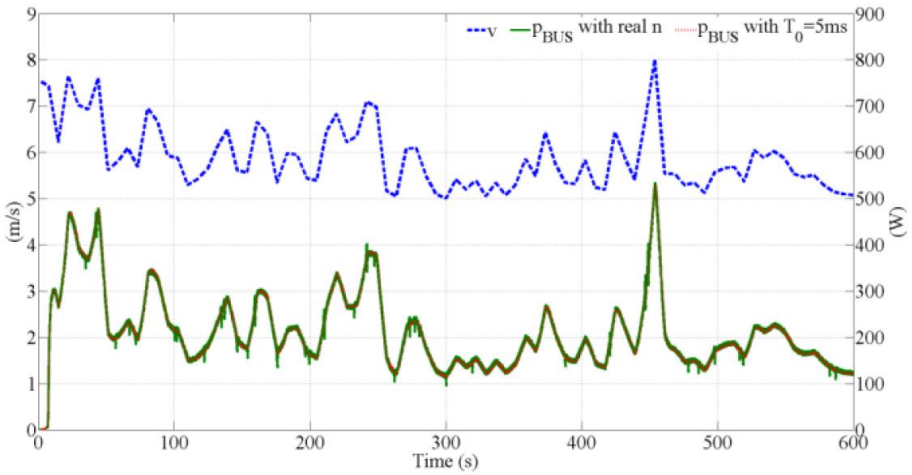

Figure 61. Evolution of the power generated in 10 minutes for the 15 January in Compiegne [160]

In this section a small-scale wind generator PMSM-based associated with an indirect MPPT method was studied. Choosing an active energy conversion structure and a sensorless PMSM, to control the system a speed estimator is required.

Facing to other methods, the EKF model-based estimator allows sensorless drive control in a wide speed range and estimates the rotation speed with a rapid response. Knowing that the voltage and current sensors are required for security issues, therefore, the use of the estimator does not induce additional costs. Furthermore, it saves a speed sensor that can generally represent more than 10% of the price of a small scale wind generator.

The EKF parameters tuning is solved by introducing an adaptive method, i.e. adaptive-tuning EKF. This adaptive estimation approach is innovative by using a covariance matching technique. This new method for adaptive-tuning of parameters of the EKF for a small scale wind generator allows easy operation of the EKF. It is implemented and then validated experimentally. The experimental results prove that the proposed method is technically feasible with good performances within some limits. One of these limits concerns the observation horizons T_0 whose values have to be both close and inferior to the electrical time constant in order to obtain the best performance. Therefore, as the observation horizons should be variable, further work will aim to find a criterion to determine the best value of T_0 for each operating point and adapt it in real time.

Anyway this observation horizon simplifies the procedure of choosing the values of various elements of Kalman matrices.

III.5. Conclusion

In this chapter, several sensorless methods allowing position and speed observation of the PMSM are presented. The most used methods in the estimation of the PMSM position and speed techniques were illustrated. At low speeds, although the techniques are numerous, injecting high frequency alternative signals appears to be the most accurate method. A state of the art is proposed to choose the methods the most appropriate depending on operating conditions. For the near nominal operation, we introduced four types of estimation methods.

Firstly, we considered the fixed coordinate system α-β. Two methods were presented of which the first is a sliding mode observer. The second is to estimate directly the speed and the position using a flux estimator plus PLL.

A model in the rotating frame d-q then is considered. In this case, the estimate of the speed comes before the position estimate that is derived by a simple integration of the speed. Luenberger observer of reduced order is presented for this aim. Experimental results were carried out for each case so that the position estimation is verified experimentally by using these mentioned methods. Then the estimation is verified at low speed begin from 4m/s then for higher speed (5m/s, 6m/s 7m/s and 8m/s). The EKF method is applied to synthesize a reduced observer for observing the position and speed of the machine. Experimental results were acceptable in the nominal case of position estimation but it needs elaborated work to design the covariance matrices.

Finally, the case of EKF with adaptive tuning approach is studied in order to find a solution to covariance matrices tuning. The EKF observer with adaptive tuning approach is presented in this section and tested in the test bench. As EKF sensorless approach with adaptive auto tuning of its matrices components it is found that this approach has improved the performance of the observer even at low speed.

There are other types of observers in the literature that have not been presented in this thesis, as it focuses on the methods most used. For example for other methods, sliding mode observer of higher order presented in [66], the interconnected adaptive observers [163], the observer Matsui [164], etc.

General conclusion and perspectives

In an ecological context more and more significant, this thesis makes a contribution to the field of renewable energies, particularly in the sector said the “small-scale wind turbines". The main objective of this study involved the propose of a small-scale wind power system whose structure is simplified to offer a compromise cost - reliability - satisfactory performance.

In the first chapter, a state of the art focused on renewable energies especially the "small-scale wind turbine" has shown us the various systems used in wind power generation. This bibliographic study is to highlight what our needs in order to simplify the system while preserving its energy efficiency. It is found that the simplest passive architecture has no active power control therefore no energy optimization; hence it was not chosen to be studied. Fully controlled architecture has been tested experimentally and it has a good optimization but it still of high cost. MPPT controls require more or less complex architectures, but it is found that they have good power optimization. So, the chosen system is "passive" rectifier added to it a boost converter with MPPT strategy because it incorporates power control hence power optimization. A permanent magnets synchronous generator directly coupled to the three blades of the turbine is used, connected to a DC bus through a three-phase diode rectifier. The issue of grid connection is not addressed in this thesis. Therefore this chapter has helped to build the foundations of our study through the representation of all the elements of wind power system represented by different energy conversion structures. Several structures and management strategies with regard to cost criteria and energy efficiency were discussed. According to this criterion,

special attention was paid to the performance in each model. The main conclusions taken in consideration for the study concern:

- Modeling a wind profile including a significant temporal wind turbulent component.
- The generator is represented from an analytical model coupled then, via the circuits' parameters. Three models were represented. The first model is in natural base *i.e.* three-dimensional stationary base *A-B-C*; the second model, developed in two-dimensional stationary α-β. The third model is in two-dimensional rotor base *d-q*.
- This confrontation is confirmed by the experimental approach based on a generator prototype for wind emulating approach. Indeed, the circuit parameters of the prototype are also at consistency with those from the models.
- Study of the wind turbine emulator for each wind value of a static or dynamic profile. The main inertial effects are also properly taken into account.

In chapter II, these last points were taken into account. A model of small-scale wind turbine emulator, which is considered in this study, is presented along with the experimental validation. A direct MPPT algorithm is introduced with two strategies, *i.e.* fixed and variable step. According to the characteristic of the small scale wind generator, the classical fixed step P&O method and a variable step P&O method are implemented to achieve MPPT. Experiments results suggest that both algorithms correctly find out the MPP whatever the wind speed increases or decreases. With the physical restrictions, extracted energies for two methods are not significantly different, but the variable step MPPT clearly suppresses the oscillation amplitude when generator system operates close to the MPP. Then a simple and robust MPPT indirect method was validated. For small-scale wind turbines with a high mechanical time constant, the indirect method of MPPT gives the best results. Moreover, this method is not only for experts of MPPT methods, it is fast to implement and add to that its simplicity. The hindrance of this method is its need to speed/position sensor; the price of a mechanical sensor can be up to 20% of the total price of a small-scale wind turbine. To utilize an indirect MPPT of less cost, estimating the speed becomes a fundamental matter, which lead to focus on this point in the third chapter.

In the third chapter, a presentation of the various works carried out on the position estimation of synchronous machine rotor with permanent magnets has been conducted. In this chapter, the principle of control without mechanical sensor has been developed. Methods that estimate the rotor speed/position were presented. The state of the art to estimate the initial position of the rotor that has been proposed in the literature was included. After analyzing the different techniques for detecting the position, thus, different methods proposed in literatures are considered and classified to be studied in details, and then the most effective and widely used one were verified experimentally for the studied

system. The methods which are chosen are SMO, rotor flux estimation with PLL, Luenberger observer of reduced order and EKF.

Experimental tests for each method were performed to compare the performance of speed/position estimation. Opposite to other methods, the EKF model-based estimator permits sensorless drive control in a wide speed range and estimates the rotation speed with a rapid response. The EKF parameters tuning is the main problem to its implementation. Hence to solve this problem, the thesis introduces an adaptive method, *i.e.* adaptive-tuning EKF. As a result and grace to this approach, the total cost of conversion system is reduced and the performance is guaranteed and optimized.

Finally, the systemic approach in this thesis allowed us to identify the main models of conversion systems and controls the component elements of the small scale wind turbine, which meet the specific needs of being integrated into the microgrid at minimum cost. Thus, several perspectives can be traced, in the continuity of this work. So, this study opens a number of perspectives:

- Studying the effect of each estimation methods with other configuration of control *e.g.* fully controlled converter.
- Most estimation processes have time varying parameters. Among these parameters, one can distinguish the stator resistance of PMSM. The value of this resistance can increase to twice its nominal value due to the stator heating. Therefore, errors are occurred on the estimation of speed and rotor position. To remedy this problem, it is necessary as the stator resistance estimate for the control without mechanical sensor using *e.g.* the MRAS method.
- Exploiting the estimation techniques developed in chapter III to design an estimator for the flux of permanent magnets.
- To study and implement algorithms for detection and isolation of a default speed/position with reconfiguring the PMSM control to ensure continuity of system operation.
- Interestingly, thereafter, implementing advanced fault detection methods in chosen control without mechanical sensor, in particular defects of opening of a stator phase faults stator short-circuit and the presence of other defects at the inverter.

Publications

Article in international journals with reviewing committee

- H. Al-Ghossini, F. Locment, M. Sechilariu, L. Gagneur, C. Forgez, "Adaptive-tuning of extended Kalman filter used for small scale wind generator control", Renewable Energy, Volume 85, Pages 1237-124, January 2016.

Communications with reviewing committee published in international conferences

- H. Al-Ghossini, F. Locment and M. Sechilariu, "Experimental comparison of small wind turbine vector control with and without position sensor — Extended Kalman filter application," EPE 2013 15th European Conference on Power Electronics and Applications, pp. 1-9, Lille, 2013.

- H. Al-Ghossini, B. Wang, F. Locment and M. Sechilariu, "Energetic macroscopic representation and inversion-based control of DC micro-grid," EPE 2013 15th European Conference on Power Electronics and Applications, Lille, pp. 1-10, 2013.

- H. Al-Ghossini, H. Liu, F. Locment and M. Sechilariu, "Estimation of speed rotation for MPPT used by small scale wind generator integrated in DC microgrid experimental validation," IECON 2014 - 40th Annual Conference of the IEEE Industrial Electronics Society, Dallas, TX, pp. 2082-2088, 2014.

Communication with reviewing committee published in national conferences

- H. Al-Ghossini, "Validation expérimentale d’une commande vectorielle sans capteur mécanique à l’aide d’un filtre de Kalman étendu pour une éolienne de faible puissance", JCGE'15 Conférence des Jeunes Chercheurs en Génie Électrique, 10-11 juin, 2015.

References

[1] M. Sechilariu, F. Locment, "Connecting and Integrating Variable Renewable Electricity in Utility Grid", Urban DC Microgrid: Intelligent Control and Power Flow Optimization, Elsevier Inc., pp 1-33, ISBN :9780128037362. doi:10.1016/B978-0-12-803736-2.00001-3.

[2] B.C. Wang, M. Sechilariu, F. Locment : "Intelligent DC Microgrid with Smart Grid Communications: Control Strategy Consideration and Design", IEEE Trans. on Smart Grid, Special Issue on Intelligent Buildings and Home Energy Management in a Smart Grid Environment, vol. 3, no. 4, pp. 2148-2156, Dec. 2012. DOI:10.1109/TSG.2012.2217764.

[3] M. Sechilariu : "Urban DC microgrids for advanced local energy management with smart grid communication", 3rd ENEFM2015 (International Congress on Energy Efficiency and Energy Related Materials, Oludeniz (Turkey), 19-23 October, 2015.

[4] M. Sechilariu, B.C. Wang, and F. Locment, "Supervision control for optimal energy cost management in DC microgrid: design and simulation", International Journal of Electrical Power and Energy Systems vol. 58, pp. 140-149, Apr. 2014. doi:10.1016/j.ijepes.2014.01.018.

[5] M. Sechilariu, B.C. Wang, F. Locment, and A. Jouglet, "DC microgrid power flow optimization by multi-layer supervision control. Design and experimental validation",

Energy Conversion and Management, vol. 82, pp. 1-10, Mar. 2014. doi:10.1016/j.enconman.2014.03.010.

[6] IBM ILOG CPLEX Optimizer. Available online: http://ibm.com.

[7] N. Hatziargyriou : Microgrids: Architectures and Control. Wiley – IEEE, 2014.

[8] M. Sechilariu, F. Locment, B.C. Wang : “Photovoltaic electricity for sustainable building. Efficiency and energy cost reduction for isolated DC microgrid”, Energies, Special Issue on Solar Photovoltaics Trilemma: Efficiency, Stability and Cost, vol. 8, no.8, pp 7945-7967, MDPI Ed., August 2015. doi:10.3390/en8087945.

[9] B. T. Patterson, "DC, Come Home: DC Microgrids and the Birth of the "Enernet"", IEEE Power & Energy Mag., vol. 10, no. 6, pp. 60-69, 2012.

[10] F. Locment, “Contribution à la modélisation et à la commande des sources renouvelables dans les micro-réseaux urbains”, Accreditation to supervise research (HDR Habilitation à la Direction de Recherches), Université de la Technologie de Compiegne, 2015

[11] http://en.wikipedia.org/wiki/History_of_wind_power/

[12] http://www.gwec.net/

[13] A. Abdelli "Optimisation multicritère d'une chaîne éolienne passive", Thèse de doctorat, Université de Toulouse, 2007.

[14] http://www.vestas.com/en/media/images#!turbines/

[15] https://en.wikipedia.org/wiki/Wind_power/

[16] http://www.ecosources.info/

[17] A.R. Jha, "Wind Turbine Technology", [handbook], Taylor & Francis Group, Boca Raton, U.S., 2011.

[18] C. Nichita, S. Pierre, M. Baïlo Camara and B. Dakyo, "Control strategy of a wind turbine simulation system designed for a hybrid wind-tidal real time emulator," Renewable Power Generation Conference (RPG 2014), 3rd, Naples, 2014, pp. 1-6.

[19] F. Locment, "Conception et modélisation d’une machine synchrone à 7 phases à aimantspermanents et flux axial : commande vectorielle en modes normal et dégradé", Thèse de doctorat, USTL, L2EP, 2006.

[20] X. Kestelyn and E. Semail, "A Vectorial Approach for Generation of Optimal Current References for Multiphase Permanent-Magnet Synchronous Machines in Real Time," in IEEE Transactions on Industrial Electronics, vol. 58, no. 11, pp. 5057-5065, Nov. 2011.

[21] M. Sechilariu, B.C. Wang, and F. Locment, "Building-integrated microgrid: advanced local energy management for forthcoming smart power grid communication", Energy and Building, vol. 59, no. 1, pp. 236-243, Apr. 2013.

[22] D. Salomonsson and A. Sannino, "Low-voltage DC distribution system for commercial power systems with sensitive electronic loads", IEEE Trans. Power Del., vol. 22, no. 3, pp. 1620-1627, Jul. 2007.

[23] T. L. Vandoorn, F. M. de Belie, T. J. Vyncke, J. A. Melkebeek, and P. Lataire, "Generation of multisinusoidal test signals for the identification of synchronous machine parameters by using a voltage-source inverter," IEEE Trans. Ind. Electron., vol. 57, no. 1, pp. 430–439, Jan. 2010.

[24] L. N. Tutelea, C. K. Myung, M. Topor, J. Lee, and I. Boldea, "Linear permanent magnetic oscillatory machine: comprehensive modeling for transients with validation by experiments," IEEE Trans. Ind. Electron., vol. 55, no. 2, pp. 492–500, Feb. 2008.

[25] N. A. Orlando, M. Liserre, R. A. Mastromauro and A. Dell'Aquila, "A Survey of Control Issues in PMSG-Based Small Wind-Turbine Systems", IEEE Trans. Ind. Inform., vol. 9, no. 3, pp. 1211-1221, Aug. 2013.

[26] Y. S. Park, S. M. Jang, M. M. Koo, J. Y. Choi and S. Y. Sung, "Comparative Investigation on Integrated System of Permanent Magnet Synchronous Generator and Power Converter Based on Machine Topology for Small-Scale Wind Power Application", IEEE Trans. Magnetics, vol. 49, no. 7, pp. 3846-3849, 2013.

[27] C. Belalahy, "Dimensionnement d'une manchine synchro-reluctante à exitation homopolaire par reseaux de permeances", [Thèse], Université de Nancy - INPL, 2008.

[28] T. Senjyu, Y. Ochi, Y. Kikunaga, M. Tokudome, A. Yona, E.B. Muhando, N. Urasaki, T. Funabashi, "Sensor-less maximum power point tracking control for wind generation system with squirrel cage induction generator", Renewable Energy, vol. 34, no. 4, pp. 994-999, 2009.

[29] H. Liu, F. Locment, M. Sechilariu, "Maximum Power Point Tracking Method for Small Scale Wind Generator Experimental validation", International Conference on Instrumentation, Control, Information Technology and System Integration (SICE 2015), Hangzhou (China), July 2015.

[30] H. Al-Ghossini, H. Liu, F. Locment, M. Sechilariu, "Estimation of speed rotation for MPPT used by small scale wind generator integrated in DC microgrid experimental validation", IEEE Annual Conference on Industrial Electronics Society (IECON 2014), Dallas (USA), November 2014.

[31] D.H. Tran, B. Sareni, X. Roboam, C. Espanet, "Integrated Optimal Design of a Passive Wind Generator System: An Experimental Validation", IEEE Trans. on Sustainable Energy, vol. 1, pp. 48-56, 2010.

[32] C.T. Pan, Y.L. Juan, "A novel sensorless MPPT controller for a high-efficiency microscale wind power generator system", IEEE Trans. on Energy Conversion, vol. 25, pp. 207-216, 2010.

[33] M.K. Hong, H.H. Lee, "Adaptive maximum power point tracking algorithm for variable speed wind power systems", International conference on life system modeling and intelligent computing (LSMS 2010), and International conference on Intelligent computing for sustainable energy and environment (ICSEE 2010), pp. 380-388, Wuxi (China), 2010.

[34] R. Kot, M. Rolak, M. Malinowski, "Comparison of maximum peak power tracking algorithms for a small wind generator", Mathematics and Computers in Simulation, vol. 91, pp. 29-40, 2013.

[35] Y. Daili, J.P. Gaubert, L. Rahmani, "Implementation of a new maximum power point tracking control strategy for small wind energy conversion systems without mechanical sensors", Energy Conversion and Management, vol. 97, pp. 298–306, 2015.

[36] Z. Qi, E. Lin, "Integrated power control for small wind power system", Journal of Power Sources, vol. 217, pp. 322-328, 2012.

[37] I. Kortabarria, J. Andreu, I. Martínez de Alegría, J. Jiménez, J. Ignacio Gárate, E. Robles, "A novel adaptative maximum power point tracking algorithm for small wind turbines", Renewable Energy, vol. 63, pp. 785-796, 2014.

[38] Z.M. Dalala, Z. Ullah Zahid, W. Yu, Y. Cho, J.S. Lai, "Design and Analysis of an MPPT Technique for Small-Scale Wind Energy Conversion Systems", IEEE Trans. on Energy Conversion, vol. 28, pp. 756-767, 2013.

[39] Z.M. Dalala, Z. Ullah Zahid, J.S. Lai, "New Overall Control Strategy for Small-Scale WECS in MPPT and Stall Regions With Mode Transfer Control", IEEE Trans. on Energy Conversion, vol. 28, pp. 1082-1092, 2013.

[40] J.C. Wu, Y.H. Wang, "Power conversion interface for small-capacity wind power generation system", IET Generation Transmission & Distribution, vol. 8, pp. 689–696, 2014.

[41] A. Urtasun, P. Sanchis, I. San Martín, J. López, L. Marroyo, "Modeling of small wind turbines based on PMSG with diode bridge for sensorless maximum power tracking", Renewable Energy, vol. 55, pp. 138-149, 2013.

[42] A. Urtasun, P. Sanchis, L. Marroyo, "Small Wind Turbine Sensorless MPPT: Robustness Analysis and Lossless Approach", IEEE Trans. on Industry Applications, vol. 50, pp. 4113-4121, 2014.

[43] H. Zhao, Q. Wu, C. Nygaard Rasmussen, M. Blanke, "L1 Adaptive Speed Control of a Small Wind Energy Conversion System for Maximum Power Point Tracking", IEEE Trans. on Energy Conversion, vol. 29, pp. 576-584, 2014.

[44] A. Bravo Cuesta, F. Javier Gomez-Gil, J. Vicente Martín Fraile, J. Ausín Rodríguez, J. Ruiz Calvo, J. Peláez Vara, "Feasibility of a Simple Small Wind Turbine with Variable-Speed Regulation Made of Commercial Components", Energies, vol. 6, pp. 3373-3391, 2013.

[45] C.Y. Lee, P.H. Chen, Y.X. Shen, "Maximum power point tracking (MPPT) system of small wind power generator using RBFNN approach", Expert Systems with Applications, vol. 38, pp. 12058-12065, 2011.

[46] K. Nan Yu, C. Kang Liao, "Applying novel fractional order incremental conductance algorithm to design and study the maximum power tracking of small wind power systems", Journal of Applied Research and Technology, vol. 13, pp. 238-244, 2015.

[47] K. S. Muhammad Raza, H. Goto, H. J. Guo and O. Ichinokura, "A novel speed-sensorless adaptive hill climbing algorithm for fast and efficient maximum power point tracking of wind energy conversion systems," 2008 IEEE International Conference on Sustainable Energy Technologies, Singapore, pp. 628-633, 2008.

[48] R. Bharanikumar, A. Yazhini, and A. Kumar, "Modeling and simulation of wind turbine driven permanent magnet generator with new mppt algorithm", Asian Power Electronics Journal, 4(2), (2010).

[49] E. Koutroulis and K. Kalaitzakis, "Design of a maximum power tracking system for wind-energy-conversion applications," in IEEE Transactions on Industrial Electronics, vol. 53, no. 2, pp. 486-494, April 2006.

[50] Q. Trinh, and H. Lee, "Fuzzy logic controller for maximum power tracking in PMSG-based wind power systems". Advanced Intelligent Computing Theories and Applications. With Aspects of Artificial Intelligence, pages 543–553, (2010).

[51] I. Houssamo, F. Locment, M. Sechilariu, “Maximum power tracking for photovoltaic power system: Development and experimental comparison of two algorithms”, Renewable Energy, Vol.35, pp. 2381-2387, 2010.

[52] I. Houssamo, F. Locment, M. Sechilariu, “Experimental analysis of impact of MPPT methods on energy efficiency for photovoltaic power systems”, Electrical Power and Energy Systems, Vol. 46 pp. 98-107, 2013.

[53] Q. Huynh, F. Nollet, N. Essounbouli, and A. Hamzaoui, "Fuzzy control of variable speed wind turbine using permanent magnet synchronous machine for stand-alone system." In Sustainability in Energy and Buildings: Proceedings of the 3rd International Conference in Sustainability in Energy and Buildings (SEB 11), volume 12, page 31. (2012).

[54] M. Lopez, and J. Vannier, “Stand-alone wind energy conversion system with maximum power transfer control”. Ingeniare. Revista chilena de ingenieria, 17(3): 329–336, (2009).

[55] M. Hong, and H. Lee, "Adaptive maximum power point tracking algorithm for variable speed wind power systems", Life System Modeling and Intelligent Computing, pages 380–388, (2010).

[56] B. Beltran, "Contribution à la Commande Robuste des Eoliennes à Base de Génératrices Asynchrones Double Alimentation : Du Mode Glissant Classique au Mode Glissant d’Ordre Supérieur.", PhD thesis, Université de Bretagne occidentale-Brest, (2010).

[57] A. Mirecki, "Etude comparative de chaînes de conversion d’énergie dédiées à une éolienne de petite puissance", PhD thesis. (2005).

[58] N. Kasa, T. Iida and Liang Chen, "Flyback Inverter Controlled by Sensorless Current MPPT for Photovoltaic Power System," in IEEE Transactions on Industrial Electronics, vol. 52, no. 4, pp. 1145-1152, Aug. 2005.

[59] R. Kot, M. Rolak and M. Malinowski, "Comparison of maximum peak power tracking algorithms for a small wind turbine", Mathematics and Computers in Simulation, vol. 91, pp. 29-40, May. 2013.

[60] Z. Zhing, Commande à haute performance et sans capteur mécanique du moteur synchrone à aimants permanents [thèse], Toulouse, L'institut National Polytechnique de Toulouse, 2008.

[61] P. P. Acarnely and J. F. Watson, "Review of Position Sensorless Operation of Brushless Permanent Magnet Machines," IEEE Trans. Ind. Electron., vol. 53, no. 2, pp. 352-362, APR. 2006.

[62] D. Luenberger, “An introduction to observers.” In IEEE Transactions on Automatic Control, vol. 16, no. 6, pp. 596–602, DEC. 1971.

[63] E. Cherrier, “Estimation de l’état et des entrées inconnues pour une classe de systèmes non linéaires.” Thèse de doctorat, Institut National Polytechnique de Lorraine, France. (2006).

[64] E. Busvelle, J. Gauthier, “Observation and identification tools for nonlinear systems: application to a fluid catalytic cracker.” International Journal of Control, 78(3) :208 –234. 2005.

[65] M., Fliess, C., Join, and H. Sira-Ramírez, “Non-linear estimation is easy.” International Journal of Modelling Identification and Control, vol. 4, no. 1, pp. 12–27, 2008.

[66] M. Mohamed Moustafa Ezzat. “Commande non linéaire sans capteur de la machine synchrone à aimants permanents.” PhD thesis, École Centrale de NANTES, 2011.

[67] G. Zhu, A. Kaddouri, L-A. Dessaint, and O. Akhrif, "A Nonlinear State Observer for the Sensorless Control of a Permanent Magnet AC Machine," IEEE Trans. Ind. Electron., vol. 48, no. 6, pp. 1098-1108, DEC. 2001.

[68] B. N-Mobarakeh, F. M-Tabar, and F-M. Sargos, "Back e.m.f Estimation Based Sensorless Control of PMSM Robustness With Respect to Measurement Errors and Inverter Irregularities," IEEE Trans. Ind. Appl., vol. 43, no. 2, pp. 485-494, MAR/APR. 2007.

[69] B. N-Mobarakeh, F. M-Tabar, and F-M. Sargos, "Mechanical Sensorless Control of PMSM With Online Estimation of Stator Resistance," IEEE Trans. Ind. Appl., vol. 40, no. 2, pp. 457-471, MAR/APR. 2004.

[70] C. D. Angelo, G. Bossio, J. Solsona, G. O. Garcia, and M. I. Valla, "Mechanical Sensorless Speed Control of Permanent Magnet AC Machines Driving an Unknown Load," IEEE Trans. Ind. Electron., vol. 53, no. 2, pp. 406-414, APR. 2006.

[71] H. Kim, M. C. Harke, and R. D. Lorenz, "Sensorless Control of Interior Permanent Magnet Machine Drives With Zero Phase Lag Position Estimation," IEEE Trans. Ind. Appl., vol. 39, no. 6, pp. 1726-1733, NOV/DEC. 2003.

[72] M. Jansson, L. Harnefors, O. Wallmark, and M. Leksell, "Synchronization at Startup and Stable Rotation Reversal of Sensorless Nonsalient PMSM Drives," IEEE Trans. Ind. Electron., vol. 53, no. 2, pp. 379-387, APR. 2006.

[73] V. D. Colli, R. D. Stefano, and F. Marignetti, "A System on Chip Sensorless Control for a Permanent Magnet Synchronous Machine," IEEE Trans. Ind. Electron., vol. 57, no. 11, pp. 3822-3829, NOV. 2010.

[74] F. Genduso, R. Miceli, C. Rando, and G. R. Galluzzo, "Back e.m.f Sensorless Control Algorithm for High Dynamic Performance PMSM ," IEEE Trans. Ind. Electron., vol. 57, no. 6, pp. 2092-2100, JUN. 2010.

[75] R. Mizutani, T. Takeshita, and N. Matsui, "Current Model Based Sensorless Drives of Salient Pole PMSM at Low Speed and Standstill," IEEE Trans. Ind. Appl., vol. 34, no. 4, pp. 841-846, JUL/AUG. 1998.

[76] T. Noguchi and S. Kohno, "Mechanical Sensorless Permanent Magnet Machine Drive Using Relative Phase Information of Harmonic Currents Caused by Frequency Modulated Three

Phase PWM Carriers," IEEE Trans. Ind. Appl., vol. 39, no. 4, pp. 1085-1092, JUL/AUG. 2003.

[77] T. Noguchi, K. Takehana, and S. Kondo, "Mechanical Sensorless Robust Control of Permanent Magnet Synchronous Machine Using Phase Information of Harmonic Reactive Power," IEEE Trans. Ind. Appl., vol. 37, no. 6, pp. 1786-1792, NOV/DEC. 2001.

[78] K-Y Lian, Ch-H Chiang, and H-W Tu, "LMI-Based Sensorless Control of Permanent Magnet Synchronous Machines," IEEE Trans. Ind. Electron., vol. 54, no. 5, pp. 2769-2778, OCT. 2007.

[79] Z. Chen, M. Tomita, Sh. Doki and Sh. Okuma, "An Extended Electromotive Force Model for Sensorless Control of Interior Permanent Magnet Synchronous Machines," IEEE Trans. Ind. Electron., vol. 50, no. 2, pp. 288-295, APR. 2003.

[80] Sh. Ichikawa, M. Tomita, Sh. Doki, and Sh. Okuma, "Sensorless Control of Permanent Magnet Synchronous Machines Using Online Parameter Identification Based on System Identification Theory ," IEEE Trans. Ind. Electron., vol. 55, no. 2, pp. 363-372, APR. 2006.

[81] Sh. Morimoto, K. Kawamoto, M. Sanada, and Y. Takeda , "Sensorless Control Strategy for Salient Pole PMSM Based on Extended e.m.f in Rotating Reference Frame," IEEE Trans. Ind. Appl., vol. 38, no. 4, pp. 1054-1061, JUL/AUG. 2002.

[82] J. X. Shen, Z. Q. Zhu, and K. Howe, "Sensorless Flux Weakening Control of Permanent Magnet Brushless Machines Using Third Harmonic Back e.m.f," IEEE Trans. Ind. Appl., vol. 40, no. 6, pp. 1629-1636, NOV/DEC. 2004.

[83] S. Bolognani, L. Tubiana, and M. Zigliotto, "Extended Kalman Filter Tuning in Sensorless PMSM Drives," IEEE Trans. Ind. Appl., vol. 39, no. 6, pp. 1741-1747, NOV/DEC. 2003.

[84] S. Bolognani, M. Zigliotto, and M. Zordan, "Extended Range PMSM Sensorless Speed Drive Based on Stochastic Filtering," IEEE Trans. Power Electron., vol. 16, no. 1, pp. 110-117, JAN. 2001.

[85] S. Bolognani, R. Oboe, and M. Zigliotto, "Sensorless Full Digital PMSM Drive With EKF Estimation of Speed and Rotor Position," IEEE Trans. Ind. Electron., vol. 46, no. 1, pp. 184-191, FEB. 1999.

[86] R. Dhaouadi, N. Mogan, and L. Norum, "Design and Implementation of an Extended Kalman Filter for the State Estimation of a Synchronous Machine," IEEE Trans. Power Electron., vol. 6, no. 3, pp. 440-449, JUL. 1991.

[87] A. Arias, C. A. Silva, G. M. Asher, J. C. Clare, and P. W. Wheeler, "Use of a Matrix Converter to Enhance the Sensorless Control of a Surface Mount Permanent Magnet AC

Machine at Zero and Low Frequency," IEEE Trans. Ind. Electron., vol. 53, no. 2, pp. 440-449, APR. 2006.

[88] Sh. Shinnaka, "A New Speed Varying Ellipse Voltage Injection Method for Sensorless Drive of Permanent Magnet Synchronous Machines With Pole Saliency—New PLL Method Using High Frequency Current Component Multiplied Signal," IEEE Trans. Ind. Appl., vol. 44, no. 3, pp. 777-788, MAY/JUN. 2008.

[89] Md. E. Haque, L. Zhong, and M. F. Rahman, "A Sensorless Initial Rotor Position Estimation Scheme for a Direct Torque Controlled Interior Permanent Magnet Synchronous Machine Drive," IEEE Trans. Power Electron., vol. 18, no. 6, pp. 1376-1383, NOV. 2003.

[90] J. Holtz, "Acquisition of Position Error and Magnet Polarity for Sensorless Control of PM Synchronous Machines," IEEE Trans. Ind. Appl., vol. 44, no. 4, pp. 1127-1180, JUL/AUG. 2008.

[91] J-H. Jang, J-I Ha, M.Ohto, K. Ide, and S-K. Sul, "Analysis of Permanent Magnet Machine for Sensorless Control Based on High Frequency Signal Injection," IEEE Trans. Ind. Appl., vol. 40, no. 6, pp. 1595-1604, NOV/DEC 2004.

[92] J-I Ha,K. Ide, T. Sawa, and S-K. Sul, "Sensorless Rotor Position Estimation of an Interior Permanent Magnet Machine From Initial States," IEEE Trans. Ind. Appl., vol. 39, no. 3, pp. 761-767, MAY/JUN. 2003.

[93] J-H. Jang, S-K. Sul, J-I Ha, K. Ide, and M. Sawamura, "Sensorless Drive of Surface Mounted Permanent Magnet Machine by High Frequency Signal Injection Based on Magnetic Saliency," IEEE Trans. Ind. Appl., vol. 39, no. 4, pp. 1031-1039, JUL/AUG. 2003.

[94] Piippo, M. Henkkanen, and J. Luomi, "Adaptation of Machine Parameters in Sensorless PMSM Drives," IEEE Trans. Ind. Appl., vol. 48, no. 1, pp. 203-212, JAN/FEB 2009.

[95] Piippo, J. Salomaki, and J. Luomi, "Signal Injection in Sensorless PMSM Drives Equipped With Inverter Output Filter," IEEE Trans. Ind. Appl., vol. 44, no. 5, pp. 1614-1620, SEP/OCT. 2008.

[96] Piippo, M. Henkkanen, and J. Luomi, "Analysis of an Adaptive Observer for Sensorless Control of Interior Permanent Magnet Synchronous Machines," IEEE Trans. Ind. Electron., vol. 55, no. 2, pp. 570-576, FEB. 2008.

[97] M. Boussak, "Implementation and Experimental Investigation of Sensorless Speed Control With Initial Rotor Position Estimation for Interior Permanent Magnet Synchronous Machine Drive," IEEE Trans. Power Electron., vol. 20, no. 6, pp. 1413-1422, NOV. 2005.

[98] T. D. Batzel and K. Y. Lee, "An Approach to Sensorless Operation of the Permanent Magnet Synchronous Machine Using Diagonally Recurrent Neural Networks," IEEE Trans. Energy Conv., vol. 18, no. 1, pp. 100-106, MAR. 2003.

[99] T. D. Batzel and K. Y. Lee, "Electric Propulsion With the Sensorless Permanent Magnet Synchronous Machine Model and Approach," IEEE Trans. Energy Conv., vol. 20, no. 4, pp. 818-825, DEC. 2005.

[100] Sh. Shinnaka, "New “D-state Observer” Based Vector Control for Sensorless Drive of Permanent Magnet Synchronous Machines," IEEE Trans. Ind. Appl., vol. 41, no. 3, pp. 825-833, MAY/JUN. 2005.

[101] Sh. Shinnaka, "New Sensorless Vector Control Using Minimum Order Flux State Observer in a Stationary Reference Frame for Permanent Magnet Synchronous Machines," IEEE Trans. Ind. Electron., vol. 53, no. 2, pp. 388-398, APR. 2006.

[102] M. Hasegawa, S. Yoshioka, and K. Matsui, "Position Sensorless Control of Interior Permanent Magnet Synchronous Machines Using Unknown Input Observer for High Speed Drives," IEEE Trans. Ind. Appl., vol. 45, no. 3, pp. 938-946, MAY/JUN. 2009.

[103] J. Lee, J. Hong, K. Nam, R. Ortega, L. Praly, and A. Astolfi, "Sensorless Control of Surface Mount Permanent Magnet Synchronous Machines Based on a Nonlinear Observer," IEEE Trans. Ind. Electron., vol. 25, no. 2, pp. 290-297, FEB. 2010.

[104] M. Rashed, P. F. A. MacConnell, A. F. Stronach, and P. Acarnley, "Sensorless Indirect Rotor Field Orientation Speed Control of a Permanent Magnet Synchronous Machine With Stator Resistance Estimation ," IEEE Trans. Ind. Electron., vol. 54, no. 3, pp. 1664-1675, JUN. 2007.

[105] M. Pacas, “Sensorless drives in industrial applications,” IEEE Industrial Electronics Magazine, vol. 5, no. 2, pp. 16–23, june 2011.

[106] M. J. Corley and R. D. Lorenz, “Rotor position and velocity estimation for a salient-pole permanent magnet synchronous machine at standstill and high speeds,” IEEE Transactions on Industry Applications, vol. 34, no. 4, pp. 784–789, 1998.

[107] F. Briz and M. Degner, “Rotor position estimation,” IEEE Industrial Electronics Magazine, vol. 5, no. 2, pp. 24–36, june 2011.

[108] R. Wu and G. Slemon, “A permanent magnet motor drive without a shaft sensor,” IEEE Transactions on Industry Applications, vol. 27, no. 5, pp. 1005–1011, sep/oct 1991.

[109] M. Hamida, J. De Leon, A. Glumineau, and R. Boisliveau, “An adaptive interconnected observer for sensorless control of pm synchronous motors with online parameter

identification," IEEE Transactions on Industrial Electronics, vol. 60, no. 2, pp. 739–748, 2013.

[110] J. Hu, D. Zhu, Y. Li, and J. Gao. Application of sliding observer to sensorless permanent magnet synchronous motor drive system. In IEEE Power Electronics Specialists Conference, (PESC), 1994.

[111] Y. S. Han, J. S. Choi, and Y. S. Kim. Sensorless PMSMdrive with a sliding mode control based adaptive speed and stator resistance estimator. IEEE Trans. Magn., vol. 36, no.5 :pp. 3588 – 3591, 2000.

[112] G. Ya, L. Weiguo, and Y. Qian. Study of position sensorless control based on sliding mode observer. In International Conference on Electrical Machines and Systems (ICEMS), 2011.

[113] H. Kim, J.Son, and J. Lee. A high-speed sliding-mode observer for the sensorless speedcontrol of a PMSM. IEEE Trans. Ind. Electron., vol. 58, no. 9 :pp. 4069 – 4077, 2011.

[114] Z. Qiao, T. Shi, Y. Wang, Y. Yan, C. Xia, and X. He. New sliding-mode observer for position sensorless control of permanent-magnet synchronous motor. IEEE Trans. Ind. Electron., vol. 60, no. 2 :pp. 710 – 719, 2013.

[115] V. Srikanth and A. A. Dutt. A comparative study on the effect of switching functions in SMO for PMSM drives. In IEEE International Conference on Power Electronics, Drives and Energy Systems (PEDES), 2012.

[116] Y. Feng, J. Zheng, X. Yu, and N. V. Truong. Hybrid terminal sliding-mode observer design method for a permanent-magnet synchronous motor control system. IEEE Trans. Ind. Electron., vol. 56, no. 9 :pp. 3424 – 3431, 2009.

[117] J. Liu, T. A. Nondahl, P. B. Schmidt, S. Royak, and M. Harbaugh. Rotor position estimation for synchronous machines based on equivalent EMF. IEEE Trans. Ind. Appl., vol. 4, no. 3 :pp. 1310 – 1318, 2011.

[118] S. Alahakoon, T. Fernando, H. Trinh, V. Sreeram, "Unknown input sliding mode functional observers with application to sensorless control of permanent magnet synchronous machines" Journal of the Franklin Institute, Volume 350, Issue 1, February 2013, Pages 107-128.

[119] R. Nalepa, T. Orlowska-Kowalska, "Optimum Trajectory Control of the Current Vector of a Nonsalient-Pole PMSM in the Field-Weakening Region," Industrial Electronics, IEEE Transactions on , vol.59, no.7, pp.2867,2876, July 2012.

[120] Ma. Zhixun, Jianbo Gao; R. Kennel, "FPGA Implementation of a Hybrid Sensorless Control of SMPMSM in the Whole Speed Range," Industrial Informatics, IEEE Transactions on , vol.9, no.3, pp.1253,1261, Aug. 2013.

[121] Vosmik, David; Smidl, Vaclav; Peroutka, Zdenek, "Sensorless PMSM control: Hybrid rotor position estimator using maximum likelihood model selection," Industrial Electronics (ISIE), 2013 IEEE International Symposium on , vol., no., pp.1,6, 28-31 May 2013.

[122] S. Sayeef, G. Foo, M.F. Rahman, "Rotor Position and Speed Estimation of a Variable Structure Direct-Torque-Controlled IPM Synchronous Motor Drive at Very Low Speeds Including Standstill," Industrial Electronics, IEEE Transactions on , vol.57, no.11, pp.3715,3723, Nov. 2010.

[123] H. Al-Ghossini, F. Locment, and M. Sechilariu, "Experimental comparison of small wind turbine vector control with and without position sensor — Extended Kalman filter application," Power Electronics and Applications (EPE), 2013 15th European Conference, pp. 1-9, (2013).

[124] Y. Aite Driss, D. Yousfi, "PMSM sensorless control using back-EMF based position and speed estimation method," Renewable and Sustainable Energy Conference (IRSEC), 2013 International , vol., no., pp.436,440, 7-9 March 2013.

[125] R. Ortega, L. Praly, A. Astolfi, J. Lee, and K. Nam, “Estimation of rotor position and speed of permanent magnet synchronous motors with guaranteed stability,” IEEE Transactions on Control Systems Technology, vol. 19, no. 3, pp. 601–614, may 2011.

[126] A. M. Salamah, S. J. Finney, and B. W. Williams, “Three-phase phase-lock loop for distorted utilities,” IET Electric Power Applications, vol. 1, no. 6, pp. 937–945, 2007.

[127] C. Wen; G. Lu; P. Wang; Zh. Li; X. Liu; Z. Fan, "Vector control strategy for small-scale grid-connected PMSG wind turbine converter," Innovative Smart Grid Technologies (ISGT Europe), 2011 2nd IEEE PES International Conference and Exhibition on , vol., no., pp.1,7, 5-7 Dec. 2011.

[128] D. Flieller, D. Ould Abdeslam, P. Wira, and J. Mercklé, “Distortions identification and compensation based on artificial neural networks using symmetrical components of the voltages and the currents,” Electronic Power System Research, vol. 79, no. 7, pp. 1145–1154, 2009.

[129] Y. H. Kim, K. S. Kim, B. K. Kwon, and C. H. Choi, “A fast and robust pll of mcfc pcs under unbalanced grid voltages,” Power Electronics Specialists Conference, pp. 4712–4716, 2008.

[130] S. Sarpturk, Y. Istefanopulos, and O. Kaynak, “On the stability of discretetime sliding mode control systems,” IEEE Transactions on Automatic Control, vol. 32, no. 10, pp. 930 – 932, oct 1987.

[131] H. Sira-Ramirez, “Nonlinear discrete variable structure systems in quasi sliding mode,” Int. J. Control, vol. 54, no. 5, pp. 1171–1187, oct 1991.

[132] Z. Qiao, T. Shi, Y. Wang, Y. Yan, C. Xia, and X. He, “New sliding-mode observer for position sensorless control of permanent-magnet synchronous motor,” IEEE Transactions on Industrial Electronics, vol. 60, no. 2, pp. 710–719, 2013.

[133] G. Wang, R. Yang, and D. Xu, “DSP-based control of sensorless IPMSM drives for wide-speed-range operation,” IEEE Transactions on Industrial Electronics, vol. 60, no. 2, pp. 720–727, feb 2013.

[134] R. Morales-Caporal, E. Bonilla-Huerta, M. Arjona, and C. Hernandez, “Sensorless predictive DTC of a surface-mounted permanent-magnet synchronous machine based on its magnetic anisotropy,” IEEE Transactions on Industrial Electronics, vol. 60, no. 8, pp. 3016–3024, 2013.

[135] V. Utkin, “Sliding mode control design principles and applications to electric drives,” IEEE Transactions on Industrial Electronics, vol. 40, no. 1, pp. 23–36, feb 1993.

[136] D. G. Luenberger. Observing the state of a linear system. IEEE Transactions on Miltary Electronics, vol. 8 :pp. 74 – 80, 1964.

[137] D. G. Luenberger. Observers for multivariable systems. IEEE Trans. Autom. Control., vol. 11 :pp. 190 – 197, avril 1966.

[138] M. Boussak, Implementation and exprimental investigation of sensorless speed control with initial rotor position estimation for interior permanent magnet synchronous motor drive, IEEE Trans. Power Electron., vol. 20, no. 6, pp. 1413–1421, Nov. 2005.

[139] R.E. Kalman, "A new approach to linear filtering and prediction problems", Trans. of the ASME, pp. 35-45, 1960.

[140] M. Kojabadi, M. Ghribi, MRAS-based adaptive speed estimator in PMSM drives, Proceedings of Advanced Motion Control conference, pp. 569–572, 2006.

[141] Y. Liang, Y. Li, Sensorless control of PM synchronous motors based on MRAS method and initial position estimation, Proceedings of the Sixth International on Electrical Machines and Systems Conference, pp. 96–99, 2003.

[142] S. Maiti, C. Chakraborty, S. Sengupta, Simulation studies on model reference adaptive controller based speed estimation technique for the vector controlled permanent magnet

synchronous motor drive, Simulation Modelling Practice and Theory, vol. 17, pp. 585–596, Apr. 2009.

[143] Y. Liu, J. Wan, G. Li, C. Yuan and H. Shen, "MRAS speed identification for PMSM based on fuzzy PI control," Industrial Electronics and Applications, 2009. ICIEA 2009. 4th IEEE Conference on, Xi'an, pp. 1995-1998, 2009.

[144] K. Liu, Q. Zhang, Z Q. Zhu, J. Zhang, A W. Shen, P. Stewart, Comparison of two novel MRAS based strategies for identifying parameters in permanent magnet synchronous motors, International Journal of Automation and Computing, vol. 4, pp. 516–524, Nov. 2010.

[145] D.J. Atkinson, P. Acarnley, J. Finch, "Observers for induction motor state and parameter estimation", IEEE Trans. on Industry Applications, vol. 27, no. 6, pp. 1119-1127, 1991.

[146] C. Lee, C.L. Chen, "Speed sensorless vector control of induction motor using kalman filter assisted adaptive observer", IEEE Trans. on Industrial Electronics, vol. 45, no. 2, pp. 359-361, 1998.

[147] Z. Peroutka, Development of sensorless PMSM drives: application of extended Kalman filter, Proceedings of the ISIE' 05, pp. 1647–1652, 2005.

[148] Y H. Kim, Y S. Kook, High performance IPMSM drives without rotational position sensors using reduced-order EKF, IEEE Trans. Energy Conversion., vol. 14, no. 4, pp. 868–873, Dec. 1999.

[149] C. Forgez, "Contribution à la modélisation et à l'identification temps réel pour les systèmes à énergie électrique embarquée", Habilitation à diriger des recherches, UTC, LEC, 2009.

[150] S. Bolognani, M. Zigliotto, and M. Zordan, "Extended-range PMSM sensorless speed drive based on stochastic filtering," IEEE Transactions on Power Electronics, vol. 16, no. 1, pp. 110–117, 2001.

[151] O. Aydogmus, S. Sünter, "Implementation of EKF based sensorless drive system using vector controlled PMSM fed by a matrix converter" International Journal of Electrical Power & Energy Systems, Volume 43, Issue 1, December 2012, Pages 736-743.

[152] K. C. Yu Kent, N. R. Watson, J. Arrillaga, An adaptive Kalman filter for dynamic harmonic state estimation and harmonic injection tracking, IEEE Trans. on power delivery, Vol. 20, No 2, 2005.

[153] G. Besançon, J. de Leon-Morales, O. Huerta-Guevara On adaptive observers for state affine systems, International Journal of Control, Vol.79, No. 6, p 581-591, 2006.

[154] F.D. Busse, J.P. How, J. Simpson, Demonstration of Adaptive Extended Kalman Filter for Low-earth-orbit Formation Estimation using CDGPS Navigation. Journal of the Institute of Navigation, v 50, n 2, p 79-93, 2003.

[155] J.-P. Gauthier, H. Hammouri, S. Othman, A simple observer for nonlinear systems, IEEE Trans. Aut. Control, 37, pp. 875–880, 1992.

[156] V. Smidl, Z. Peroutka, Advantages of square-root extended Kalman filter for sensorless control of AC drives, Ind. Electron. IEEE Trans. Ind. Electron. 59 (11) (2012) 4189-4196.

[157] F. Jiancheng, Y. Sheng, Study on innovation adaptive EKF for in-flight alignment of airborne POS, IEEE Trans. Instrum. Meas. 60 (4) (2011) 1378-1388.

[158] J. Ali, Strapdown inertial navigation system/astronavigation system data synthesis using innovation-based fuzzy adaptive Kalman filtering, IET Sci. Meas. Technol. 4 (5) (2010) 246-255.

[159] M. Saha, R. Ghosh, B. Goswami, Robustness and sensitivity metrics for tuning the extended Kalman filter, IEEE Trans. Instrum. Meas. 63 (4) (April 2014) 964-971.

[160] H. Al-Ghossini, F. Locment, M. Sechilariu, L. Gagneur, C. Forgez: "Adaptive-tuning of extended Kalman filter used for small scale wind generator control", Renewable Energy, vol.85, pp. 1237-1245, 2016.

[161] P.D. Larminate, "Analysis, Control of Linear Systems", Wiley, 2007.

[162] L. Gagneur, C. Forgez, A.L.D. Franco, "On-line adaptive tuning of a lithium-ion battery cell state of charge observer", IEEE Energy Conversion Congress and Exposition (ECCE), pp. 307-314, Denver (USA), 2013.

[163] M. A. Hamida, J. De Leon, A. Glumineau, and R. Boisliveau. An adaptive interconnected observer for sensorless control of PM synchronous motors with online parameter identification. IEEE Trans. Ind. Electron., vol. 60, no. 2 :pp. 739 – 748, 2013.

[164] N. Matsui. Sensorless PM brushless DC motor drives. IEEE Trans. Ind. Electron., vol.43, no. 2: pp. 300–308, Avril 1996.

Appendixes

Appendix 1: Parameters measurement of PMSM

Appendix 2: Modeling of PMSM

Appendix 3: Geometric and mechanical parameters

Appendix I. Parameters measurement of PMSM

From the early days of the energy distribution, which means late twenties of the last century, the grid engineers understood how important is an accurate model of the synchronous machine in calculating the stability, or in general, the dynamic behavior of the power grid. Since the synchronous machine model is based on its parameters, the need for a reliable set of electrical parameters is obvious. The parameters can be calculated analytically or via a magnetic field analysis procedure during the design stage of the machine. The parameters can be obtained also by tests at the factory or on site. Two groups may classify the techniques to settle on electrical-machine model parameters: frequency and time domain tests. Some of them can be applied online, while others are used when the machine is at a standstill. Online tests, such as the sudden short circuit, open circuit, load rejection, and field flux decay, have been reported in literature [23]. Tests, such as the sudden short circuit and load rejection, are considered to be prohibitive due to the possible damage of the machine. Moreover, a great amount of research has been reported to characterize the *d*–*q*-axis machine model with standstill tests. Some of them are the well-known standstill frequency response, DC step voltage, and DC flux decay. A set of inductances and resistances is always needed in modeling and simulating the synchronous machine dynamic behavior or for its controller design [24].

1. Measurement of constant electromotive force

The constant of back-electromotive force (EMF) can be obtained by measuring the machine phase voltage in the state of no-load while it is driven through the shaft at a constant speed Ω. The constant k gives a ratio between back- EMF voltage and the angular electrical frequency ω. From the same test, the ratio between the mechanical and electrical speed also gives the number of pole pairs. To achieve this test it requires oscilloscope, at least one voltage probe. The motor is set to spin at a constant speed. Then, the generated phase voltage is measured and the constant k is calculated by (62):

$$k = \frac{v}{\omega} \tag{62}$$

Various rotation speeds have been applied on the machine to get more accurate value of back-EMF constant. After measuring the phase voltage terminal, this constant are calculated by (62) considering that this speed has an amplifying ratio by 7 due to gearbox from manufactory. The constant k can be rewritten as in (63):

$$k = \frac{V}{\frac{2\pi.\omega}{60} \times 7} \tag{63}$$

Results are shown in Table 4:

Table 5. Results of no-load test

Rotational speed [rpm]	Voltage phase [V]	Back-EMF constant [V.r^{-1}.s]	Back-EMF constant [V.rad^{-1}.s]
350	20.2	2.448	0.389
700	39.9	2.418	0.384
1050	59.6	2.408	0.383
1400	79.6	2.412	0.383
Average value		2.421	0.385

At the same time, by applying Fast Fourier Transform to the output signal, electrical frequency is obtained and then number of poles pairs can be calculated. For rotation speed of 1050rpm, meaning 110rad.s^{-1}, and electrical frequency measures 90Hz, meaning 556rad.s^{-1}. Hence, the number of poles pairs is verified to be 5 pairs of poles.

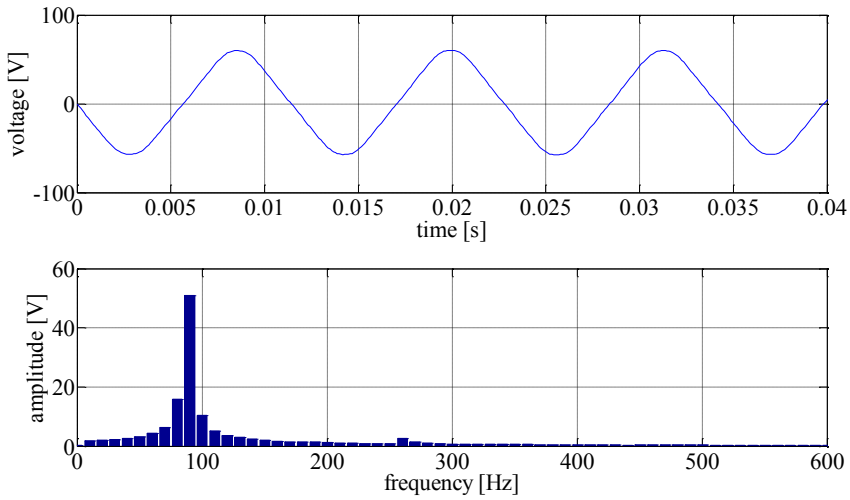

Figure 62. Voltage signal Fast Fourier Transform in no-load test

2. *Measurement of phase resistance*

To measure the resistance R (recall that the resistances of the three phases are equal and therefore only one measurement is sufficient), a voltage-current method can be used where it is necessary to impose a DC voltage between a phase and the machine neutral point. Hence, as the current is also continuous, so $L \cdot di/dt = 0$ and impose a zero rotational speed (which leads to $E = k.\Omega = 0$). In this way, voltage equation of the machine becomes $V = R \cdot I$. A portable multi-meter (of type FLUKE 87V) is used to measure the voltage of phase and a numeric multi-meter (of type FLUKE 8846A 6-1/2) to measure the current phase. A DC voltage source (of type AX 502 Metrix) has been utilized to feed the circuit. To obtain a more real value of resistance, various measurements were taken at the nominal value of current with different period of time to allow the machine get hotter. Results are presented in Table 6:

Table 6. Results of resistance value

Time (min)	Voltage(V)	Current (A)	R (Ω)
T=0	6.58	5	1.316
T=15	6.72	5	1.344
T=30	6.79	5	1.358
T=45	6.84	5	1.368
Average value			1.346

3. *Measurement of phase inductance*

One phase can only be used to measure the inductance value. By imposing a voltage to one phase, only the self-inductance can be considered, the other two phases are in effect under zero voltage, it will not induces mutual inductance. In this test, the converter is used as a chopper to inject a square-wave voltage in the phase so that induces a step response gives an image of time constant τ. So inductance can be calculated from $\tau = L / R$. The DC source is connected to the converter bus and phase A to the first arm and the neutral point to the negative terminal of the bus. A dSPACE 1103 is used to generate chopper pulses that produce the appropriate wave at the chopper output. This dSPACE is also used to obtain the two signals, the injected voltage into the machine and the response step of phase current, as presented in Figure 63:

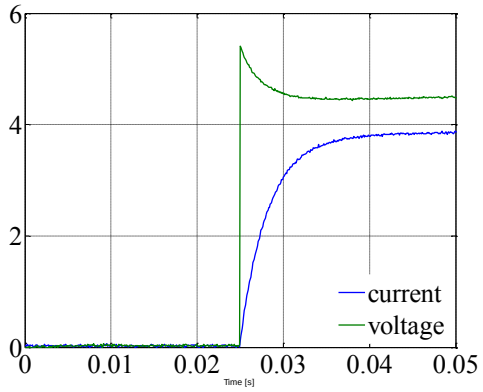

Figure 63. Voltage step and current response

Signals are filtered and treated through MATLAB and final result is obtained that gives the time constant value, so that inductance value can be determined, as it is in Table 7.

Table 7. Results of inductance value

Chopper frequency (Hz)	Time constant τ (s)	Inductance L (mH)
2	0.0038	4.9
5	0.0036	4.7
15	0.0034	4.4
25	0.0032	4.2

4. *Measurement of mutual inductance*

Mutual inductance can be calculated if it is placed under the same conditions as the same in experimental measurement of phase inductance (but sinusoidal voltage imposed on a single phase) and measure the EMF induced in the two other phases. A linear three-phase amplifier (of type PA-1000-AB x 3 and of 3kVA power) that emulates the national grid is used to produce sinusoidal voltage. A produced voltage in the other phase terminal is measured. Also, the previous inductance value can be verified by measuring voltage and current phase, and determine the angle phase of it. This test doesn't need dSPACE or converter, but just an oscilloscope to figure and store signals data. By imposing an alternative voltage whose an effective value of 4.8V and a frequency of 50Hz in phase A, an alternative current flows through machine phase, and its effective value equals 1.72A shows the signals of voltage and current in machine phase, current vector is lagged to voltage by 126°, thus, the power factor of 0.5878. Hence, the inductance value can be verified through Ohm's law as voltage, current and frequency values are known; its value is 5.6mH.

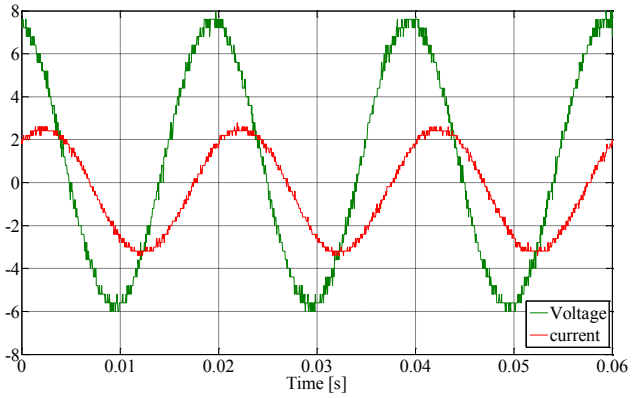

Figure 64. Voltage and current signals in machine phase

Figure 65 show the voltage induced at open-terminal phase B, which represents an image of the mutual flux with phase A.

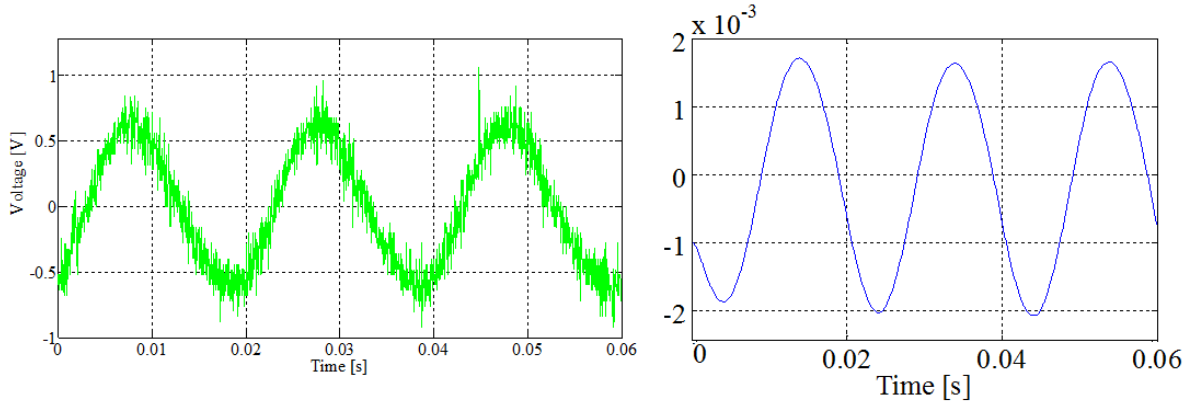

Figure 65. Induced voltage and flux signals at open-terminal phase

Mutual inductance can be obtained through integrating voltage so getting magnetic flux. Flux induced in phase B has a calculated maximum value of 0.002wb. Current maximum value is 1.72A. So mutual inductance can be calculated and it results 1.2mH.

Appendix II. Modeling of PMSM

In this appendix, the mathematical model of PMSM will be developed in fixed frames, both the natural three-phase reference *A-B-C* and stationary two-phase reference α-β. The analysis of machine power and torque will be given as well. The first step of a control guideline synthesis is the modeling of control PMSM process; this modeling is established in terms of differential equations and is essentially based on the Clarke transformation. Thus, the purpose of this part is to present the modeling of permanent magnet synchronous machines associated with a 3-ph diode bridge. It begins with the three-phase model and the model obtained by decomposition in the two axes (Clarke transformation).

1. Simplifying assumptions

A PMSM is a complex system, whose modeling conformed to the following simplifying assumptions:

- The voltage system is balanced.
- The distribution of the magneto-motive force created by the stator windings is sinusoidal.
- The magnetic circuits are not saturated (operating in the linear zone).
- There are no rotor's damper windings (effect of the shock absorbers is neglected).
- Losses by eddy current and hysteresis are neglected.

2. Equation development of PMSM in A-B-C frame

To establish simple relationships between voltage power sources and motor currents, the model of ideal synchronous machine is considered. Figure 66 represents the geometrical diagram of PMSM. From this schema, electrical equations can be obtained.

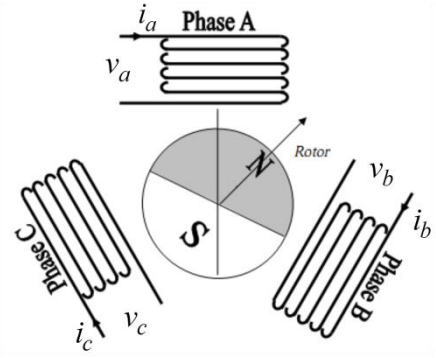

Figure 66. Equivalent diagram of PMSM in *A-B-C* frame

In the context of simplifying assumptions listed above and taking into account the geometrical schema mentioned earlier, the equations of PMSM can be written as (64):

$$
\begin{aligned}
v_A &= R_S.i_A + \frac{d\varphi_A}{dt} \\
v_B &= R_S.i_B + \frac{d\varphi_B}{dt} \\
v_C &= R_S.i_C + \frac{d\varphi_C}{dt}
\end{aligned} \tag{64}
$$

with $\varphi_A, \varphi_B, \varphi_C$ stator flux in *A*-*B*-*C* reference (Wb), v_A, v_B, v_C phase voltages in *A*-*B*-*C* reference (V), i_A, i_B, i_C phase currents in *A*-*B*-*C* reference (A) and R_S Phase resistance (Ω).

In matrix form (65) it is obtained:

$$
\begin{bmatrix} v_A \\ v_B \\ v_C \end{bmatrix} = \begin{bmatrix} R_S & 0 & 0 \\ 0 & R_S & 0 \\ 0 & 0 & R_S \end{bmatrix} \begin{bmatrix} i_A \\ i_B \\ i_C \end{bmatrix} + \frac{d}{dt} \begin{bmatrix} \varphi_A \\ \varphi_B \\ \varphi_C \end{bmatrix} \tag{65}
$$

Under the assumption of a sinusoidal spatial distribution of induction, the induced flux by the magnet in the three-phase of stator 'a, b, c' are given in (66):

$$
\begin{aligned}
\phi_{FA} &= \phi_F \cos\theta \\
\phi_{FB} &= \phi_F \cos\left(\theta - \frac{2\pi}{3}\right) \\
\phi_{FC} &= \phi_F \cos\left(\theta - \frac{4\pi}{3}\right)
\end{aligned} \tag{66}
$$

with ϕ_F Induced flux by the permanent magnets (Wb) and where the produced flux in each stator winding is sum of four terms. For example, to the phase 'a', the flux is sum of the following terms:

Self-flux phase 'a' to 'a': $\phi_{AA} = L_0 i_A$

Mutual flux of phase 'b' to 'a': $\phi_{BA} = M_S i_B$

Mutual flux of phase 'c' to 'a': $\phi_{CA} = M_S\, i_C$

Mutual flux of the magnet on phase 'a': ϕ_{FA}

Hence, the expression of the total flux in the phase 'a' is given by (67):

$$
\phi_A = \phi_{AA} + \phi_{BA} + \phi_{CA} + \phi_{FA} = L_0 I_A + M_S \left(I_B + I_C\right) + \phi_{FA} \tag{67}
$$

because the machine is balanced by isolated star point, then: $i_A + i_B + i_C = 0$. That is to say, $i_B + i_C = -i_A$. So, the expression of the flux in phase 'a' is reduced to (68):

$$
\phi_A = \left(L_0 - M_S\right) i_A + \phi_{FA} = L_S i_A + \phi_{FA} \tag{68}
$$

Therefore, the expressions for flux in the other two phases are expressed as (69):

$$\begin{aligned}\phi_B &= L_S i_B + \phi_{FB} \\ \phi_C &= L_S i_C + \phi_{FC}\end{aligned} \tag{69}$$

By replacing the expressions for the flux in the voltage system, the equations in (70) are obtained:

$$\left.\begin{aligned} v_A &= R_S.i_A + L_S\frac{di_A}{dt} + \frac{d\phi_{FA}}{dt} \\ v_B &= R_S.i_B + L_S\frac{di_B}{dt} + \frac{d\phi_{FB}}{dt} \\ v_C &= R_S.i_C + L_S\frac{di_C}{dt} + \frac{d\phi_{FC}}{dt} \end{aligned}\right\} \Leftrightarrow \begin{bmatrix} v_A \\ v_B \\ v_C \end{bmatrix} = [R]\begin{bmatrix} i_A \\ i_B \\ i_C \end{bmatrix} + [L]\frac{d}{dt}\begin{bmatrix} i_A \\ i_B \\ i_C \end{bmatrix} + \begin{bmatrix} e_A \\ e_B \\ e_C \end{bmatrix} \tag{70}$$

where $[R]$ is a diagonal matrix (no coupling between phases) and $[L]$ symmetric matrix and in circulation. These matrices and electromotive forces are expressed by (71):

$$[R] = \begin{bmatrix} R_S & 0 & 0 \\ 0 & R_S & 0 \\ 0 & 0 & R_S \end{bmatrix};\ [L] = \begin{bmatrix} L_0 & M_S & M_S \\ M_S & L_0 & M_S \\ M_S & M_S & L_0 \end{bmatrix};\ \begin{bmatrix} e_A \\ e_B \\ e_C \end{bmatrix} = \varphi_F \begin{bmatrix} \cos\theta \\ \cos\left(\theta - \frac{2\pi}{3}\right) \\ \cos\left(\theta - \frac{4\pi}{3}\right) \end{bmatrix} \tag{71}$$

From (70), the electrical schema is simplified as given in Figure 67:

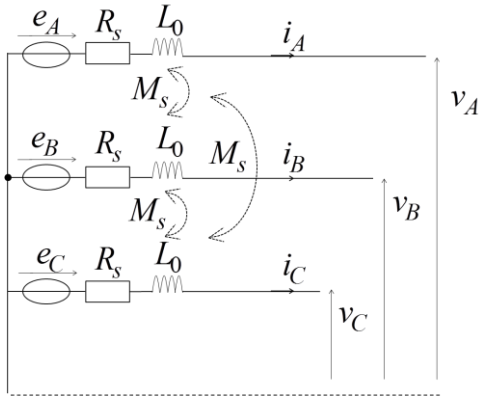

Figure 67. Electrical schema of PMSM

From (70) and (71), (72) can be concluded:

$$\begin{bmatrix} v_A \\ v_B \\ v_C \end{bmatrix} = [R]\begin{bmatrix} i_A \\ i_B \\ i_C \end{bmatrix} + [L]\frac{d}{dt}\begin{bmatrix} i_A \\ i_B \\ i_C \end{bmatrix} + \varphi_F \begin{bmatrix} \cos\theta \\ \cos\left(\theta - \frac{2\pi}{3}\right) \\ \cos\left(\theta - \frac{4\pi}{3}\right) \end{bmatrix} \tag{72}$$

3. *Equation development of PMSM in α-β frame*

The two-phase model consists of two perpendicular coils with respect to each other (Figure 68) and traversed with currents phased by π/2. In order to model the three-phase system described above through a two-phase model, Clarke transform with its inverse transformation are used. Considering the simplifying assumptions mentioned above and in case of stator windings connected in star and a balanced three-phase system, the zero sequence components of the current, voltage and flux become zero. Therefore, equations can be deduced based on simplified Clarke transform given by (73):

$$\left.\begin{aligned}\begin{bmatrix} v_\alpha, i_\alpha \\ v_\beta, i_\beta \end{bmatrix} &= \frac{2}{3}\begin{bmatrix} 1 & -\frac{1}{2} & -\frac{1}{2} \\ 0 & \frac{\sqrt{3}}{2} & -\frac{\sqrt{3}}{2} \end{bmatrix}\begin{bmatrix} v_A, i_A \\ v_B, i_B \\ v_C, i_C \end{bmatrix} \\ \begin{bmatrix} v_A, i_A \\ v_B, i_B \\ v_C, i_C \end{bmatrix} &= \begin{bmatrix} 1 & 0 \\ -\frac{1}{2} & \frac{\sqrt{3}}{2} \\ -\frac{1}{2} & -\frac{\sqrt{3}}{2} \end{bmatrix}\begin{bmatrix} v_\alpha, i_\alpha \\ v_\beta, i_\beta \end{bmatrix}\end{aligned}\right\} \tag{73}$$

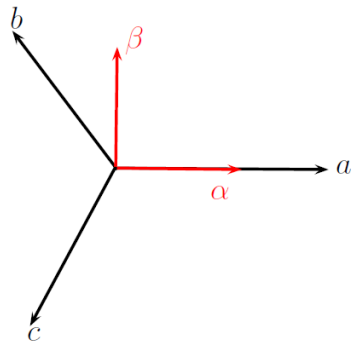

Figure 68. Natural three-phase reference *A-B-C* and stationary two-phase reference *α-β*

Applying this transformation on voltages, currents and flux, the two-phase PMSM model is given by the equation (74):

$$\begin{bmatrix} v_\alpha \\ v_\beta \end{bmatrix} = R_S\begin{bmatrix} i_\alpha \\ i_\beta \end{bmatrix} + L_S\frac{d}{dt}\begin{bmatrix} i_\alpha \\ i_\beta \end{bmatrix} + K\omega\begin{bmatrix} \sin\theta \\ -\cos\theta \end{bmatrix} \tag{74}$$

with v_α, v_β voltages in *α-β* reference (V), i_α, i_β currents in *α-β* reference (A), K flux magnets constant, ω electrical speed rotation ($\omega = p\Omega$ with p number of pole pairs, five here) and θ ($\theta = \omega t$) electrical position.

Appendix III. Geometric and mechanical parameters

Blade radius: $R = 1.25\text{m}$;

Interpolation factors of c_P:

$a_7 = -4.1\times10^{-8}; a_6 = -4.2\times10^{-6}; a_5 = 2.1\times10^{-4};$

$a_4 = -4.2\times10^{-3}; a_3 = 1.65\times10^{-2}; a_2 = -1.9\times10^{-2};$

$a_1 = 1.7\times10^{-2}; a_0 = -1.9\times10^{-3};$

Inertia: $J = 1.5\text{kg}\cdot\text{m}^2$;

Viscous damping coefficient: $F = 0.06\text{Nm}/\text{rad}$.

PMSM parameters

number of pole pairs	5
measured phase resistance	1.46Ω
measured flux linkage of the magnets	0.393Wb
self inductance in average	0.0051H
mutual inductance in average	0.0005H
inertia of rotor	$42.6\times10^{-5}\text{kg}\cdot\text{m}^2$

BRUSHLESS MOTORS
NX430EAJ
ELECTRONIC DRIVE (1)
DIGIVEX 7.5/15 et DIGIVEX 8/16
(230 V) (400 V)

PARVEX

Torque at low speed	M_o	Nm		5.5	
Permanent current at low speed	I_o	A_{rms}		5.24	
Peak torque	M_p	Nm		18.8	
Current for the peak torque	I_p	A_{rms}		21	
Back emf constant at 1000 rpm (25°C)*	Ke	V_{rms}		65.6	
Torque sensitivity	Kt	Nm/A_{rms}		1.05	
Winding resistance (25°C)*	Rb	Ω		2.33	
Winding inductance*	L	mH		10.9	
Rotor inertia	J	kgm^2x10^{-5}		42.6	
Thermal time constant	Tth	min		18	
Motor mass	M	kg		4.8	
Voltage of the mains	UR1 UR2 UR3	V_{rms}	230	400	480
Rated speed	Nn1 Nn2 Nn3	rpm	3200	5500	6200
Rated torque	Mn1 Mn2 Mn3	Nm	4.68	3.35	2.82
Rated current	In1 In2 In3	A_{rms}	4.53	3.31	2.83
Rated power	Pn1 Pn2 Pn3	W	1570	1930	1830

All data are given in typical values under standard conditions

** Phase to phase* *(1) Please check the availability of this drive with 480 V*

Voltages and currents are given in rms values

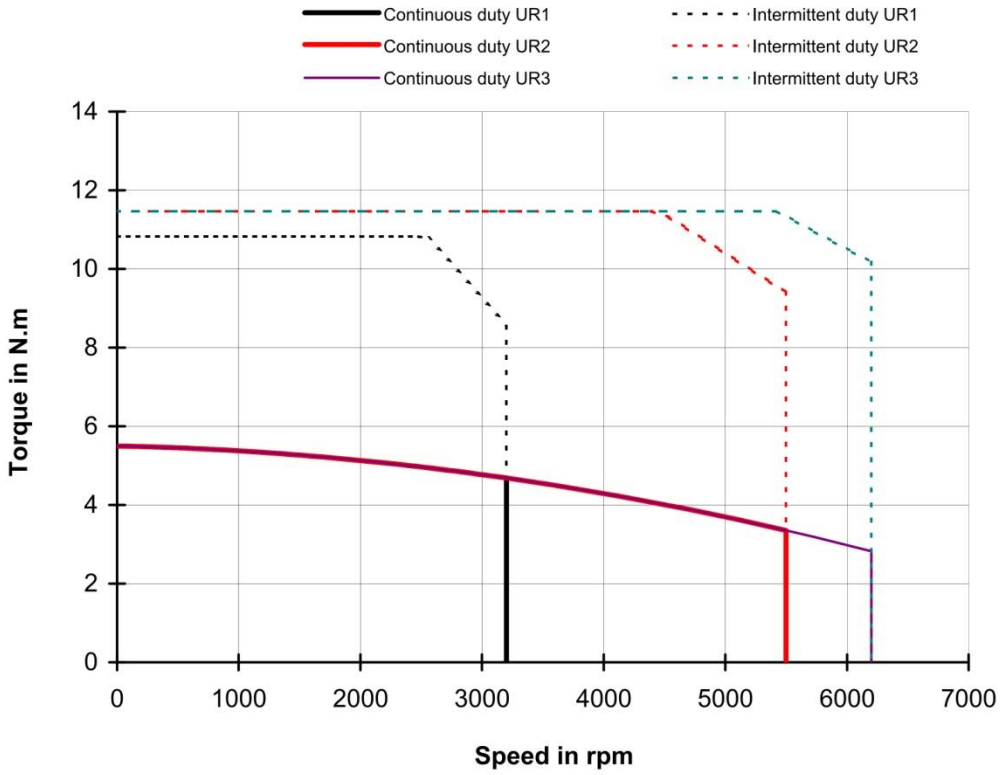

Characteristics are given for an optimal drive of the motor FICHE-009

Création: 11 mai 2000	Edition:	10/févr/2005	NX430EAJ	. -